PSI

Paul Scherrer Institut

Labor für Reaktorphysik und Systemtechnik

Shielding Performance of the NET Vacuum Vessel

J. J. Arkuszewski, J. F. Jaeger

Shielding Performance of the NET Vacuum Vessel *

J. J. Arkuszewski, J. F. Jaeger

Paul Scherrer Institute, (formerly EIR)

5303 Würenlingen

Switzerland

August 12, 1988

Abstract

To corroborate 1-D deterministic shielding calculations on the Next European Torus (NET) vacuum vessel/shield and shielding blanket, 3-D Monte Carlo calculations have been done with the MCNP code. This should provide information on the poloidal and the toroidal variations. Plasma source simulation and the geometrical model are described, as are other assumptions. The calculations are based on the extended plasma power of 714 MW. The results reported here are the heat deposition in various parts of the device, on the one hand, and the neutron and photon currents at the outer boundary of the vacuum vessel, on the other hand. The latter are needed for the detailed design of the super-conducting magnetic coils.

A reasonable statistics has been obtained on the outboard side of the torus, though this cannot be said for the inboard side. The inboard is, however, much more toroidally symmetric than the outboard, so that other methods could be applied such as 2-D deterministic calculations, for instance.

Contents

1 Introduction

The *next fusion experiment in the Euratom after JET*, which should demonstrate ignition, i.e. plasma burning without external heating, long term plasma burning, and also the fiability of the technology used is the Next European Torus (NET). In designing the vacuum vessel/shield and the shielding blanket, the following aspects must be considered:

- the radiation load on the superconducting coils

- the power deposition in both the vacuum vessel and the shielding blanket

- tritium breeding in the case that the shielding blanket is upgraded by using lithium compounds

1-D deterministic shielding calculations have been done by the NET team to this purpose as these are quicker to set up and use less computer time than full 3-D ones. Done well, they give an accurate overall picture. To corroborate these 1-D calculations done with the ANISN code, 3-D Monte Carlo calculations have been done with the MCNP code (A General Monte Carlo Code for Neutrons and Photon Transport) - Version 3A[1]. This should provide information on the poloidal and the toroidal variations caused, in particular, by large vacuum pumping ducts, division of the vessel into parallel and wedge segments, and the D-shape of the plasma, as well as provide a check of the adequacy of the 1-D calculations.

The Monte Carlo method emerged from work done at Los Alamos during World War II. It is a simulation of neutron and photon transport based on a statistical consideration of the physical processes actually taking place. The MCNP is a general purpose code with many sophisticated methods to increase the accuracy, especially where thick shields are concerned. It uses, in the present case, point-wise cross-section libraries for the various reactions.

The 32-fold reflective symmetry of the device allows one to compute a $11.25°$ sector only. The present calculations provide, in particular, neutron and photon currents at the outer boundary of the vacuum vessel. These are needed for the detailed design of the super-conducting magnetic coils, where the problem of heat deposition is crucial, as this has to be extracted at the temperature of liquid helium. The shielding blanket, however, is less important at this point.

The following note describes some of the assumptions used for the calculations: the plasma source simulation in Sec. 2, the modeling of the shielding blanket and the vacuum vessel in Sec. 3, and the description of the tallies used in Sec. 4. The main results are presented in Sec. 5 and discussed in Sec. 6.

2 Plasma Source Simulation

The D-shaped plasma contours are described by the following set of parametric equations, which represent fairly realistically the results of the plasma physics:

$$R(\alpha,a) = R_p + a\cos(\alpha + \frac{a}{a_p}c_p\sin\alpha) + \epsilon_p a_p(1 - \frac{a^2}{a_p^2})$$

$$Z(\alpha,a) = \frac{a}{a_p}b_p\sin\alpha$$

$$S(a) = S_0(1 - \frac{a^2}{a_p^2})^{c_{pk}}$$

$$0 \leq \alpha < 2\pi$$

These equations define the contour surfaces, $(R(\alpha,a), Z(\alpha,a))$, of equal source strength, $S(a)$, for given values of the horizontal minor radius a. The values of the constants for the NET Extended Plasma are:

R_p	-	plasma major radius	-	541	cm
a_p	-	horizontal plasma minor radius	-	168	cm
b_p	-	vertical plasma minor radius	-	366	cm
ϵ_p	-	radial plasma shift	-	0.17	
c_p	-	triangularity	-	0.62	
e_{pk}	-	peaking exponent	-	4	

The geometry can be defined in MCNP by surfaces up to the second order and by tori. Thus, the above contours have to be approximated by such surfaces. Every contour has been replaced by an envelope consisting of a rotational hyperboloid and an elliptical torus on the inboard side and a rotational ellipsoid and another elliptical torus on the outboard side. This is illustrated in Fig. 1, where the exact contours for 10 evenly spaced values of a are drawn with solid lines and the corresponding envelope elements with dashed lines. The optimum envelopes have been found for positive values of z for the sets of points 1, 19, 26, 36, 51 out of 51 equidistant points in the α interval of $(0, \pi)$. These support points together with their symmetrical counterparts have been marked with crosses. This construction has been calculated by an auxilliary program PLASMA, which produced, at the same time, appropriate surface cards for the MCNP input including the z-axis virtual cylinders through points no. 26, which delimit the region defined by the outboard ellipsoids.

The code MCNP-3A has a very powerful source generation facility, which makes it possible to sample source particles from the very large class of phase space subspaces, including dependences between different phase space variables.

The source definition card has the form:

SDEF   ERG=D1 CEL=D2   X FCEL D3   Y FCEL D4   Z FCEL D5   EFF=0.05

4

The neutron energy distribution is designated as no. 1. It is a Gaussian fusion spectrum for D-T fusion at 10 keV. Its probability distribution is:

$$p(E) = Ce^{-(\frac{E-b}{a})^2}$$

where $a = 0.33605$ is the width in MeV and $b = 14.076$ is the average neutron energy in MeV for D-T fusion at 10 keV. The width here is defined as the ΔE above b where the value of the exponential is equal to e^{-1}.

The discrete distribution among cells is defined by the distribution no. 2, represented as a histogram of unnormalized probability density values for cell midpoints, interpolated from the $S(a_i)$ values. The three variables x, y, and z are sampled from distributions no. 3, 4, and 5, respectively, which depend on the cell number. Each cell is enclosed in a parallelepiped which is sampled uniformly in x, y, and z variables. If the sampled point is found to be inside the cell it is accepted, otherwise it is rejected and another point is sampled. The parameter EFF provides an efficiency criterion for the above process. The angular velocity distribution is isotropic and there is no biasing.

The exact cell volumes can be found for the plasma contour model from the formula:

$$V_i = T_i - T_{i-1}$$

where $i = 1, \ldots, I$, $T_0 = 0$, and:

$$T_i = 2\pi \int_0^\pi R^2(\alpha, a_i) \frac{\partial Z(\alpha, a_i)}{\partial \alpha} d\alpha$$

or,

$$T_i = \frac{2\pi^2 a_i b_p}{c_p} \{2[R_p + \epsilon_p a_p(1 - \frac{a_i^2}{a_p^2})]J_1(\frac{a_i}{a_p}c_p) - \frac{a_i}{4}[J_2(2\frac{a_i}{a_p}c_p) + J_3(2\frac{a_i}{a_p}c_p)]\}$$

with J_n. $n = 1, 2, 3$ denoting the Bessel functions of n-th order. The volumes of the 10 approximate cells has also been computed stochastically by the MCNP code. Table 1 presents the comparison of the volumes obtained analytically and stochastically for a 22.5° sector as well as the cell emission probability density.

As the statistical error in the MCNP calculation is smaller than 1% the systematic growth of the above error can be attributed to the contour approximation. The peripheral cells, however, produce much fewer neutrons than the inner ones, so the approximation as a whole can be considered as satisfactory. The above source model has been implemented in a test MCNP input. The comparison of sampled and expected values is presented in Fig. 2.

The MCNP code computes all tallies for 1 source particle, so, for the plasma total power of 714 MW and a D-T reaction energy release of 17.58 MeV, the normalization factor for a 11.25° torus sector is:

$$S_0 = \frac{714}{1.6021892.10^{-19} \cdot 17.58 \cdot 32} = 7.9216.10^{18} \frac{n}{s}$$

5

Cell	Prob. Density	Analytic Volume	MCNP Volume	Error (%)
1	2..77150-1	4.3143+5	4.2952+5	-0.44
2	2.222249-1	1.2869+6	1.2832+6	-0.28
3	1.884614-1	2.1201+6	2.1244+6	0.20
4	1.453179-1	2.9169+6	2.9296+6	0.44
5	9.996436-2	3.6635+6	3.7077+6	1.21
6	5.944822-2	4.3473+6	4.4510+6	2.38
7	2.890151-2	4.9568+6	5.0870+6	2.66
8	1.036231-2	5.4818+6	5.6487+6	3.05
9	4.444497-3	5.9138+6	6.1705+6	4.34
10	1.600019-4	6.2459+6	6.6196+6	5.98
Total	1.0	3.7364+7	3.8451+7	2.91

Table 1: Source Cell Volumes

3 Shielding Blanket and Vacuum Vessel MCNP Model

The reference profile of the internal vacuum vessel surface is shown in Fig. 3. This profile has been approximated by the envelope of the following surfaces:

- Inboard cylinder.

- Two circular "small" tori on the inboard side shifted ± 360 cm along the z-axis.

- A "large" elliptical torus from the vertex down on the outboard side.

- A rotational ellipsoid on the outboard side.

The above approximation is shown in Fig. 4. All other poloidal surfaces that define both the shielding blanket and the vacuum vessel are parallel forming a sandwich structure. The poloidal cross-section through the wedge sector is shown in Fig. 5. The vacuum vessel possesses a 32-fold rotational symmetry, therefore it is sufficient to deal with a 11.25° sector of the torus cut by reflective surfaces. Additionally, this sector is divided into so called parallel and wedge parts, which have different radial structures. The inner region beyond the outer boundary of the vessel on the inboard side is a black body, so no neutrons or gammas get back to the torus across the torus center, whether from neighbouring segments or those lying on the opposite side of the torus. This approximates the dense coil inner region. However, this is less applicable to the present machine with super-conducting coils than to one with a large transformer iron yoke. Inclusion of an extra layer with a material representative of the coils would increase the flow of neutrons and gammas from one sector to the next and provide some backscatter

6

from this region. The outer region beyond the outer boundary on the outboard side is also a black body. Inclusion of coils there would cause some backscatter too. However, the model is sufficiently large as it is, in terms of computing time for instance, that such effects should be rather investigated with simpler, 1-D or 2-D, codes.

The modelled layers correspond to those of the real design with water in the cooling pipes, simply homogenized. Empty structural spaces taken up by bolt endings have been homogenized as well and the electrical insulation between sectors disregarded. The stainless steel, SS, composition corresponds to the standard AISI 316 LN, with alloying elements and impurities taken near the upper limit of the standard range. Copper, cobalt, and boron have been neglected. Borated water contains 40 g/l of H_2BO_3, with natural boron. The inboard and outboard blanket is separated by a sloping divertor made of molybdenium steel and cooled with water. The material used is composed of 67.6% TZM (Ti, Zr, Mo), 13% SS, and 19.4% water and fills the whole volume. At the time of the calculations, the detail design was not yet known. In fact, the divertor will probably be only a slab of a similar material with a void packed with pipe headers and connections behind it. As a result, the divertors absorb too much neutrons and gammas compared to present design concepts. Material compositions are listed in Table 2. In the wedge, in three cases the actual materials were approximated by similar ones from the table:

- a material with 9.45% water (WI1/2), is approximated by one with 9.95% water, M4;

- a material with 4.55% water (WI3) is almost exactly M5 with 4.53% water;

- and 0.0012% water is neglected (WO5).

The materials and thicknesses used at $z = 0$ are shown in Table 3 for both wedge and parallel regions. The cross-sections through the $z = 0$ plane of the inboard and outboard parts are shown in Figs. 6 and 7, respectively, together with the material designations[1]. In the wedge, the outermost zone from 255.0 cm to 290.5 cm on the inboard side, Fig. 6, is probably too long (35.5 cm), but the wedge is very narrow at this point and thus contributes only a small fraction of the total neutron and gamma currents.

The lower part of the wedge sector opens onto the vacuum duct (Fig. 5 and 8). The wedge shape of the vertical part of the duct (Fig. 9) is there to leave space for the coils. In the vacuum vessel and outside the torus, the walls of the duct have been modelled as a uniform material (SS with 25% water, M2, at present), by means of planes (vertical and inclined), vertical cylinders, and in the lower part a quadrant of tori in a vertical plane with their axes of symmetry tangential to the tokamak torus (Fig. 8). This last feature represents a simplification on the far right hand side for a duct finally sloping downwards, but it should not have much effect on the tallies around the tokamak torus.

---

[1] Material 0 designates void.

Nuclide	Mass Fraction						
	M1 Graphite	M2 SS 25%water	M3 13% SS 67.6%TZM 19.4%water	M4 SS 9.95%water	M5 SS 4.53%water	M6 Water	M7 SS 1.76% water
^{1}H	-	0.00456	0.00207	0.00154	0.00067	0.11191	0.00026
B	-	-	-	-	-	-	-
^{12}C	1.00000	0.00029	0.00004	0.00029	0.00030	-	0.00030
^{14}N	-	0.00156	0.00020	0.00154	0.00160	-	0.00156
^{16}O	-	0.03639	0.02125	0.01241	0.00537	0.88809	0.00204
Si	-	0.00959	0.00125	0.00982	0.00993	-	0.01003
^{31}P	-	0.00043	0.00006	0.00045	0.00044	-	0.00044
^{32}S	-	0.00028	0.00004	0.00029	0.00029	-	0.00030
Ti	-	-	0.00420	-	-	-	-
Cr	-	0.16492	0.02100	0.16973	0.17056	-	0.17060
^{55}Mn	-	0.01918	0.00251	0.01964	0.01985	-	0.01993
Fe	-	0.60985	0.07968	0.62703	0.63295	-	0.63553
Ni	-	0.12902	0.01680	0.13256	0.13325	-	0.13414
Zr	-	-	0.00084	-	-	-	-
Mo	-	0.02394	0.84931	0.02469	0.02478	-	0.02487
W	-	-	0.00017	-	-	-	-
Gram Density ($g \cdot cm^{-3}$)	1.8	6.1	8.095	7.129	7.505	1.0	7.679
Atomic Density ($b^{-1}cm^{-1}$)	9.03300-2	8.88454-2	7.38776-2	8.66398-2	8.59738-2	1.00306-1	8.53990-2

Nuclide	Mass Fraction					
	M8 Borated water	M9 SS .266%water	M10 SS	M11 SS .969%water	M12 SS .236%water	M13 SS 1.51%water
^{1}H	0.10865	0.00004	-	0.00014	0.00003	0.00022
B	0.00673	-	-	-	-	-
^{12}C	-	0.00030	0.00030	0.00030	0.00030	0.00030
^{14}N	-	0.00160	0.00160	0.00160	0.00160	0.00160
^{16}O	0.88462	0.00030	-	0.00111	0.00027	0.00174
Si	-	0.01001	0.01001	0.00995	0.01001	0.00999
^{31}P	-	0.00045	0.00045	0.00045	0.00045	0.00045
^{32}S	-	0.00030	0.00029	0.00030	0.00030	0.00030
Ti	-	-	-	-	-	-
Cr	-	0.17201	0.17180	0.17194	0.17202	0.17124
^{55}Mn	-	0.01990	0.02000	0.02004	0.01990	0.01998
Fe	-	0.63541	0.63593	0.63476	0.63543	0.63437
Ni	-	0.13478	0.13462	0.13445	0.13479	0.13492
Zr	-	-	-	-	-	-
Mo	-	0.02490	0.02500	0.02495	0.02490	0.02491
W	-	-	-	-	-	-
Gram Density ($g \cdot cm^{-3}$)	1.04	7.79	7.8	7.734	7.79	7.708
Atomic Density ($b^{-1}cm^{-1}$)	1.02547-1	8.52901-2	8.51572-2	8.53015-2	8.52635-2	8.54881-2

Table 2: Material Composition

8

	Parallel Segments			Wedge Segments		
	Material	Δr (cm)	R_o (cm)	Material	Δr (cm)	R_o (cm)
Vessel:			**255.0**			**255.0**
	M10	12.0	267.0			
	M8	5.0	272.0	M10	35.5	290.5
	M9	20.0	**292.0**	void	1.5	**292.0**
	M8	4.5	296.5			
	M7	11.0	307.5	M13	14.0	306.0
	M6	1.5	309.0	M6	2.0	308.0
	M5	7.0	**316.0**	≈M5	8.0	**316.0**
	M4	4.0	320.0			
	void	3.0	**323.0**	≈M4	7.0	**323.0**
Blanket:	void	5.0	328.0			
	M2	20.0	348.0		same as	
	M1	2.0	350.0			
Vacuum			373.0			
Plasma			709.0			
Vacuum			726.0		parallel	
Blanket:	M1	2.0	728.0			
	M2	3.0	731.0			
	void	7.7	738.7		(see note)	
	M2	19.6	758.3			
	void	7.7	766.0			
Vessel:				M11	6.0	772.0
	void	7.5	773.5	M6	1.5	773.5
	M4	4.0	777.5			
	M5	7.0	784.5			
	M6	1.5	786.0	M12	18.0	791.5
	M7	11.0	**797.0**	M6	5.5	**797.0**
	M8	6.5	803.5	≈M10	18.0	815.0
				M8	3.0	818.0
	M9	20.0	**823.5**	M10	5.5	**823.5**

Table 3: Materials and Thicknesses

Bold faced radii are the same for parallel and wedge segments.
Note: the blanket is not divided into wedge and parallel parts.

For the sake of some better computational accuracy the whole duct has been segmented into several cells. These are, nevertheless, too coarse for reliable results in the duct itself, but serve as a suitable boundary condition (neutron reflector) for the main torus. They should also help to provide a reliable set of boundary currents as inputs to a local duct computation. The sandwich nature of the vessel is retained in all but the lowest outboard vertical wedge segment, where material M2 is used. This explains the rather artificial limits of the sandwich. In the blanket region the sandwich structure is maintained and the duct is simply an opening bounded by a cone. The blanket sandwich extends past the top edge of the duct to simulate the rather complicated lip which protects the duct from line of sight radiation from inside the plasma core.

The heat generation in the duct wall as well as the current at its outer surface is not a subject of the present calculation. No tallies are present in this area. The duct has been modelled to provide a template MCNP input for future applications. This may include, among others, the more accurate modelling of the blanket lip.

Both vacuum vessel and shielding blanket are sectioned into segments. The outboard side (Figs. 5 and 10) is divided into 12 segments, the last one being the duct structure. The inboard side also consists of 12 segments (Fig. 11).

The final input to the code contains the following features:

Cross Section Data. The default MCNP library has been used. This library, BM-CCS, compiled at the Los Alamos National Laboratory, contains recommended unclassified data (Table 4). Three of the nuclides ^{31}P, ^{32}S, and ^{55}Mn have no

ZAID	Length	Nuclide	Evaluation	ID No.
1001.04C	2214	^{1}H	ENDF/B IV (T404 Rev.1)	1269
5000.01C	4169	B	LLL-Howerton, 1/73	510
6012.10C	7962	^{12}C	LASL Sublibrary, 13 Apr. 1976, T=0.0	102
7014.04C	17482	^{14}N	ENDF/B-IV	1275
8016.04C	19192	^{16}O	ENDF/B-IV	1276
14000.02C	18558	Si	ENDF/B-III, (T302), 20 Feb. 74	1151
15031.01C	2496	^{31}P	LLL-Howerton, 1/73, no γ prod.	520
16032.01C	2550	^{32}S	LLL-Howerton, 1/73. no γ prod.	521
22000.11C	8045	Ti	ENDF/B-IV, 19 May 77, T=300.0, NJOY	1286
24000.11C	34291	Cr	ENDF/B-IV, 24 Feb. 76, T=300.0	1191
25055.01C	3109	^{55}Mn	LLL-Howerton, 1/73, no γ prod.	527
26000.11C	46819	Fe	ENDF/B-IV, 24 Feb. 76, T=300.0	1192
28000.11C	30213	Ni	ENDF/B-IV, 24 Feb. 76, T=300.0	1190
40000.02C	7944	Zr	LLL-Howerton, 3/75	7141
42000.01C	5147	Mo	LLL-Howerton, 1/73	533
74000.01C	2850	W	LLL-Howerton, 1/73	541

Table 4: Cross Section Data

gamma production tables. However, they occur in small quantities, therefore an underestimation of gamma effects can be expected to be negligible. The gamma

library, MCPL, also belongs to the recommended set created at LANL and contains cross-sections for coherent and incoherent scattering, pair production, and the photoelectric effect together with appropriate form factors, energy deposition, and fluorescence data. No (γ,n) reactions are considered.

Volume and Surface Areas. None of the volumes and surface areas required by the code could be computed analytically by the code itself. A special run has, therefore, been done to estimate them stochastically for $1 \cdot 10^6$ particles starting inwards from a large sphere encompassing the whole system. A random choice of these estimated quantities[2] could be recalculated by hand; the results did not deviate by more than 1 to 4 %.

Physical and Weight Cutoffs. An analog Monte Carlo game has been chosen for the neutrons for the entire energy range from 0 to 20 MeV as well as for the photons from 0.001 to 100 MeV. The detailed physical treatment has been used for the photons[1].

Weight Windows and Exponential Transform. The outboard weight windows for both neutrons and photons were generated from a series of relatively short runs with hand adjustment. As the reference tally for the outboard side, the total heat generation at the outer shell of segment 5 was selected. One energy bin was used for both types of particles and a set of stretching parameters $p = \Sigma_a/\Sigma_t$ in directions normal to the sandwich structure has been used for the exponential transform. The weight windows for the inboard and the outboard sides are different and for this reason two sets of corresponding calculations were done with, respectively, different sets of weight windows. In fact, the generated outboard weight window set was transferred with appropriate adjustments to the inboard side. In both cases the less important sides (inboard for the outboard case and vice-versa) were treated with source-cell weight window values. In this way no time was wasted for transport in areas remote from tallies of interest, while the few particles reflected from the distant side of the facility were entering the game with relatively high weight and their scores was not lost. In the duct cells as well as in some top and bottom cells the weight windows were switched off to prevent oversplitting and underrouletting.

4 Tallies

The results of the calculations have been collected in the following tallies:

1. Power load (MW/m^2) on the first wall. This tally has been designed to check the correctness of the power normalization.

---

[2]For example volumes and areas on the inboard side.

11

2. Neutron power release per unit mass (W/g) in all cells of the shielding blanket and the vacuum vessel with the exception of the duct walls.

3. Ditto for photons.

4. Ditto for neutrons and photons, together.

5. Neutron current at the vacuum vessel outer surface split into 24 segments[3] (Figs. 10, 11). The current is binned in 7 energy bins.

6. Ditto for photons but without binning.

The statistical error[4] R is understood as the estimated standard deviation of the mean of a tally divided by the mean:

$$R \cong \left[\frac{1}{N} \left(\frac{\overline{f^2}}{\overline{f}^2} - 1 \right) \right]^{\frac{1}{2}}$$

This error represents approximately a 1σ confidence interval, i.e. the tally is correct to within $\pm R$ about 68% of the time or to within $\pm 2R$ about 95% of the time.

5 Results

The power load on the first wall is largest, 1.37 MW/m^2, at the mid-outboard region and least, 0.67 MW/m^2, at the divertors, Table 5. The overall mean is 1.03 MW/m^2, with a 0.2% error. The second set of values refer to the power load from the virgin neutrons. This calculation has been done in a separate fast MCNP run with all materials removed and exact surface area values. The remaining $\approx 20\%$ of the power load comes from back-scattering. The virgin power load poloidal distribution is shown in Fig. 12.

The total net neutron power crossing the first wall is 574.4 MW. This is close, $\approx 0.6\%$, to the total power of the virgin neutrons in the plasma of 571.2 MW. This provides a check of the input, the more so if one remembers that areas and volumes have themselves been computed stochastically and may have errors up to $\approx 1-4\%$.

The overall spectrum of neutron induced photons is shown in Fig. 13. The average photon energy is 2.4 MeV, which represents indirect evidence that most of the gamma radiation is created in a capture process that leads to high energy photons. The low energy part of the photon spectrum comes from inelastic scattering. The code produces very detailed statistics of the neutron and photon activity with respect to each nuclide. The effect of material composition on the photon production and absorption is illustrated by Fig. 14, where neutron induced weight creation and weight absorption are given for a few significant nuclides. It should be noted that neutrons are captured preferentially

---

[3]Segments 1 and 2 have been tallied together.

[4]This quantity is called the *relative* error in the MCNP terminology.

Location	All neutrons		Virgin Neutrons	
	Power Load (MW/m^2)	Error (%)	Power Load (MW/m^2)	Error (%)
Mid-outboard	1.37	0.3	1.16	0.1
Top and bottom outboard	0.79	0.7	0.63	0.3
Top divertor	0.68	1.8	0.51	0.8
Bottom divertor	0.67	1.8	0.51	0.8
Mid-inboard	0.80	0.7	0.63	0.3
Total average	1.03	0.2	0.845	0.0

Table 5: Power Load on the First Wall

in iron, whereas gammas are best absorbed in chromium. This could be of importance when defining the composition of the steel.

The outboard power release distributions for wedge segments are given in Tables 8 to 12 and for parallel segmei .s in Tables 13 to 18. Some of these results are also illustrated in Figs. 15 to 20. The outgoing particle currents on the outboard are given in Tables 19 to 21, as well as in Figs. 21 to 23. The poloidal distributions of the neutron and photon total currents are given in Figs. 24 and 25, respe. .vely. On the inboard side, the power release distributions for wedge segments are given in Tables 22 to 27 and for parallel segments in Tables 28 to 33. They are also plotted in Figs. 26 to 37. The outgoing particle currents on the inboard are given in Tables 34 and 35 at mid-section and in Table 21 at top and bottom as well as in Figs. 38 to 40. The poloidal distributions of the neutron and photon total currents are given in Figs. 41 and 42, respectively. The power release distribution is given in Tables 36 and 37, for the outboard and inboard parts of the blanket, respectively, and Table 38 for the two divertors. The poloidal distribution of the power release on the inner side of the blanket is given in Figs. 43 and 44, for the outboard and inboard respectively.

Auxilliary programs analyze both the input and the output of the code and compute neutron, photon, and total power generation in metal and water for all segments. The total power released in the blanket, in the inboard, and in the outboard vacuum vessel is given in Tables 39 to 41, respectively, and the totals summarized in Table 42. The overall total, 811 MW, is considerably more than the energy of the virgin neutrons at birth. It corresponds to 20.0 MeV per source neutron, a gain of 5.9 MeV in the blanket alone. This unusually high value is due to the fact that the principal neutron capture material is stainless steel - iron, chromium, and nickel - all with a neutron binding energy around 7 MeV, instead of the more usual lithium with only 4.8 MeV present in blankets constrained to breed tritium.[2,3] Furthermore, the energy multiplication is significantly enhanced by a strong contribution from (n,xn) reactions, particularly in iron, molybdenum, chromium, nickel, and manganese. These reactions create $\approx$12%

extra neutron weight with an average energy loss of ≈ 0.27 MeV. In other words, the neutron energy spectrum is shifted down and as a result the rate of exothermic capture increases. This is to be compared with $\approx 12\%$, also, from the ^7Li $(n, n'\alpha)$ T reaction[4] with an average energy loss of ≈ 0.3 MeV, if a tritium breeding blanket is used in a Reversed Field Pinch Reactor.

6 Discussion

6.1 Heat Generation

Heat Deposition	Major >1% (%)	Small <1-2% (%)
Vessel		
– outboard	3 – 5	≤ 10
– except:-		
· segment 12	4 – 7	18
– inboard	5 – 8	≤ 10
– except:-		
· segments 13, 14, 23, 24	≤ 20	e.g. 57
Blanket		
– outboard	2 – 4	–
– inboard, mid-section	4 – 7	–
– divertors	5 – 6	≤ 18

Table 6: Statistical Errors in Heat Generation

Neutron and Photon Currents	Total Neutrons & Neutrons 0.11 < E < 1.0 MeV (%)	Minor Partial Neutron Currents (%)	Total Photons (%)
– outboard	≤ 8	≤ 15	≤ 11
– except:-			
· bottom	22	unreliable	27
– inboard			
– parallel	≤ 8	≤ 19	≤ 10
– wedge	14	≤ 51	≤ 32
– except:-			
· top & bottom	≤ 29	unreliable	≤ 32

Table 7: Statistical Errors in Currents

If we consider the heat generation in the segments of the vessel or blanket, we must distinguish between those layers where a major portion of the heat is generated and those where the heat generation is small, less than 1 - 2% of the peak power release density in that segment. Whereas the statistical error, Table 6, is generally acceptable, less than $\approx 8\%$, in the major layers:

14

- vessel outboard, (Nos. 1 - 12), typically **3 - 5%**,

- vessel inboard, mid-section, (Nos. 15 -22), **5 - 8%**,

- blanket outboard, (Nos. 1 - 12), typically **2 - 4%**,

- blanket inboard,mid-section, (Nos. 15 - 22), **4 - 7%**,

there are notable exceptions:

- generally, the outermost two layers of the vessel, $\leq 10\%$, (small deposition)

- the outer layer of the divertor, which has a heat deposition at least an order of magnitude smaller than the inner layer, so that the total for both layers stays acceptable: $\leq 18\%$

- segment 12 of the vessel, which is nearest the duct, where small contributions have errors up to 18%,

- top and bottom segments of the vessel on the inboard side, (Nos. 13, 14, 23, and 24) which are adjacent to divertors. Statistical errors range up to 20% in some major contributions, $\geq 1\%$, and even higher, up to 57%, for contributions which are small.

6.2 Neutron and Photon Currents

Again, if we consider the statistical errors in the neutron and photon currents escaping from the vessel, Table 7, we must distinguish between:

- the total neutron current and the partial current carrying the main contribution, for $0.11 < E < 1.0$ MeV, on the one hand, with statistical errors $\leq 8\%$,

- all the other partial currents carrying relatively smaller currents, on the other hand, with statistical errors $\leq 15.0\%$,

- and the photon total current, for which the error is larger, $\approx 11\%$.

There are, however, notable exceptions:

- for the top and bottom segments, wedge and parallel segments have been tallied together, Table 21, to improve the statistics. Nevertheless, except for the outboard top segment, the statistical errors on the total currents are large, for the same reasons as for the heat deposition.

  - segment 12: proximity of the duct, $\leq 27\%$

  - segments 13, 14, 23, and 24: behind the divertors, $\leq 32\%$.

Partial currents are totally unreliable.

- the currents on the wedge on the inboard side are very unreliable, reaching 51% for partial neutron currents and 32% for the photon currents, but the wedge sector is relatively very narrow at this point and makes but little contribution to the total inboard leakage, even if the actual wedge neutron current is more than double the parallel one. As was noted above this is partly due to the large radial dimension (35.5 cm) of the wedge. This could be helped by zone splitting.

6.3   General Comments

A couple of reasons can be attributed to the special behaviour of the top and bottom inboard segments:

- First, the four segments

  - are behind the divertors, and as these are massive (in fact too massive compared to the present designs), the vessel is exposed to far fewer neutrons as elsewhere, (fewer events),

  - the divertors seem to be less exposed to the neutron source (viz. Table 5),

  - and produce less energetic photons due to a high Mo content (1.9 MeV vs. 2.4 MeV for Fe), so the statistics are based on fewer e ents.

- Second, the weight windows for the inboard side are not so well tuned as they are synthetically constructed from adjacent outboard and mid-inboard values.

As a result of the fewer particles, however, the power release in these four segments is, generally smaller than in the other segments by nearly an order of magnitude and, thus, this should not invalidate global conclusions, but give a stimulus instead to devoting more effort towards more accurate space, energy, and weight window modelling of this region in future analyses. Moreover, the divertors geometry is very simplified in the present case, thus more exact calculations in those regions should wait till the divertors can be modelled in more detail. The same remarks apply to the neutron and photon currents as well. The calculations can no longer be called reliable for these four, top and bottom, inboard segments, nor can the accuracy be significantly improved in view of the large computer time already expended. The poloidal variations on the inboard side are, however, much less than outboards - for one, the duct is absent - so that these regions can be modelled in 2-D, or even 1-D, toroidal symmetry and deterministic codes can be used with advantage.

One inherent approximation is to be mentioned here: the reflective planes which delimit the 11.25° sector under consideration act only at its poloidal cross-section. In other words, the inner space of the torus is assumed black, i.e. there is no radiation returning from other sectors. This approximation applies, of course, only to the inboard results.

7 Conclusions

A good geometrical model has been set up and good material compositions used, except in the area of the duct, where this was not required, and for the divertors, which were still at an early stage of design. The source description can be considered without errors.

Looking at the statistical errors shows that, in general, there is good statistical accuracy in the calculation of the heat generated especially in the **outboard** of the vacuum vessel and in the blanket. It is also a proof that the game strategy or the weight window selection can be considered as satisfactory. An improvement on the weight window selection on the inboard of the vessel could perhaps bring some slight improvement there still. In general, the currents are less satisfactory, but this pertains to a results further from the plasma than for the heat deposition and this is to be expected.

The best possible results have been obtained allowing for the considerable computing time already required. Good results have been obtained for all significant quantities. Mediocre or unreliable results are found only where their contributions to the total is small and where they thus do not invalidate global conclusions.

A novel result has been obtained. In stainless steel, neutrons are captured preferentially in iron, whereas gammas are best absorbed in chromium. This could be of importance when defining the composition of the steel.

Two recommendations can be put forward for further calculations. On the inboard, in the region of the divertors, the calculations can no longer be called reliable, nor can the accuracy be significantly improved in view of the large computer time already expended. The poloidal variations on the inboard side are, however, much less than outboards - for one, the duct is absent - so that these regions can be modelled in 2-D toroidal symmetry, or even 1-D, and deterministic codes can be used with advantage. The source can either be simulated in 2-D, using the same input as now, or surface currents can be obtained from MCNP and used as a boundary condition. Second, as far as the ducts are concerned, currents in the vessel can be tallied and used as boundary conditions for a detailed calculation, 'bootstrap method'. The same applies to the superconducting coils, where the currents already obtained can be used as a boundary condition.

Even if the present calculations do not furnish exact results for all the heat deposition rates in the vessel and blanket and for all the detailed currents escaping from the vessel, they do give a good global picture of these quantities and their poloidal and toroidal variation. It was these variations which had to be determined as these cannot be obtained from simple 1-D computations.

References

[1] MCNP - A General Monte Carlo Code for Neutron and Photon Transport - Version

17

3A, LA-7396-M, Rev. 2 (1986)

[2] C. G. Bathke, D. J. Dudziak, R. A. Krakowski, et al.. "ELMO Bumpy Torus Reactor and Power Plant," LA-8882-MS.

[3] D C. Quimby and G. L. Woodruff, "A Consistent Comparison of Neutron Multipliers for Fusion Blanket," Trans. Amer. Nucl. Soc. 28, 38 (1978).

[4] A. A. Hollis and J. T. D. Mitchell "Reversed Field Pinch Reactor Study," III. Preliminary Engineering Design. CLM-R 173.

Material	d (cm)	Volume (cm^3)	Power Release Density (W/cm^3) with Statistical Error (%)					
			Neutrons		Photons		Neutrons & Photons	
M11	6.0	1.15+5	6.72–2	3.5	5.79–1	4.0	6.47–1	3.7
M6	7.5	2.97+4	1.34–1	3.7	4.87–1	5.1	1.83–1	3.4
M12	25.5	3.65+5	1.45–2	3.9	1.34–1	3.5	1.49–1	3.4
M6	31.0	1.19+5	9.23–3	5.3	6.96–3	4.7	1.62–2	4.5
M10	49.0	4.05+5	1.27–3	4.6	1.36–2	4.2	1.49–2	4.2
M8	52.0	7.60+4	1.78–3	7.1	2.25–4	7.8	2.00–3	6.9
M10	61.3	2.26+5	5.53–5	9.3	7.30–4	7.3	7.85–4	7.3

Table 8: Heat Generation - Vessel Outboard - Segment 1

Material	d (cm)	Volume (cm³)	Power Release Density (W/cm³) with Statistical Error (%)					
			Neutrons		Photons		Neutrons & Photons	
M11	6.0	9.23+4	9.36–2	4.3	6.91–1	3.8	7.81–1	3.5
M6	7.5	2.34+4	1.85–1	3.4	6.47–2	5.0	2.53–1	3.2
M12	25.5	2.89+5	2.03–2	3.7	1.77–1	3.2	1.97–1	3.1
M6	31.0	9.27+4	1.12–2	5.2	9.85–3	4.5	2.10–2	4.3
M10	49.0	3.31+5	1.82–3	4.5	1.95–2	3.9	2.13–2	3.9
M8	52.0	6.06+4	2.19–3	6.0	3.00–4	6.2	2.50–3	5.9
M10	57.5	1.05+5	1.07–4	7.6	1.33–3	6.0	1.44–3	5.9

Table 9: Heat Generation - Vessel Outboard - Segment 3

Material	d (cm)	Volume (cm³)	Power Release Density (W/cm³) with Statistical Error (%)					
			Neutrons		Photons		Neutrons & Photons	
M11	6.0	1.12+5	1.37–1	2.2	1.04–0	2.4	1.18–0	2.2
M6	7.5	2.93+4	2.69–1	2.3	9.33–2	3.3	3.62–1	2.2
M12	25.5	3.52+5	3.08–2	2.5	2.52–1	2.2	2.84–1	2.2
M6	31.0	1.07+5	1.70–2	3.2	1.41–2	3.0	3.11–2	2.8
M10	49.0	3.67+5	2.67–3	2.9	2.87–2	2.7	3.14–2	2.7
M8	52.0	6.11+4	3.37–3	4.0	4.22–4	4.9	3.79–3	4.0
M10	57.5	1.12+5	1.87–3	5.7	2.07–3	4.6	2.25–3	4.5

Table 10: Heat Generation - Vessel Outboard - Segment 5

Material	d (cm)	Volume (cm³)	Power Release Density (W/cm³) with Statistical Error (%)					
			Neutrons		Photons		Neutrons & Photons	
M11	6.0	1.15+5	1.37–1	2.2	1.01–0	2.3	1.14–0	2.1
M6	7.5	2.88+4	2.65–1	2.3	9.07–2	3.0	3.55–1	2.1
M12	25.5	3.50+5	2.98–2	2.5	2.42–1	2.2	2.72–1	2.1
M6	31.0	1.08+5	1.65–2	3.3	1.41–2	3.0	3.06–2	2.8
M10	49.0	3.63+5	2.65–3	3.0	2.75–2	2.7	3.02–2	2.7
M8	52.0	6.14+4	3.44–3	4.0	4.48–4	5.1	3.89–3	4.0
M10	57.5	1.07+5	1.81–4	5.4	2.02–3	4.6	2.20–3	4.5

Table 11: Heat Generation - Vessel Outboard - Segment 7

Material	d (cm)	Volume (cm³)	Power Release Density (W/cm³) with Statistical Error (%)					
			Neutrons		Photons		Neutrons & Photons	
M11	6.0	9.68+4	8.82–2	3.3	6.91–1	3.0	7.81–1	2.9
M6	7.5	2.45+4	1.76–1	3.4	6.40–2	3.9	2.40–1	3.1
M12	25.5	3.00+5	2.03–2	3.7	1.76–1	3.0	1.96–1	3.0
M6	31.0	9.78+4	1.21–2	4.8	1.07–2	4.4	2.29–2	4.1
M10	49.0	3.25+5	1.87–3	4.3	2.07–2	3.8	2.25–2	3.8
M8	52.0	6.08+4	2.45–3	5.7	3.11–4	7.4	2.76–3	5.6
M10	57.5	1.02+5	1.32–4	7.7	1.48–3	8.0	1.61–3	7.7

Table 12: Heat Generation - Vessel Outboard - Segment 9

Material	d (cm)	Volume (cm³)	Power Release Density (W/cm³) with Statistical Error (%) Neutrons		Photons		Neutrons & Photons	
M4	4.0	5.06+4	8.91-2	4.0	5.41-1	4.2	6.30-1	3.9
M5	11.0	9.17+4	3.95-2	4.6	2.79-1	4.3	3.19-1	4.0
M6	12.5	2.05+4	6.91-2	4.8	2.73-2	5.2	9.64-2	4.4
M7	23.5	1.57+5	1.06-2	4.9	9.29-2	4.2	1.04-1	4.2
M8	30.0	9.03+4	2.37-2	5.0	3.58-3	5.1	2.72-2	4.8
M9	50.0	3.70+5	3.79-4	8.0	4.53-3	5.3	4.90-3	5.3

Table 13: Heat Generation - Vessel Outboard - Segment 2

Material	d (cm)	Volume (cm³)	Power Release Density (W/cm³) with Statistical Error (%) Neutrons		Photons		Neutrons & Photons	
M4	4.0	2.90+4	1.18-1	4.4	6.88-1	4.1	8.06-1	3.8
M5	11.0	5.07+4	5.66-2	4.9	3.81-1	3.9	4.01-1	3.9
M6	12.5	1.15+4	9.63-2	5.0	3.75-2	4.6	1.34-1	4.5
M7	23.5	8.64+4	1.54-2	5.1	1.30-1	4.1	1.45-1	4.1
M8	30.0	5.32+4	3.16-2	5.2	4.73-3	4.9	3.64-2	5.0
M9	50.0	1.72+5	7.64-4	8.7	8.18-3	5.2	8.96-3	5.4

Table 14: Heat Generation - Vessel Outboard - Segment 4

Material	d (cm)	Volume (cm³)	Power Release Density (W/cm³) with Statistical Error (%) Neutrons		Photons		Neutrons & Photons	
M4	4.0	3.19+4	1.81-1	3.1	9.77-1	3.3	1.16-0	3.1
M5	11.0	5.58+4	8.18-2	3.4	5.32-1	3.1	6.14-1	3.0
M6	12.5	1.20+4	1.33-1	3.6	5.08-2	4.0	1.84-1	3.3
M7	23.5	9.00+4	2.37-2	3.8	1.89-1	3.2	2.13-1	3.1
M8	30.0	5.31+4	4.95-2	3.9	7.75-3	4.2	5.72-2	3.8
M9	50.0	1.67+5	1.08-3	7.0	1.18-2	4.2	1.29-2	4.3

Table 15: Heat Generation - Vessel Outboard - Segment 6

Material	d (cm)	Volume (cm^3)	Power Release Density (W/cm^3) with Statistical Error (%)					
			Neutrons		Photons		Neutrons & Photons	
M4	4.0	3.17+4	1.75–1	3.1	9.98–1	3.3	1.17–0	3.1
M5	11.0	5.79+4	7.81–2	3.4	5.20–1	3.3	5.98–1	3.2
M6	12.5	1.26+4	1.33–1	3.6	5.29–2	4.1	1.86–1	3.3
M7	23.5	8.92+4	2.09–2	3.8	1.84–1	3.3	2.05–1	3.2
M8	30.0	5.35+4	4.61–2	3.8	7.20–3	4.2	5.32–2	3.7
M9	50.0	1.61+5	8.57–4	6.3	1.04–2	4.2	1.13-2	4.3

Table 16: Heat Generation - Vessel Outboard - Segment 8

Material	d (cm)	Volume (cm^3)	Power Release Density (W/cm^3) with Statistical Error (%)					
			Neutrons		Photons		Neutrons & Photons	
M4	4.0	3.13+4	1.26–1	4.2	7.56–1	4.1	8.77–1	3.9
M5	11.0	5.54+4	5.67–2	4.8	3.94–1	3.8	4.51–1	3.7
M6	12.5	1.18+4	1.01–1	5.1	3.44–2	4.6	1.35–1	4.6
M7	23.5	8.53+4	1.72–2	5.2	1.37–1	4.0	1.54–1	4.1
M8	30.0	5.22+4	3.55–2	5.3	5.81–3	5.0	4.13–2	5.1
M9	50.0	1.61+5	7.62–4	9.3	8.80–3	6.4	9.58–3	5.5

Table 17: Heat Generation - Vessel Outboard - Segment 10

Material	d (cm)	Volume (cm^3)	Power Release Density (W/cm^3) with Statistical Error (%)					
			Neutrons		Photons		Neutrons & Photons	
M4	4.0	5.26+4	1.34–1	4.1	8.34–1	3.6	9.70–1	3.4
M5	11.0	9.38+4	6.27–2	4.5	4.35–1	3.5	4.98–1	3.4
M6	12.5	1.99+4	1.21–1	6.8	4.13–2	4.4	1.62–1	5.7
M7	23.5	1.50+5	1.91–2	6.1	1.45–1	3.8	1.64–1	3.9
M8	30.0	9.18+4	4.76–2	6.4	8.22–3	6.4	5.58–2	6.1
M9	50.0	3.63+5	1.35–3	18	1.22–2	8.4	1.36–2	9.1

Table 18: Heat Generation - Vessel Outboard - Segment 12

Neutrons E_u (MeV)	Current ($cm^{-2}sec^{-1}$) with Statistical Error (%)							
	Segment 3		Segment 5		Segment 7		Segment 9	
4.14–7	1.16+8	10.5	2.01+8	9.9	2.04+8	9.3	1.40+8	12.1
1.01–4	8.75+8	7.4	1.28+9	6.0	1.54+9	5.3	8.93+8	7.2
9.12–3	7.87+8	7.6	1.22+9	6.1	1.46+9	5.5	9.51+8	7.4
0.11	9.58+8	7.8	1.80+9	5.7	1.88+9	5.7	1.23+9	7.4
1.0	2.87+9	7.4	4.97+9	5.2	5.00+9	5.1	3.14+9	7.0
14.9	1.14+9	11.9	2.01+9	8.5	2.12+9	8.4	1.35+9	11.6
Total	6.74+9	6.5	1.15+10	4.5	1.22+10	4.4	7.70+9	6.2
Photons	4.63+9	6.3	7.25+9	4.9	7.49+9	4.9	4.95+9	10.2
Area (cm^2)	2.02+4		2.08+4		1.97+4		2.00+4	

Table 19: Neutron and Photon Current - Outboard Wedge Midsection

Neutrons E_u (MeV)	Current ($cm^{-2}sec^{-1}$) with Statistical Error (%)							
	Segment 4		Segment 6		Segment 8		Segment 10	
4.14–7	<1.00+8		<1.00+8		<1.00+7		<1.00+7	
1.01–4	7.49+8	15.0	1.04+9	11.8	8.36+8	12.6	7.72+8	13.7
9.12–3	1.25+9	12.2	1.75+9	9.6	1.36+9	10.5	1.18+9	12.7
0.11	4.10+9	8.9	4.90+9	7.5	5.04+9	7.6	3.89+9	9.2
1.0	1.39+10	8.0	1.80+10	6.4	1.62+10	6.4	1.34+10	8.4
14.9	4.30+9	11.5	5.56+9	9.7	4.35+9	9.6	3.61+9	13.6
Total	2.43+10	7.6	3.13+10	6.0	2.78+10	5.9	2.29+10	7.9
Photons	5.74+9	11.2	8.58+9	9.1	6.38+9	9.4	6.20+9	11.2
Area (cm^2)	8.43+3		7.96+3		8.03+3		8.44+3	

Table 20: Neutron and Photon Current - Outboard Parallel Midsection

Neutrons E_u (MeV)	Current ($cm^{-2}sec^{-1}$) with Statistical Error (%)							
	Segment 1&2		Segment 12		Segment 13&14		Segment 23&24	
4.14–7	2.44+7	24.3			–			
1.01–4	2.93+8	12.0	unreliable		2.6+7	29	unreliable	
9.12–3	4.37+8	11.0			3.0+7	27		
0.11	1.16+9	9.2	data		8.1+7	30	data	
1.0	3.65+9	69			1.5+8	24		
14.9	9.29+8	11.1			4.3+7	45		
Total	6.49+9	6.0	7.40+10	22.0	3.32+8	23	3.76+9	29
Photons	1.92+9	7.7	6.39+10	27.0	1.23+8	25	7.07+8	32
Area (cm^2)	4.22+4		2.02+4		2.0+4		2.0+4	

Note:- Inboard top and bottom segments should have nearly equal currents, whereas the values calculated are ca. a factor ten different. This shows the unreliability of these values.

Table 21: Neutron and Photon Current - Outboard and Inboard Top and Bottom Segments

Material	d (cm)	Volume (cm^3)	Power Release Density (W/cm^3) with Statistical Error (%)					
			Neutrons		Photons		Neutrons & Photons	
M4	7.0	3.91+4	5.02–3	16	4.71–2	13	5.22–2	13
M5	15.0	4.71+4	1.55–3	17	1.47–2	14	1.63–2	13
M6	17.0	1.23+4	2.26–3	18	1.66–3	20	3.91–3	16
M13	31.0	8.45+4	3.95–4	15	4.08–3	14	4.47–3	13
void	32.5	8.50+3	–	–	–	–	–	–
M10	66.5	2.01+5	2.01–5	27	2.37–4	21	2.57–4	22

Table 22: Heat Generation - Vessel Inboard - Segment 13

Material	d (cm)	Volume (cm^3)	Power Release Density (W/cm^3) with Statistical Error (%)					
			Neutrons		Photons		Neutrons & Photons	
M4	7.0	2.16+4	5.43–2	5.6	4.36–1	5.9	4.90–1	5.5
M5	15.0	2.36+4	2.13–2	6.9	1.74–1	6.2	1.95–1	5.9
M6	17.0	5.40+3	3.39–2	7.7	1.68–2	7.7	5.06–2	6.6
M13	31.0	3.50+4	5.60–3	7.2	5.82–2	6.1	5.84–2	6.0
void	32.5	2.99+3	–	–	–	–	–	–
M10	68.0	5.30+4	3.18–4	9.5	3.53–3	7.7	3.84–3	7.6

Table 23: Heat Generation - Vessel Inboard - Segment 15

Material	d (cm)	Volume (cm^3)	Power Release Density (W/cm^3) with Statistical Error (%)					
			Neutrons		Photons		Neutrons & Photons	
M4	7.0	2.09+4	1.59–1	3.9	9.05–1	4.2	1.06–0	3.8
M5	15.0	2.24+4	5.97–2	4.4	4.19–1	4.3	4.79–1	4.1
M6	17.0	5.26+3	8.16–2	4.8	4.17–2	5.0	1.23–1	4.2
M13	31.0	3.28+4	1.45–2	4.6	1.36–1	4.1	1.50–1	4.0
void	32.5	3.26+3	–	–	–	–	–	–
M10	68.0	5.29+4	9.59–4	6.2	8.74–3	4.9	9.75–3	4.9

Table 24: Heat Generation - Vessel Inboard - Segment 17

Material	d (cm)	Volume (cm³)	Power Release Density (W/cm³) with Statistical Error (%)					
			Neutrons		Photons		Neutrons & Photons	
M4	7.0	2.36+4	1.64–1	3.9	8.91–1	4.2	1.06–0	3.8
M5	15.0	2.41+4	6.12–2	4.3	4.29–1	4.2	4.90–1	4.0
M6	17.0	5.43+3	8.93–2	4.9	3.82–2	4.7	1.28–1	4.3
M13	31.0	3.30+4	1.45–2	4.8	1.27–1	3.9	1.41–1	3.9
void	32.5	3.39+3	–	–	–	–	–	–
M10	68.0	5.31+4	9.44–4	6.7	8.50–3	4.7	9.44–3	4.7

Table 25: Heat Generation - Vessel Inboard - Segment 19

Material	d (cm)	Volume (cm³)	Power Release Density (W/cm³) with Statistical Error (%)					
			Neutrons		Photons		Neutrons & Photons	
M4	7.0	2.31+4	7.77–2	5.3	5.08–1	5.6	5.85–1	5.2
M5	15.0	2.45+4	2.63–2	6.3	2.12–1	5.8	2.39–1	5.6
M6	17.0	5.53+3	3.52–2	7.1	1.86–2	7.8	5.38–2	6.3
M13	31.0	3.44+4	5.92–3	6.8	5.43–2	5.5	6.03–2	5.4
void	32.5	2.84+3	–	–	–	–	–	–
M10	68.0	5.02+4	3.92–4	9.1	3.78–3	6.9	4.17–3	6.9

Table 26: Heat Generation - Vessel Inboard - Segment 21

Material	d (cm)	Volume (cm³)	Power Release Density (W/cm³) with Statistical Error (%)					
			Neutrons		Photons		Neutrons & Photons	
M4	7.0	4.08+4	2.13–2	11	1.54–1	7.9	1.75–1	7.7
M5	15.0	4.75+4	1.09–2	13	7.37–2	8.7	8.48–1	8.8
M6	17.0	1.20+4	1.98–2	16	8.97–3	12	2.88–2	13
M13	31.0	8.47+4	3.59–3	18	2.86–2	11	3.22–2	11
void	32.5	8.89+3	–	–	–	–	–	–
M10	66.5	2.06+5	3.91–4	57	2.45–3	27	2.84–3	31

Table 27: Heat Generation - Vessel Inboard - Segment 23

Material	d (cm)	Volume (cm^3)	Power Release Density (W/cm^3) with Statistical Error (%)					
			Neutrons		Photons		Neutrons & Photons	
M4	4.0	3.85+4	5.97–3	11	5.02–2	10	5.61–2	10
M5	11.0	6.76+4	2.77–3	13	2.33–2	10	2.61–2	10
M6	12.5	1.51+4	3.99–3	13	2.59–3	15	6.58–3	12
M7	23.5	1.19+5	8.14–4	14	8.91–3	12	9.75–3	11
M8	29.0	6.48+4	1.90–3	15	3.01–4	14	2.20–3	14
M9	48.0	2.34+5	5.38–5	24	5.76–4	14	6.30–4	14
M8	53.0	6.55+4	9.72–5	22	1.10-5	30	1.08–4	23
M10	61.25	1.11+5	2.99–6	30	3.82–5	28	4.13–5	28

Table 28: Heat Generation - Vessel Inboard - Segment 14

Material	d (cm)	Volume (cm^3)	Power Release Density (W/cm^3) with Statistical Error (%)					
			Neutrons		Photons		Neutrons & Photons	
M4	4.0	3.25+4	7.77–2	3.7	5.55–1	3.8	6.46–1	3.5
M5	11.0	5.68+4	3.41–2	4.1	2.78–1	3.6	3.13–1	3.5
M6	12.5	1.23+4	6.01–2	4.7	2.63–2	4.3	8.64–2	4.1
M7	23.5	9.23+4	9.29–3	4.4	8.75–2	3.7	9.68–2	3.7
M8	28.0	3.73+4	2.64–2	4.6	3.63–3	4.6	3.01–2	4.4
M9	48.0	1.64+5	5.86–4	6.7	6.95–3	4.6	7.54–3	4.7
M8	53.0	4.38+4	1.66–3	6.2	1.77–4	7.2	1.84–3	6.1
M10	65.0	9.91+4	3.86–5	8.2	5.05–4	6.9	5.44–4	6.8

Table 29: Heat Generation - Vessel Inboard - Segment 16

Material	d (cm)	Volume (cm^3)	Power Release Density (W/cm^3) with Statistical Error (%)					
			Neutrons		Photons		Neutrons & Photons	
M4	4.0	3.21+4	1.75–1	2.7	1.06–0	2.8	1.23–0	2.6
M5	11.0	5.55+4	7.96–2	2.9	5.53–1	2.6	6.33–1	2.6
M6	12.5	1.21+4	1.37–1	3.2	5.29–2	3.2	1.90–1	2.9
M7	23.5	9.28+4	2.30–2	3.2	1.93–1	2.7	2.16–1	2.6
M8	28.0	3.73+4	5.76–2	3.3	8.21–3	3.3	6.58–2	3.2
M9	48.0	1.64+5	1.57–3	4.8	1.67–2	3.2	1.82–2	3.2
M8	53.0	3.96+4	4.04–3	4.0	4.90–4	4.9	4.53–3	3.9
M10	65.0	9.62+4	1.03–4	5.4	1.29–3	4.6	1.39–3	4.5

Table 30: Heat Generation - Vessel Inboard - Segment 18

Material	d (cm)	Volume (cm^3)	Power Release Density (W/cm^3) with Statistical Error (%)					
			Neutrons		Photons		Neutrons & Photons	
M4	4.0	3.09+4	1.89–1	2.6	1.04–0	2.7	1.23–0	2.5
M5	11.0	5.37+4	8.48–2	2.8	5.64–1	2.5	6.48–1	2.4
M6	12.5	1.13+4	1.54–1	3.0	5.63–2	3.1	2.10–1	2.7
M7	23.5	8.78+4	2.60–2	3.1	2.10–1	2.6	2.37–1	2.6
M8	28.0	3.63+4	6.78–2	3.1	9.46–3	3.2	7.73–2	3.0
M9	48.0	1.62+5	1.75–3	4.6	1.83–2	3.1	2.01–2	3.2
M8	53.0	4.01+4	4.58–3	4.0	5.09–4	4.8	5.09–3	4.0
M10	65.0	9.43+4	1.05–4	5.6	1.29–3	4.6	1.40–3	4.6

Table 31: Heat Generation - Vessel Inboard - Segment 20

Material	d (cm)	Volume (cm³)	Power Release Density (W/cm³) with Statistical Error (%)					
			Neutrons		Photons		Neutrons & Photons	
M4	4.0	3.23+4	7.77–2	3.9	5.28–1	3.9	6.05–1	3.6
M5	11.0	5.58+4	3.46–2	4.2	2.81–1	3.6	3.16–1	3.5
M6	12.5	1.19+4	5.89–2	4.6	2.53–2	4.4	8.41–2	4.0
M7	23.5	8.62+4	9.83–3	4.6	9.37–2	3.8	1.04–1	3.8
M8	28.0	3.51+4	2.68–2	4.6	3.96–3	4.9	3.08–2	4.4
M9	48.0	1.57+5	6.12–4	6.6	7.61–3	4.5	8.26–3	4.5
M8	53.0	4.06+4	1.59–3	5.8	1.98–4	6.9	1.79–3	5.8
M10	65.0	9.57+4	3.71–5	7.4	5.55–4	6.7	5.92–4	6.6

Table 32: Heat Generation - Vessel Inboard - Segment 22

Material	d (cm)	Volume (cm³)	Power Release Density (W/cm³) with Statistical Error (%)					
			Neutrons		Photons		Neutrons & Photons	
M4	4.0	3.89+4	9.55–3	12	8.63–2	8.9	9.55–2	8.6
M5	11.0	6.92+4	4.90–3	14	4.14–2	8.4	4.62–2	8.6
M6	12.5	1.52+4	8.59–3	17	4.05–3	10	1.26–2	13
M7	23.5	1.18+5	1.57–3	17	1.40–2	10	1.56–2	11
M8	29.0	6.32+4	3.13–3	14	6.67–4	19	3.80–3	13
M9	48.0	2.30+5	7.56–5	19	9.89–4	12	1.07–3	12
M8	53.0	6.32+4	2.06–4	15	3.12–5	16	2.32–4	14
M10	61.25	1.12+5	4.61–6	16	8.34–5	15	8.81–5	15

Ta... 33: Heat Generation - Vessel Inboard - Segment 24

Neutrons E_u (MeV)	Current (cm^{-2}sec^{-1}) with Statistical Error (%)							
	Segment 15		Segment 17		Segment 19		Segment 21	
4.14–7	0	0	0	0	<1.00+8		0	0
1.01–4	4.11+8	26	1.04+9	18	6.72+8	19	1.77+8	32
9.12–3	5.33+8	23	1.11+9	17	1.32+9	16	3.19+8	26
0.11	2.46+9	15	5.33+9	9.0	5.37+9	8.7	2.09+9	14
1.0	4.56+9	12	1.02+10	8.1	1.04+10	9.5	3.16+9	14
14.9	1.70+8	51	6.13+8	26	7.13+8	36	1.52+8	38
Total	8.14+9	9.9	1.83+10	6.5	1.85+10	7.3	5.90+9	10.6
Photons	4.93+8	32	2.63+9	17	3.02+9	16	1.09+9	25
Area (cm^2)	7.66+2		8.02+2		8.58+2		1.03+3	

Table 34: Neutron and Photon Current - Inboard Wedge Midsection

Neutrons E_u (MeV)	Current (cm^{-2}sec^{-1}) with Statistical Error (%)							
	Segment 16		Segment 18		Segment 20		Segment 22	
4.14–7	<1.00+7		<1.00+7		≈1.00+7		<1.00+7	
1.01–4	1.48+8	14.6	3.67+8	9.4	4.35+8	8.4	1.84+8	13.1
9.12–3	2.90+8	13.5	4.96+8	8.3	6.27+8	7.6	2.29+8	12.4
0.11	4.76+8	10.4	1.10+9	6.3	1.34+9	6.2	5.70+8	9.6
1.0	1.30+9	8.0	3.03+9	5.3	3.51+9	5.5	1.25+9	8.4
14.9	2.20+8	19.2	6.39+8	10.6	5.91+8	10.9	2.01+8	15.5
Total	2.34+9	7.3	5.64+9	4.7	6.52+9	4.8	2.44+9	7.1
Photons	8.00+8	10.2	2.05+9	7.1	1.81+9	7.1	8.72+8	10.2
Area (cm^2)	7.99+3		8.20+3		8.08+3		7.91+3	

Table 35: Neutron and Photon Current - Inboard Parallel Midsection

Material	d (cm)	Volume (cm³)	Power Release Density (W/cm³) with Statistical Error (%)					
			Neutrons		Photons		Neutrons & Photons	
Segment 1&2								
M1	2.0	4.90+4	2.31–0	3.5	1.26–0	3.6	3.57–0	2.9
M2	5.0	7.77+4	2.53–0	3.3	5.17–0	2.9	7.70–0	2.7
void	12.7	2.06+5	–	–	–	–	–	–
M2	32.3	5.53+5	7.38–1	3.6	2.20–0	3.0	2.94–0	3.0
void	40.0	2.36+5	–	–	–	–	–	–
Segment 3&4								
M1	2.0	4.05+4	3.08–0	3.6	1.38–0	3.6	4.46–0	3.1
M2	5.0	6.08+4	3.23–0	3.4	5.91–0	3.0	9.14–0	2.9
void	12.7	1.55+5	–	–	–	–	–	–
M2	32.3	4.24+5	9.67–1	3.7	2.88–0	3.1	3.85–0	3.2
void	40.0	1.72+5	–	–	–	–	–	–
Segment 5&6								
M1	2.0	5.25+4	4.21–0	2.5	1.72–0	3.3	5.93–0	2.3
M2	5.0	7.77+4	4.54–0	2.4	7.65–0	2.4	1.22+1	2.2
void	12.7	2.03+5	–	–	–	–	–	–
M2	32.3	5.27+5	1.38–0	2.7	3.79–0	2.4	5.17–0	2.4
void	40.0	2.09+5	–	–	–	–	–	–
Segment 7&8								
M1	2.0	5.09+4	3.88–0	2.5	1.58–0	3.1	5.45–0	2.3
M2	5.0	7.59+4	4.38–0	2.5	7.15–0	2.5	1.15+1	2.3
void	12.7	2.02+5	–	–	–	–	–	–
M2	32.3	5.17+5	1.26–0	2.8	3.44–0	2.4	4.69–0	2.4
void	40.0	2.08+5	–	–	–	–	–	–
Segment 9&10								
M1	2.0	3.86+4	2.83–0	3.7	1.31–0	3.8	4.13–0	3.1
M2	5.0	5.66+4	3.14–0	3.5	5.77–0	3.2	8.91–0	3.0
void	12.7	1.50+5	–	–	–	–	–	–
M2	32.3	4.19+5	8.96–1	3.7	2.58–0	3.2	3.47–0	3.2
void	40.0	1.76+5	–	–	–	–	–	–
Segment 11&12								
M1	2.0	3.35+4	2.30–0	4.2	1.13–0	4.0	3.43–0	3.5
M2	5.0	5.06+4	2.48–0	4.0	4.88–0	3.3	7.36–0	3.2
void	12.7	1.36+5	–	–	–	–	–	–
M2	32.3	3.78+5	8.28–1	4.1	2.54–0	3.3	3.37–0	3.3
void	40.0	1.64+5	–	–	–	–	–	–

Table 36: Heat Generation - Blanket Outboard

Material	d (cm)	Volume (cm³)	Power Release Density (W/cm³) with Statistical Error (%)					
			Neutrons		Photons		Neutrons & Photons	
Segment 15&16								
M1	2.0	2.48+4	1.82–0	7.3	1.06–0	5.4	2.88–0	5.5
M2	22.0	2.36+5	6.60–1	6.1	2.28–0	4.7	2.94–0	4.8
void	27.0	5.74+4	–	–	–	–	–	–
Segment 17&18								
M1	2.0	2.57+4	3.19–0	5.1	1.44–0	4.5	4.64–0	4.2
M2	22.0	2.37+5	1.36–0	4.7	3.56–0	4.0	4.92–0	4.0
void	27.0	5.74+4	–	–	–	–	–	–
Segment 19&20								
M1	2.0	2.44+4	3.13–0	5.0	1.46–0	4.9	4.59–0	4.3
M2	22.0	2.36+5	1.40–0	4.6	3.51–0	4.0	4.92–0	4.0
void	27.0	5.66+4	–	–	–	–	–	–
Segment 21&22								
M1	2.0	2.44+4	1.88–0	7.3	1.06–0	5.3	2.94–0	5.5
M2	22.0	2.33+5	7.33–1	6.3	2.30–0	5.0	3.04–0	5.1
void	27.0	5.78+4	–	–	–	–	–	–

Table 37: Heat Generation - Blanket Inboard

Material	Volume (cm)	Power Release Density (W/cm³) with Statistical Error (%)					
		Neutrons		Photons		Neutrons & Photons	
Segment 13&14							
M3	2.71+5	4.70–1	5.6	4.76–0	5.3	5.23–0	5.2
M3	3.64+5	2.64–2	16	3.87–1	13	4.13–1	13
Segment 23&24							
M3	2.83+5	4.21–1	5.9	4.42–0	5.0	4.85–0	4.9
M3	3.69+5	2.21–2	18	3.85–1	14	4.07–1	14

Table 38: Heat Generation - Divertor

33

Material	Inboard blanket	Top divertor	Bottom divertor	Outboard blanket	Total
Neutron Power Release (MW)					
Graphite	7.9	–	–	26.8	34.7
Metal & Coolant	31.7	4.4	4.0	136.2	176.3
Total	39.6	4.4	4.0	163.0	211.0
Photon Power Release (MW)					
Graphite	3.9	–	–	12.0	15.9
Metal & Coolant	88.9	46.2	43.4	342.5	521.0
Total	92.9	46.2	43.4	354.5	537.0
Total Power Release (MW)					
Graphite	11.8	–	–	38.8	50.6
Metal & Coolant	120.6	50.7	47.4	478.7	697.4
Total	132.5	50.7	47.4	517.5	748.0

Table 39: Power Release in the Shielding Blanket

Material	Wedge segment	Parallel segment	Total
Neutron Power Release (MW)			
Water (incl. Boron)	0.1	0.4	0.5
Metal & Coolant	0.6	1.2	1.8
Total	0.7	1.6	2.3
Photon Power Release (MW)			
Water (incl. Boron)	0.0	0.1	0.1
Metal & Coolant	3.8	8.6	12.4
Total	3.8	8.7	12.5
Total Power Release (MW)			
Water (incl. Boron)	0.1	0.5	0.6
Metal & Coolant	4.3	9.8	14.1
Total	4.4	10.3	14.7

Table 40: Power Release in the Inboard Vacuum Vessel

Material	Wedge segment	Parallel segment	Total
Neutron Power Release (MW)			
Water (incl. Boron)	1.2	0.8	2.0
Metal & Coolant	3.2	2.1	5.3
Total	4.4	2.9	7.3
Photon Power Release (MW)			
Water (incl. Boron)	0.5	0.2	0.7
Metal & Coolant	26.0	14.3	40.3
Total	26.5	14.5	41.0
Total Power Release (MW)			
Water (incl. Boron)	1.7	1.0	2.7
Metal & Coolant	29.2	16.4	45.6
Total	30.9	17.4	48.3

Table 41: Power Release in the Outboard Vacuum Vessel

	Power Release (MW)		
	Neutron	Photon	Total
Shielding Blanket:			
–Inboard	39.6	92.9	132.4
–Top divertor	4.4	46.2	50.7
–Bottom divertor	4.0	43.4	47.4
–Outboard	163.0	354.5	517.5
–Total	211.0	537.0	748.0
Vacuum Vessel:			
–Inboard	2.3	12.5	14.7
–Outboard	7.3	41.0	48.3
–Total	9.6	53.5	63.0
Total	220.6	590.5	811.0

Table 42: Power Release in the Shielding Blanket and Vacuum Vessel

35
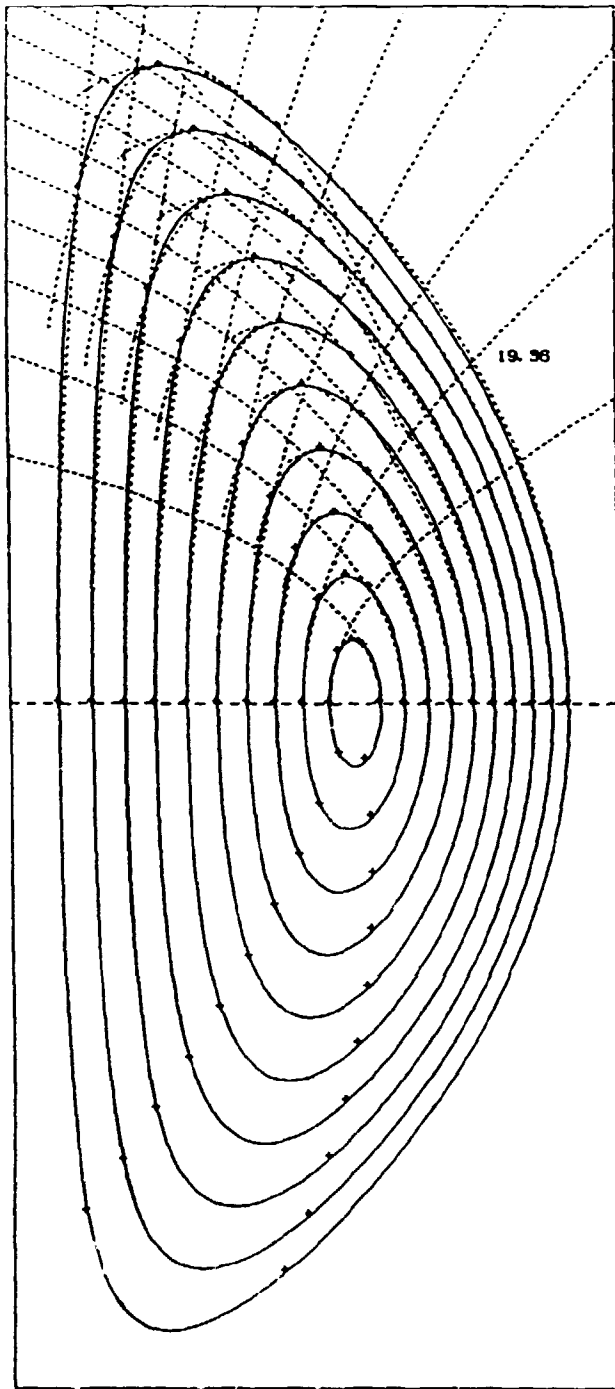
Figure 1: Surfaces of Equal Source Density, S(a)
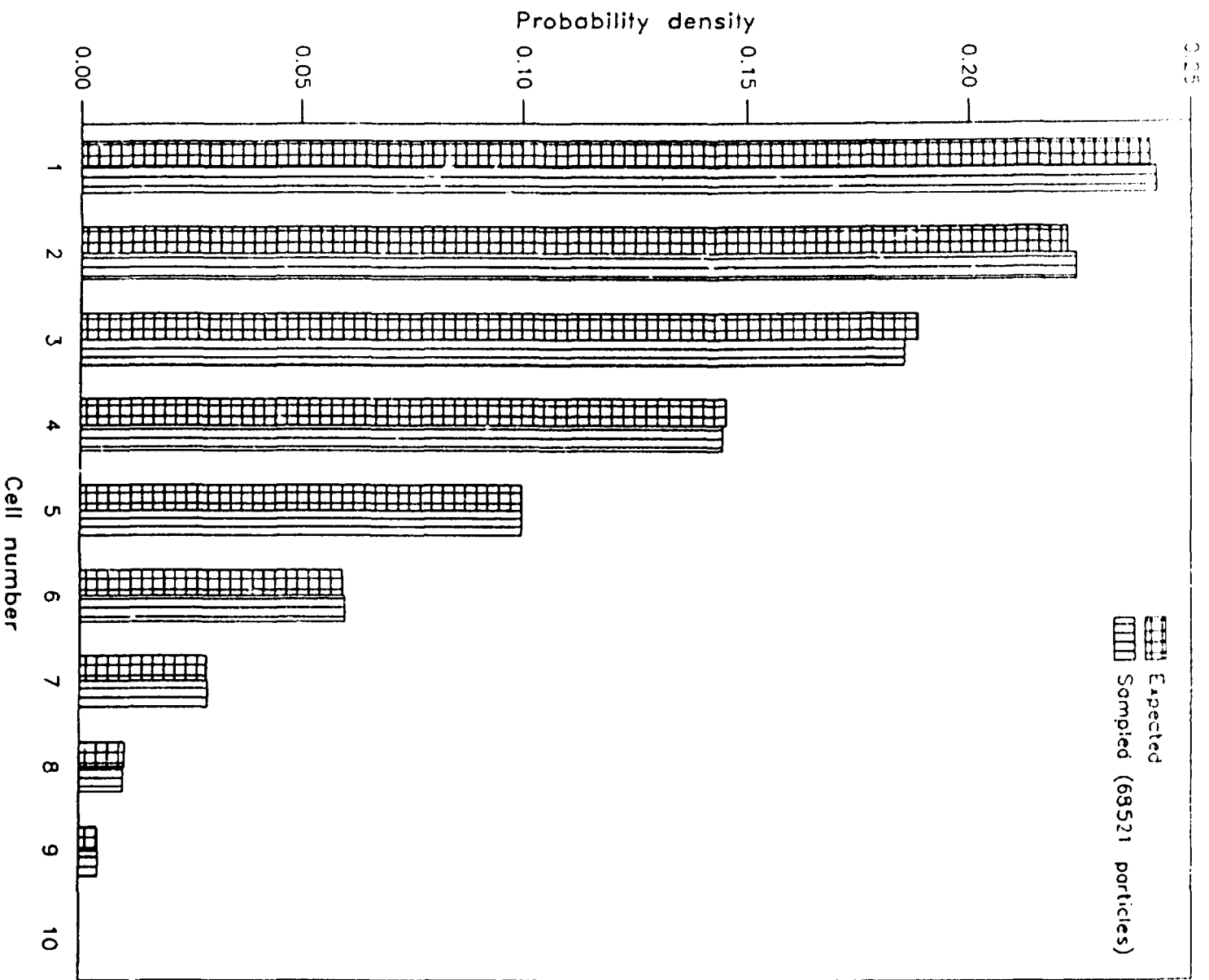
Figure 2: Sampled and Expected Source Probability Density

37

Z	R internal	external
0	0	4380.0
300	0.1	4373.6
600	0.2	4354.2
900	0.3	4321.4
1200	0.3	4274.4
1500	0.4	4212.7
1800	0.5	4135.3
2100	0.6	4041.1
2400	0.7	3928.6
2700	0.8	3796.1
3000	0.9	3641.2
3300	1.0	3461.4
3600	1.0	3249.9
3900	38.5	2991.6
4200	168.2	2667.0
4500	423.6	2231.5
4800	1294.6	1294.6
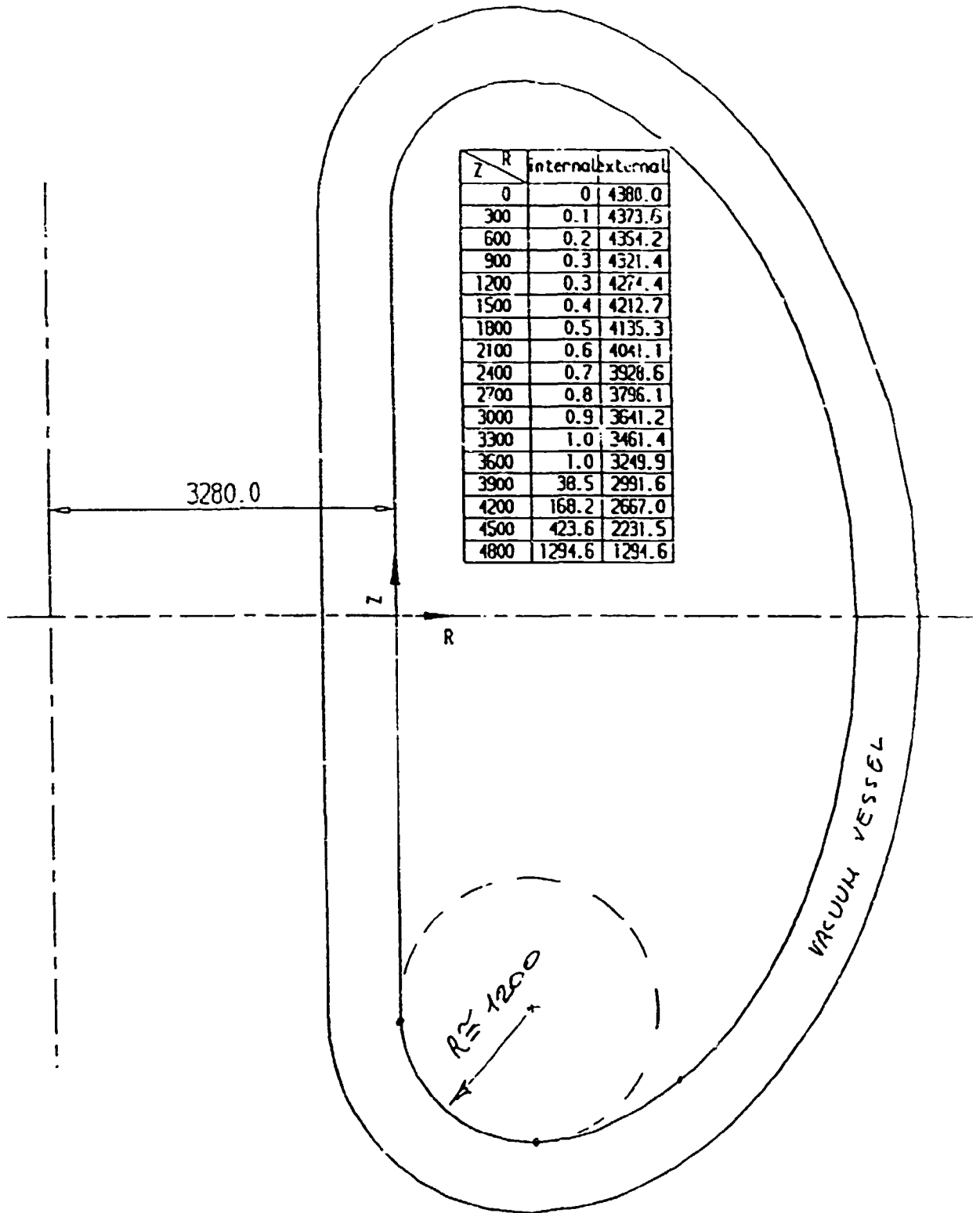
Figure 3: Vacuum Vessel Reference Profile

38
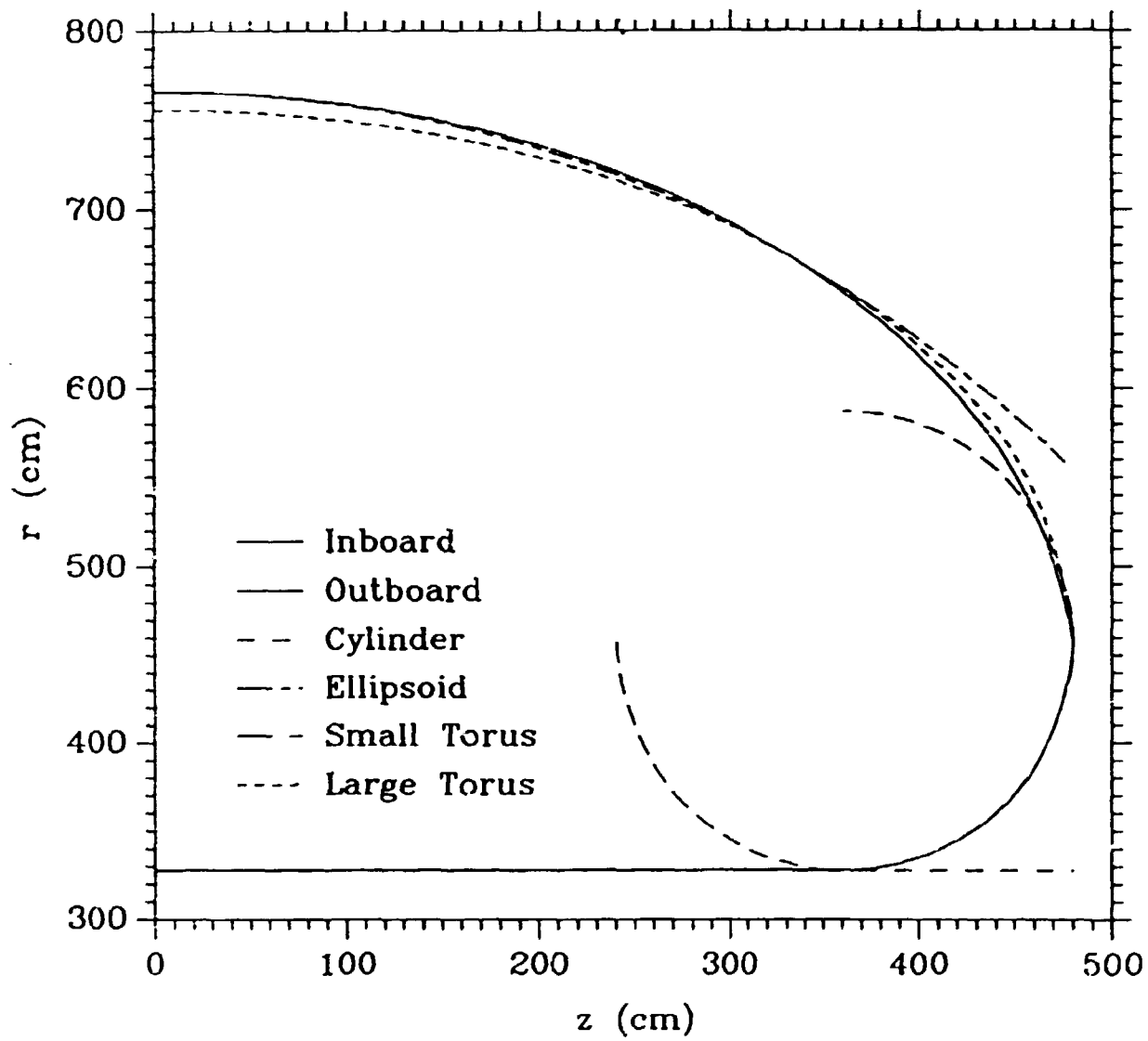
Figure 4: MCNP Approximation to Reference Profile

39
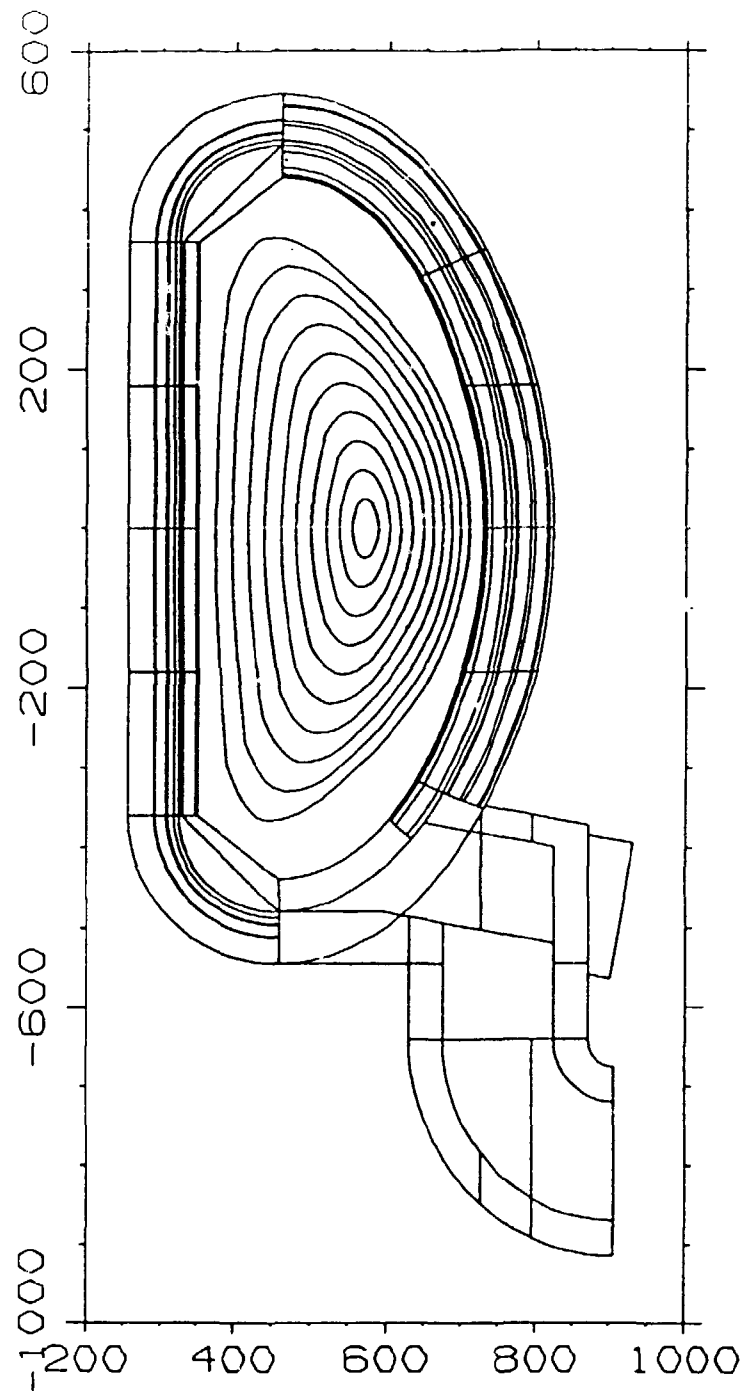
Figure 5: Poloidal Cross-section through the Wedge

see Fig. 8 and 9 for duct details.

40
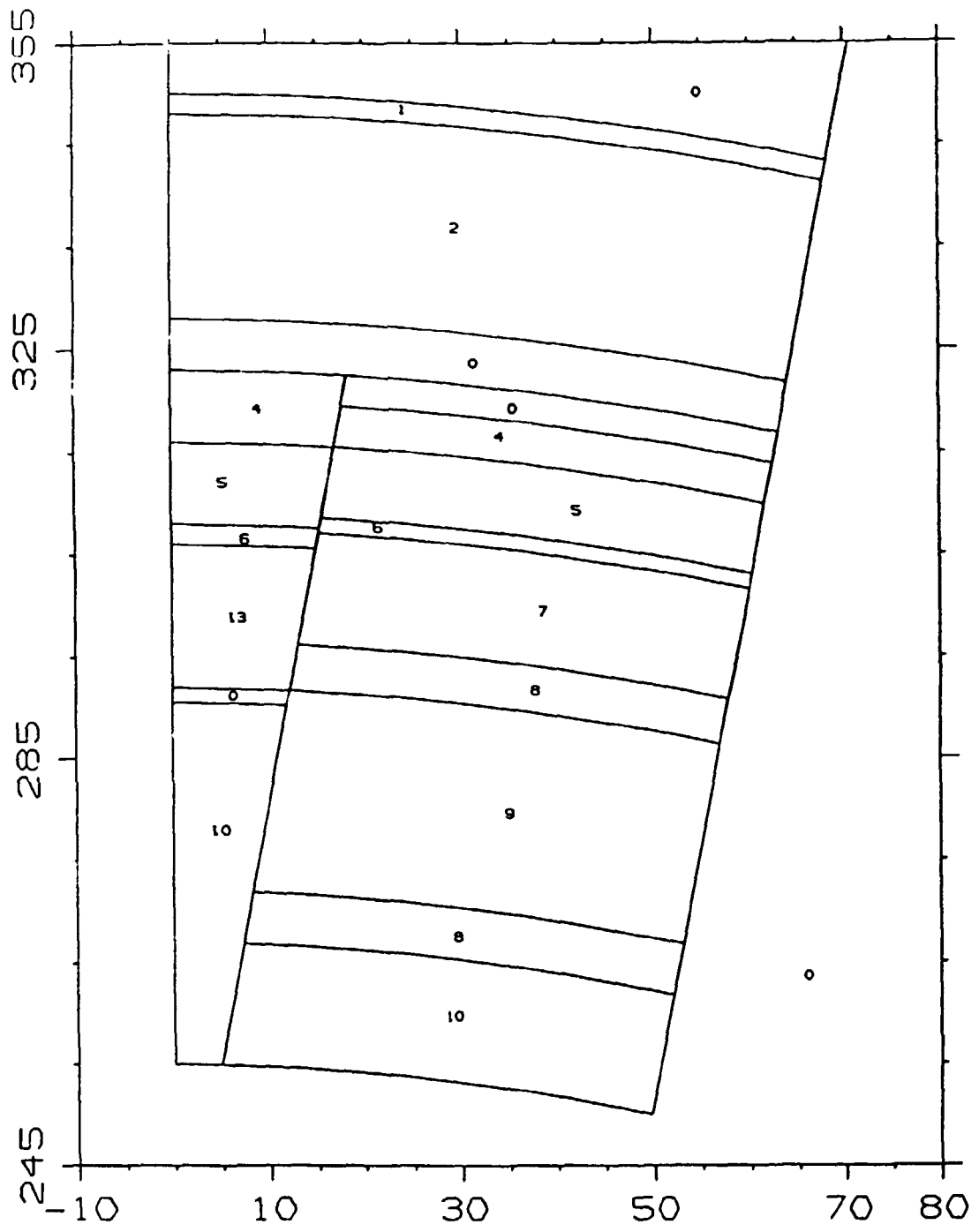
Figure 6: Inboard Horizontal Cross-section

41
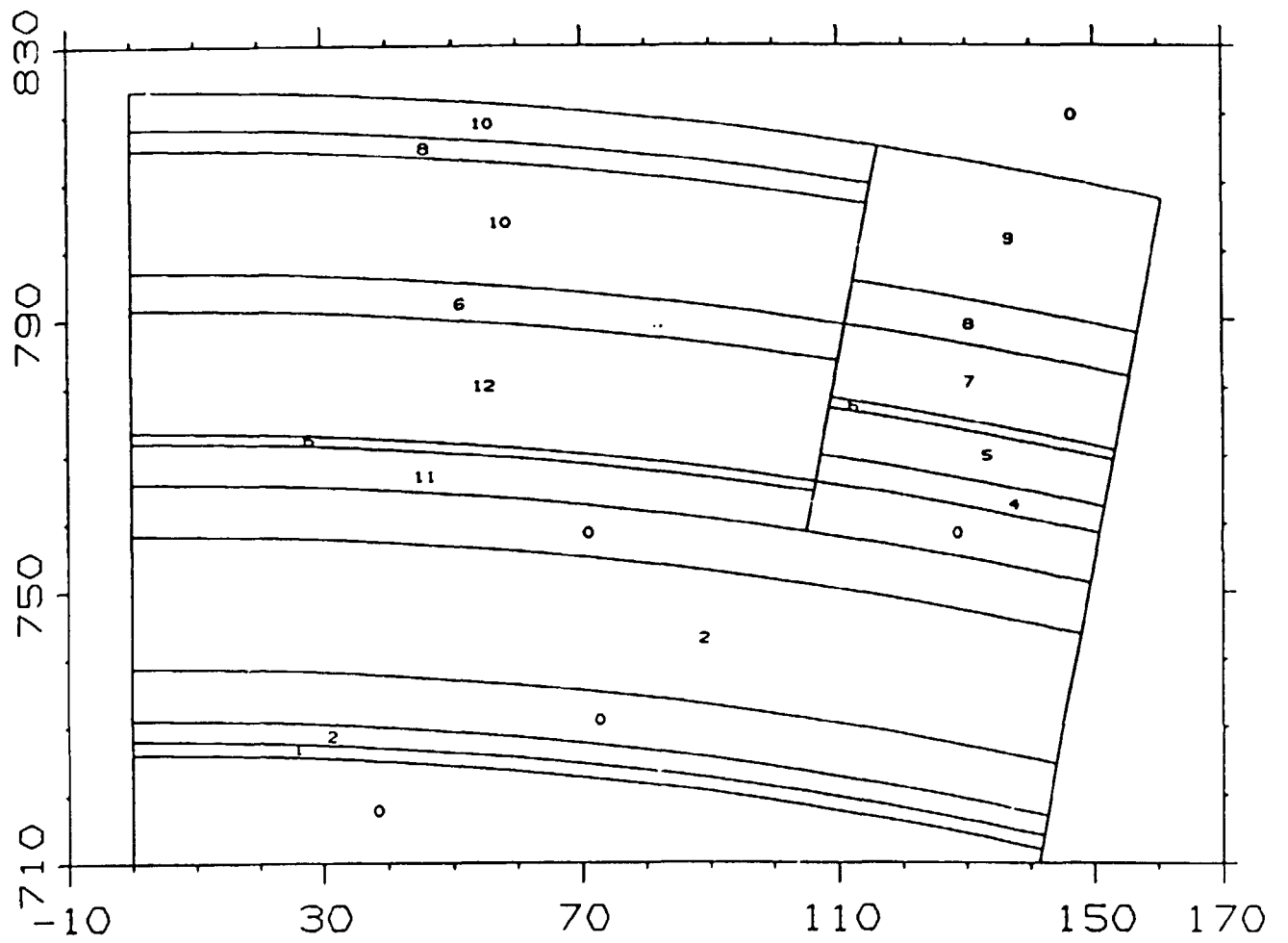
Figure 7: Outboard Horizontal Cross-section
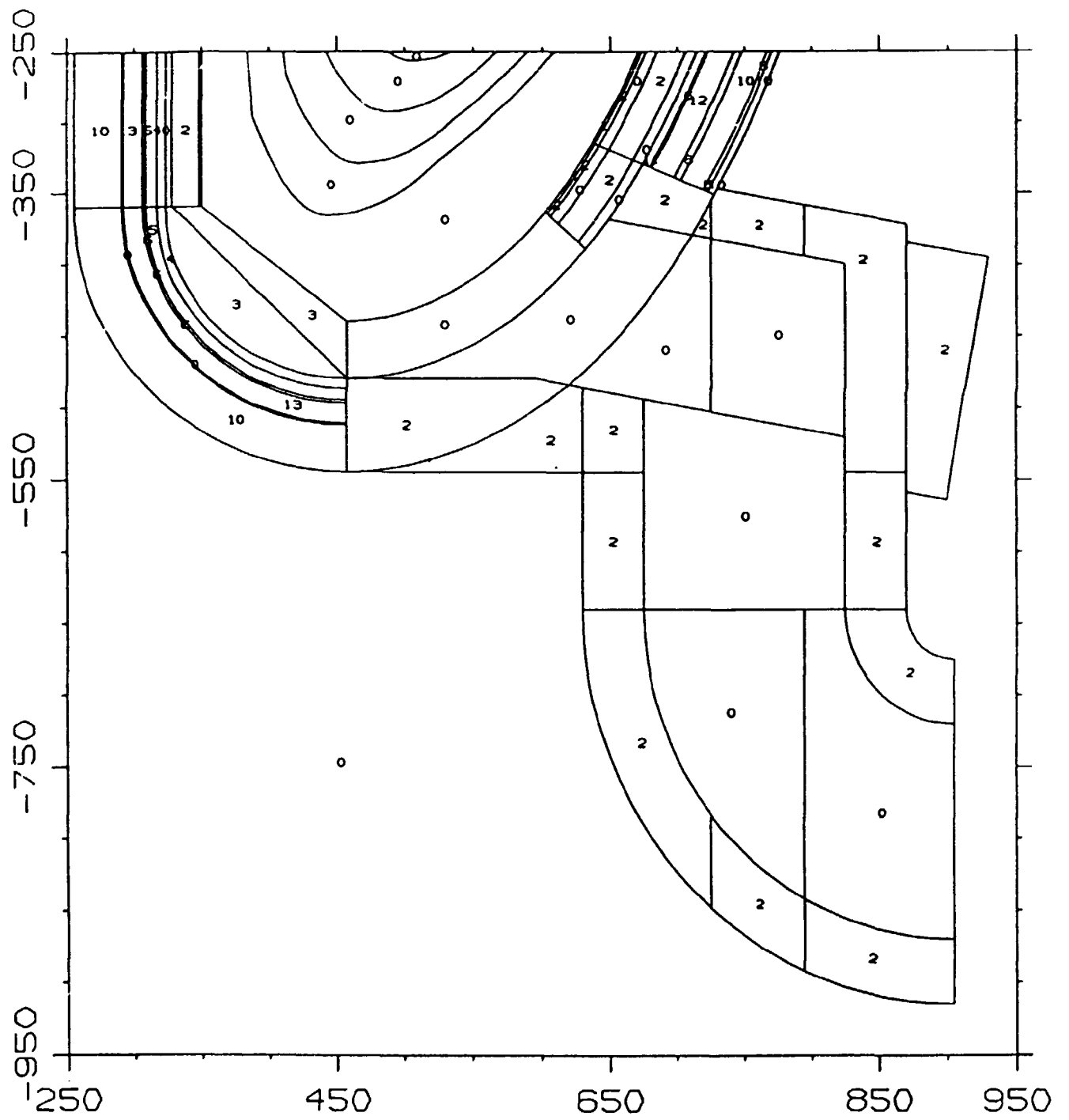
Figure 8: Vertical Cross-section through the Duct

43
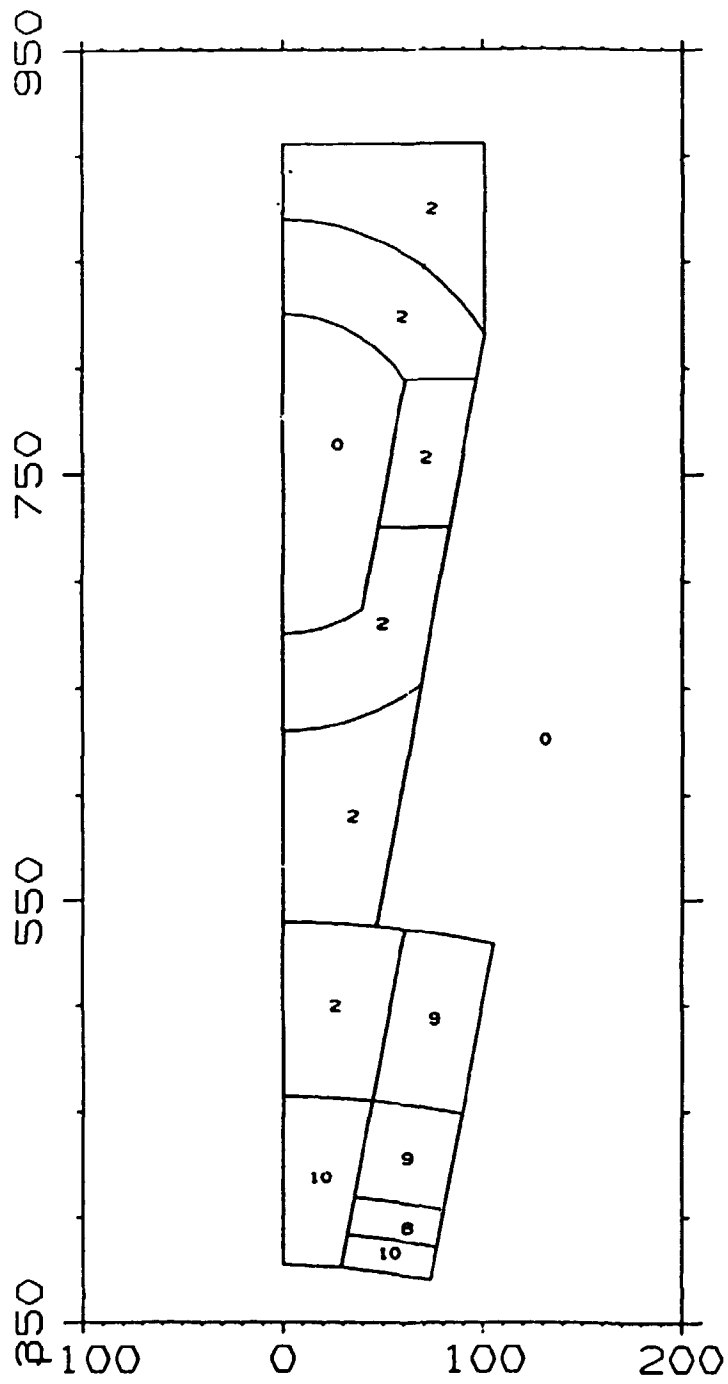
Figure 9: Horizontal Cross-section through the Vertical Duct

44
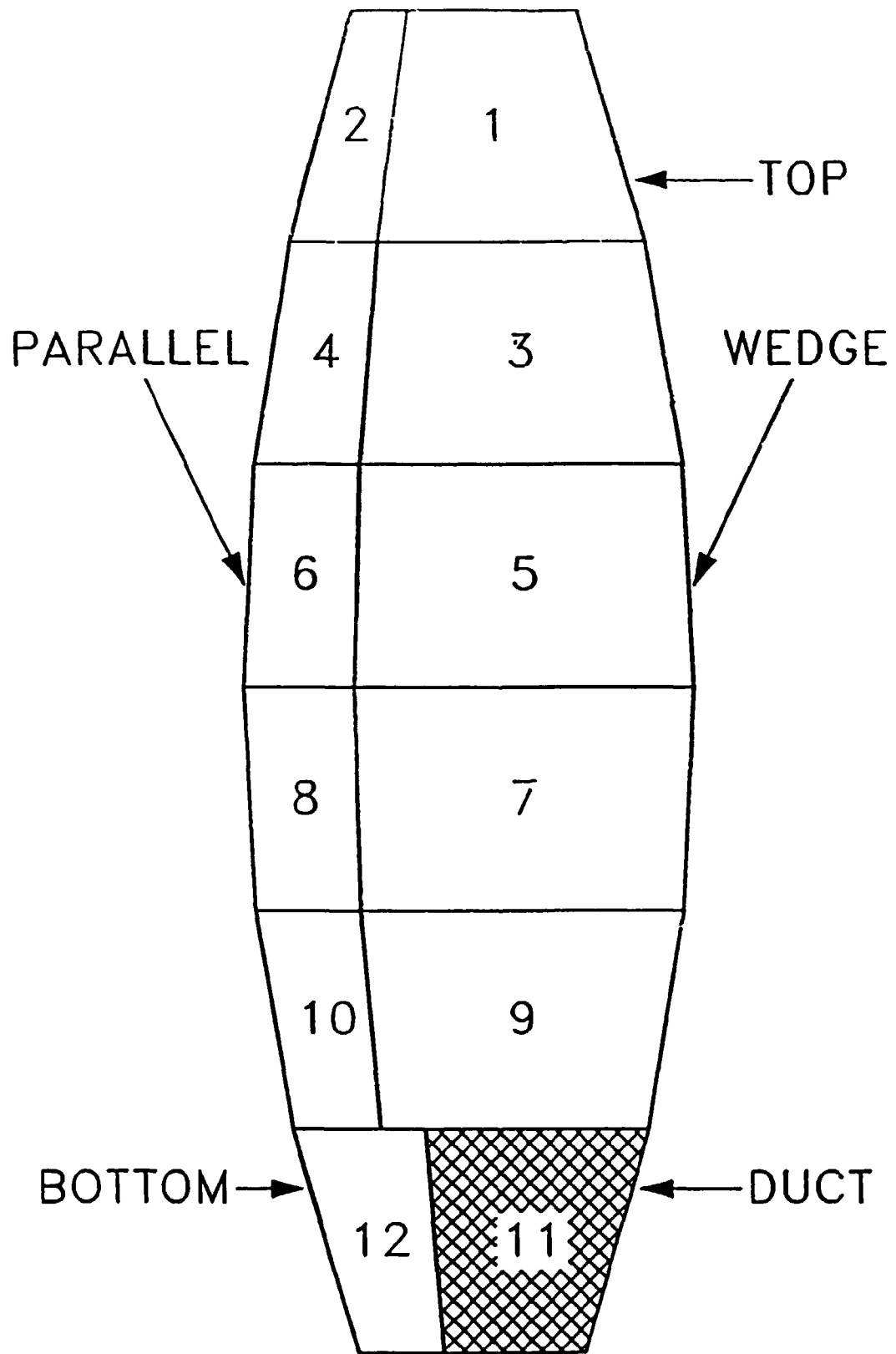
Figure 10: Scheme of Outboard Segment Disposition
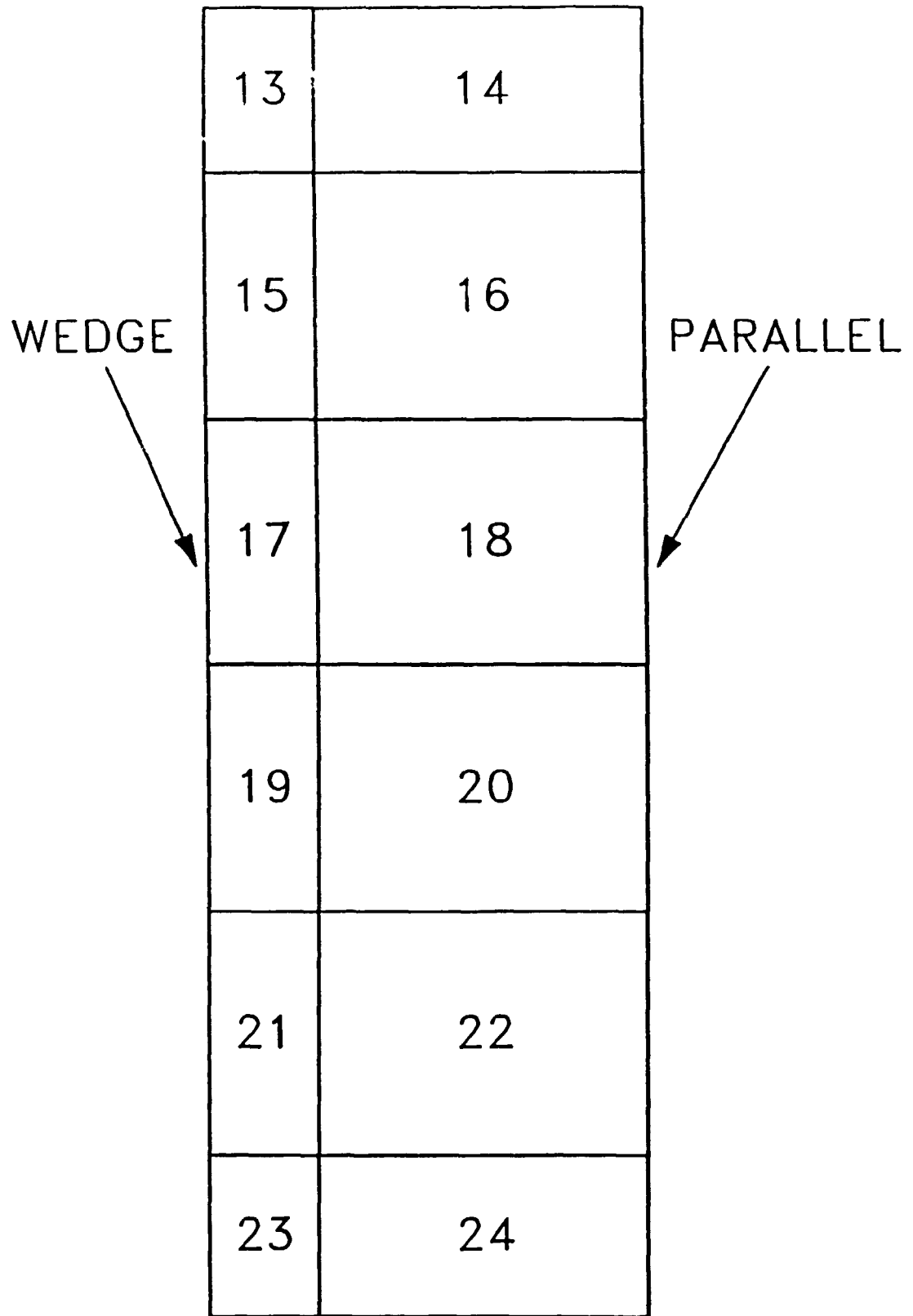
Figure 11: Scheme of Inboard Segment Disposition
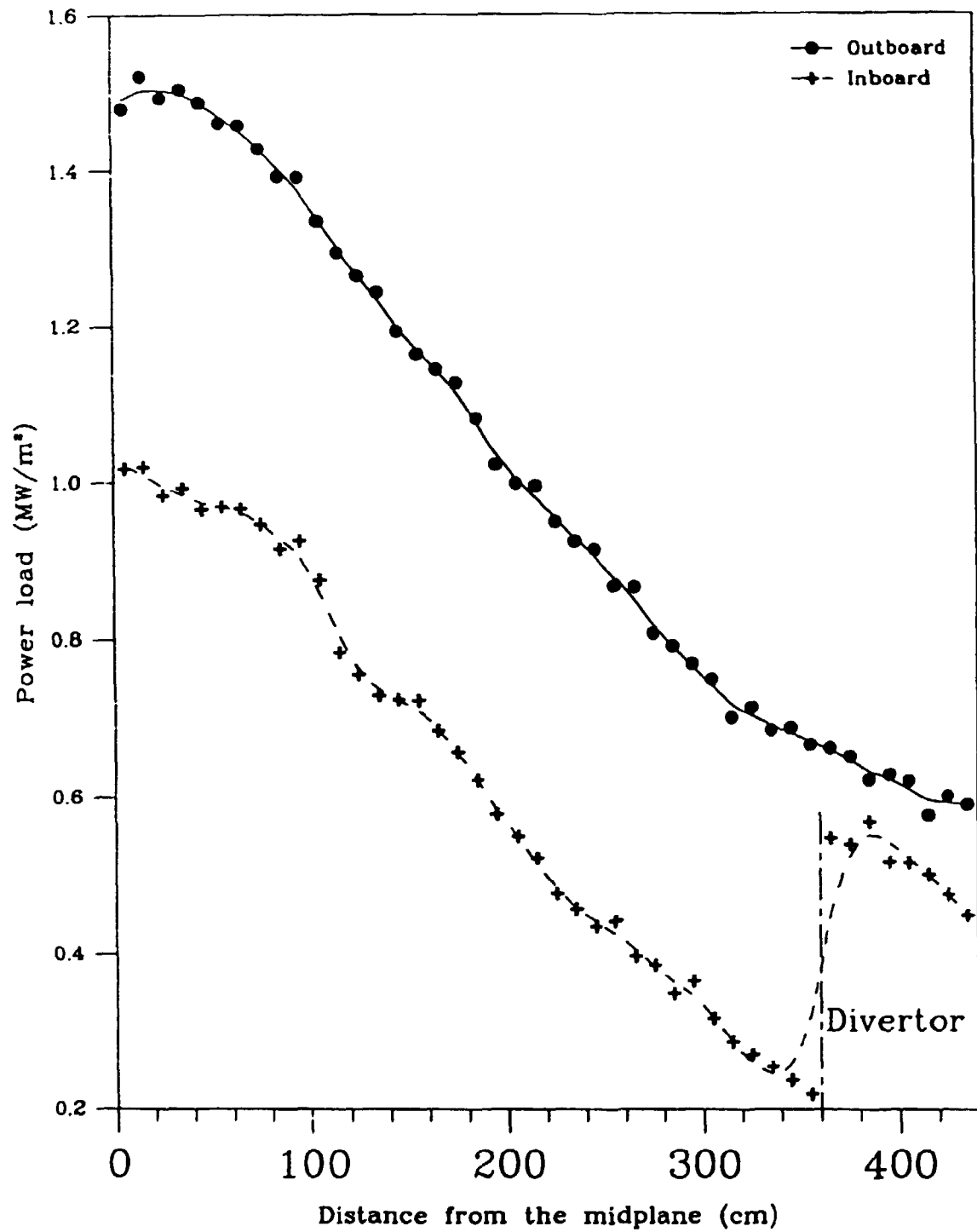
Figure 12: Poloidal Distribution of the Virgin First Wall Load

47
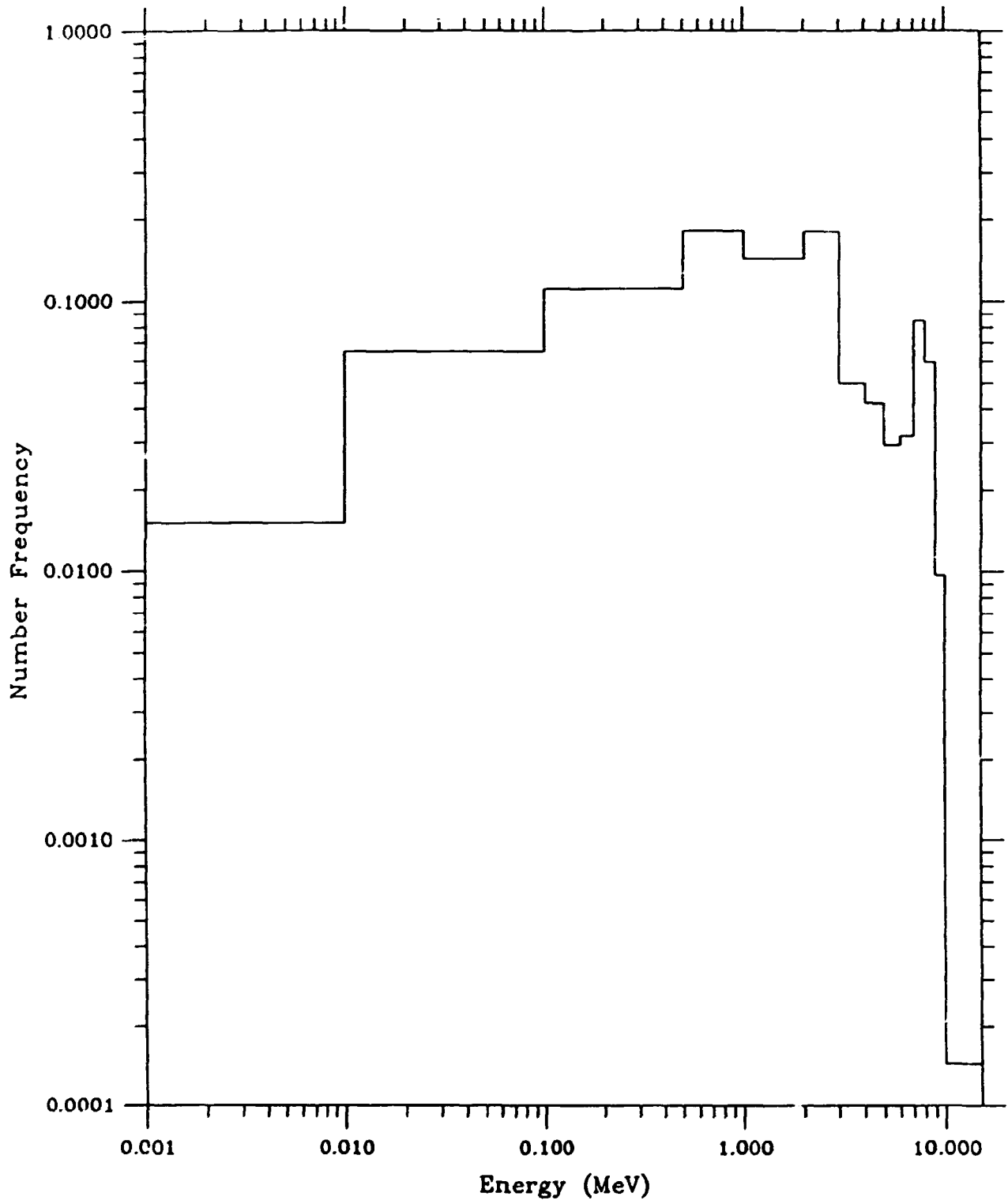
Figure 13: Spectrum of Photons Produced in Neutron Collisions

48
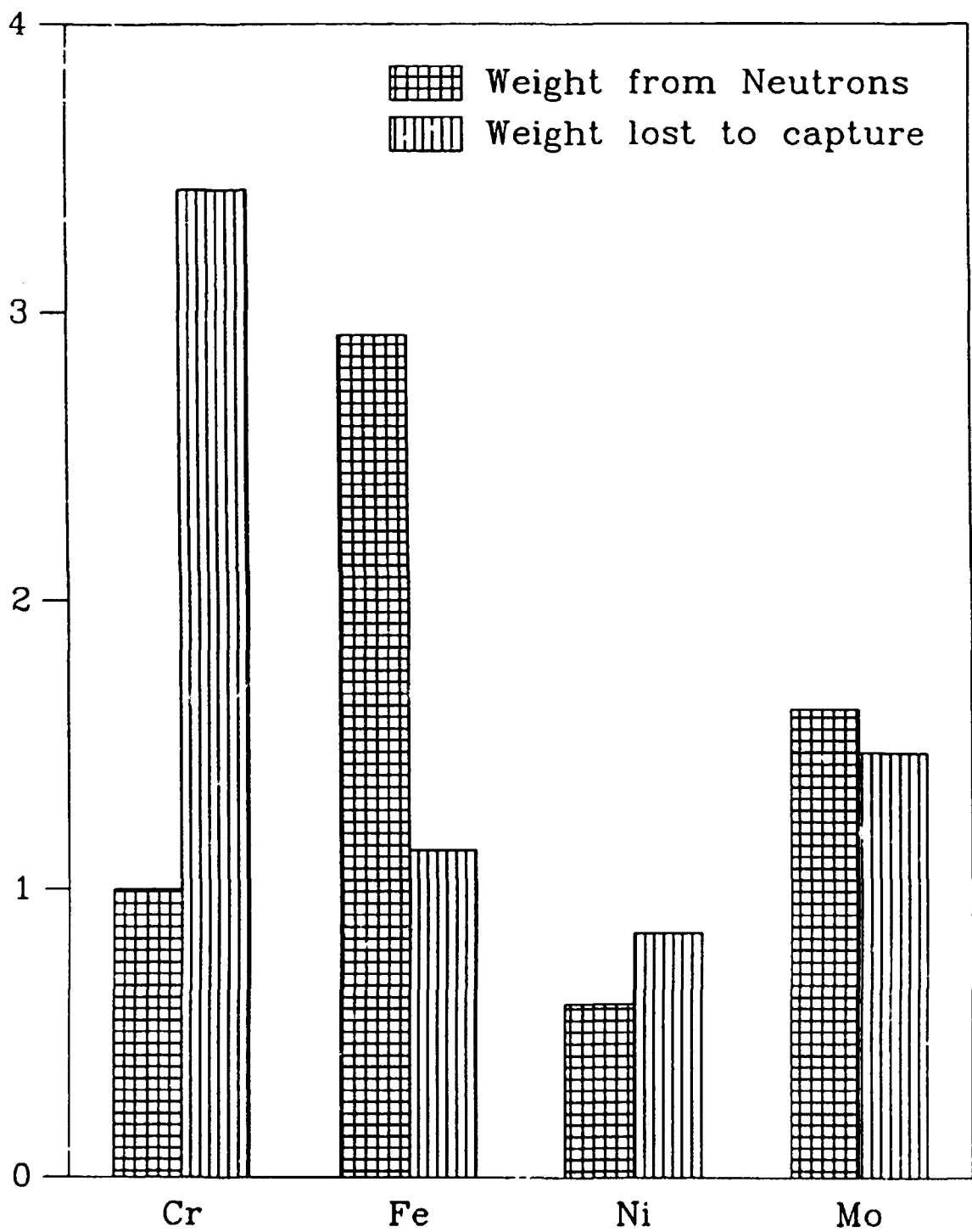
Figure 14: Photon Creation & Loss

49
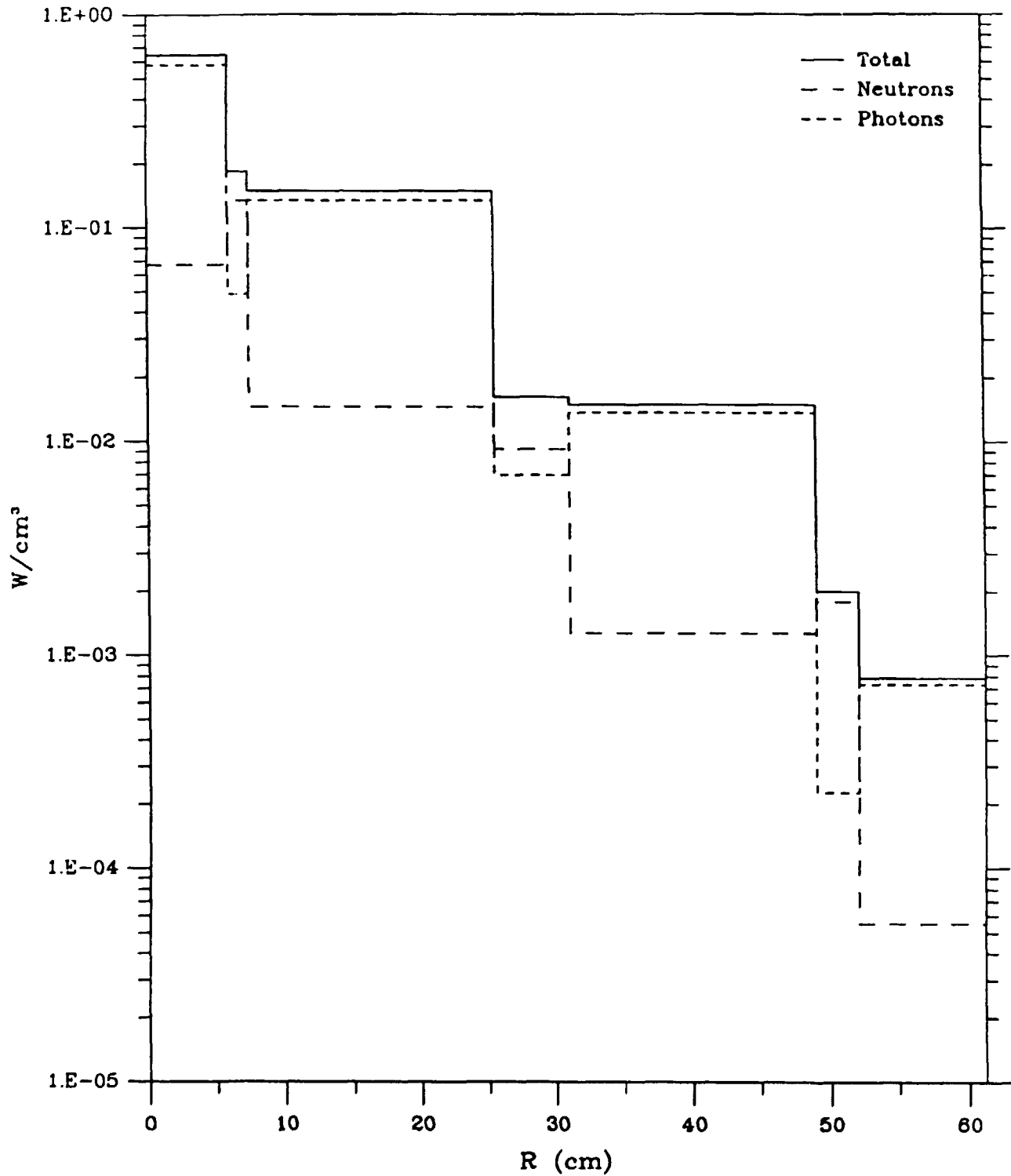
Segment 1

Figure 15: Outboard Power Release

50
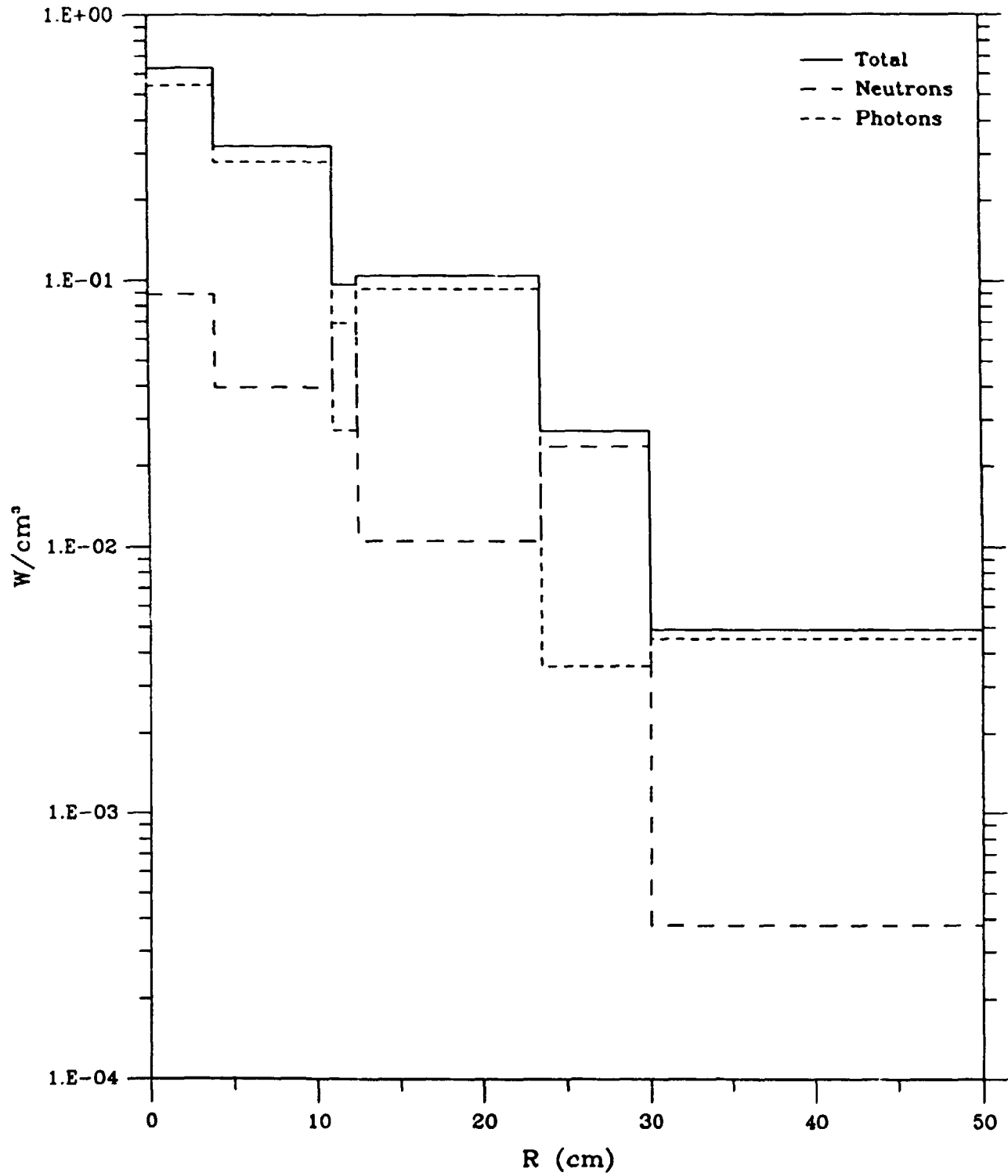
Figure 16: Outboard Power Release

51
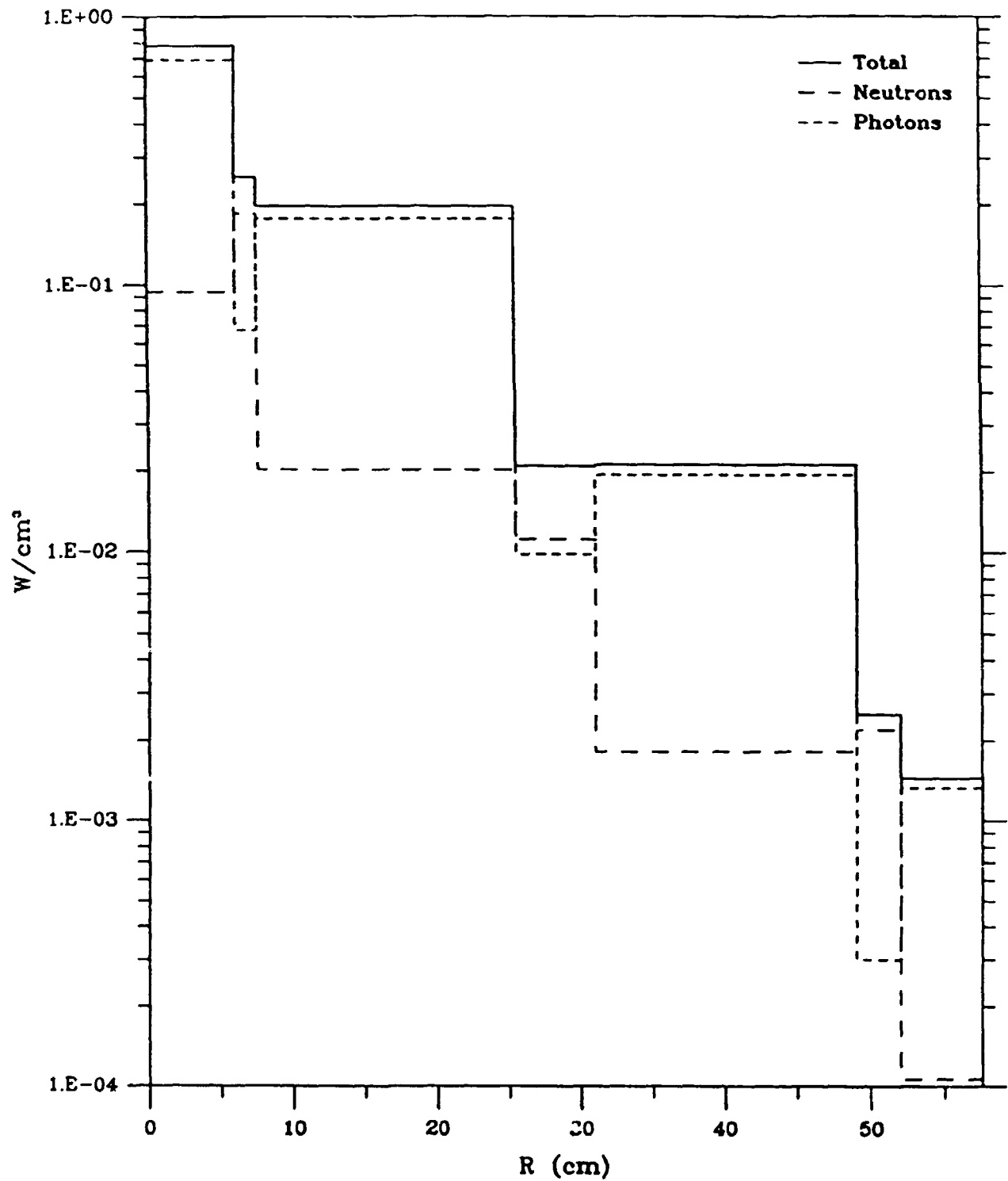
Segment 3

Figure 17: Outboard Power Release

Segment 5
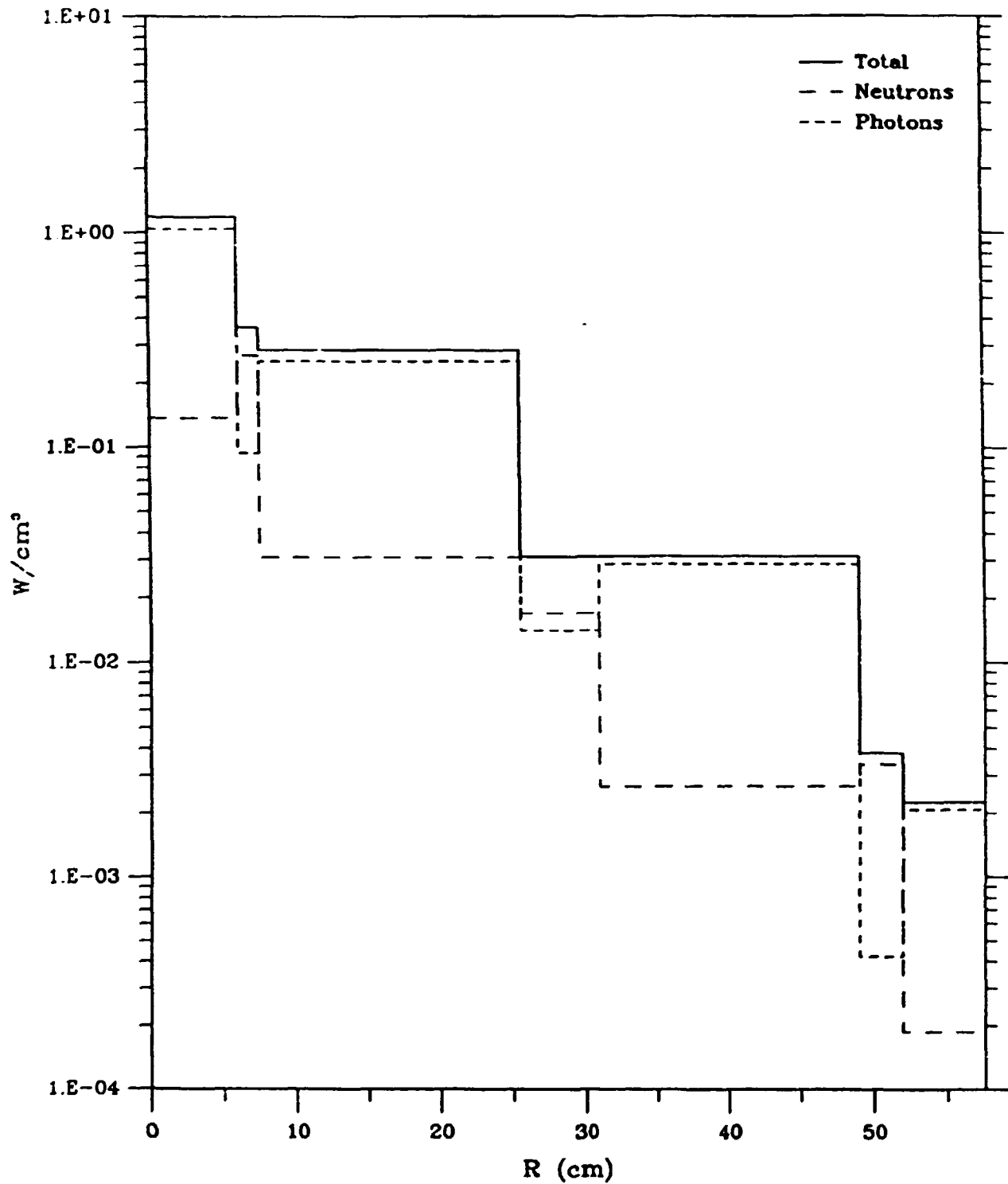
Figure 18: Outboard Power Release

Segment 6
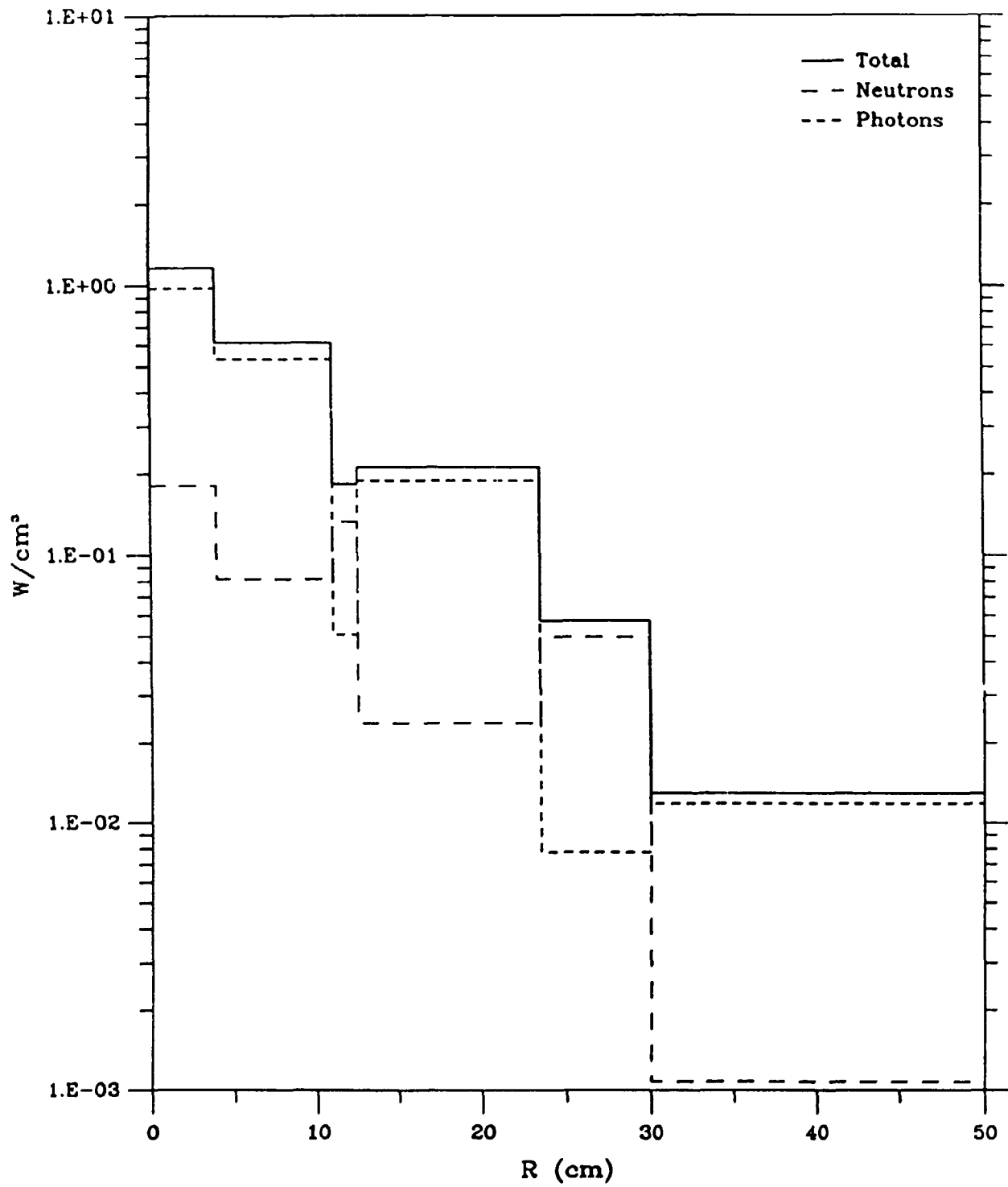
Figure 19: Outboard Power Release

54
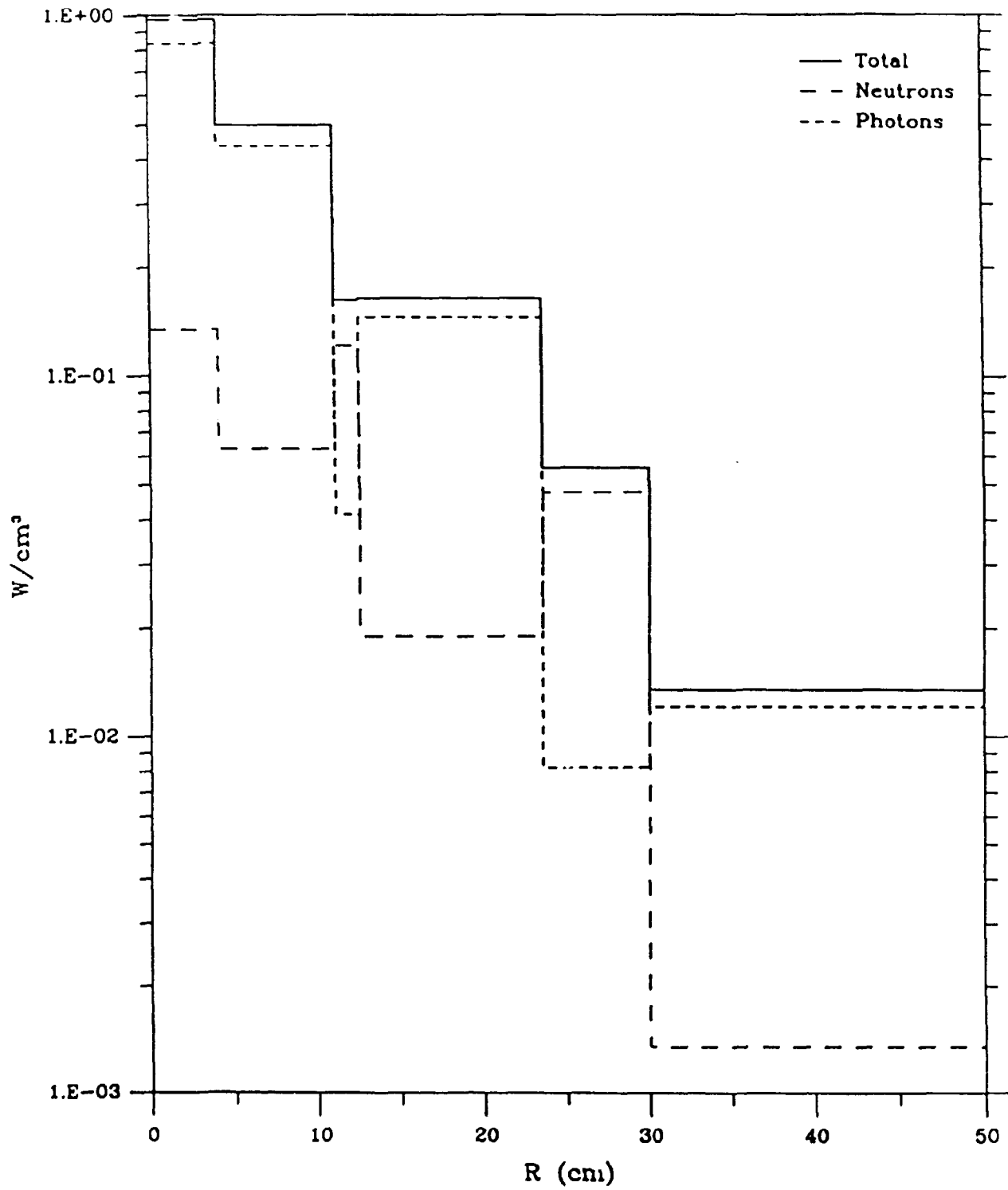
Figure 20: Outboard Power Release
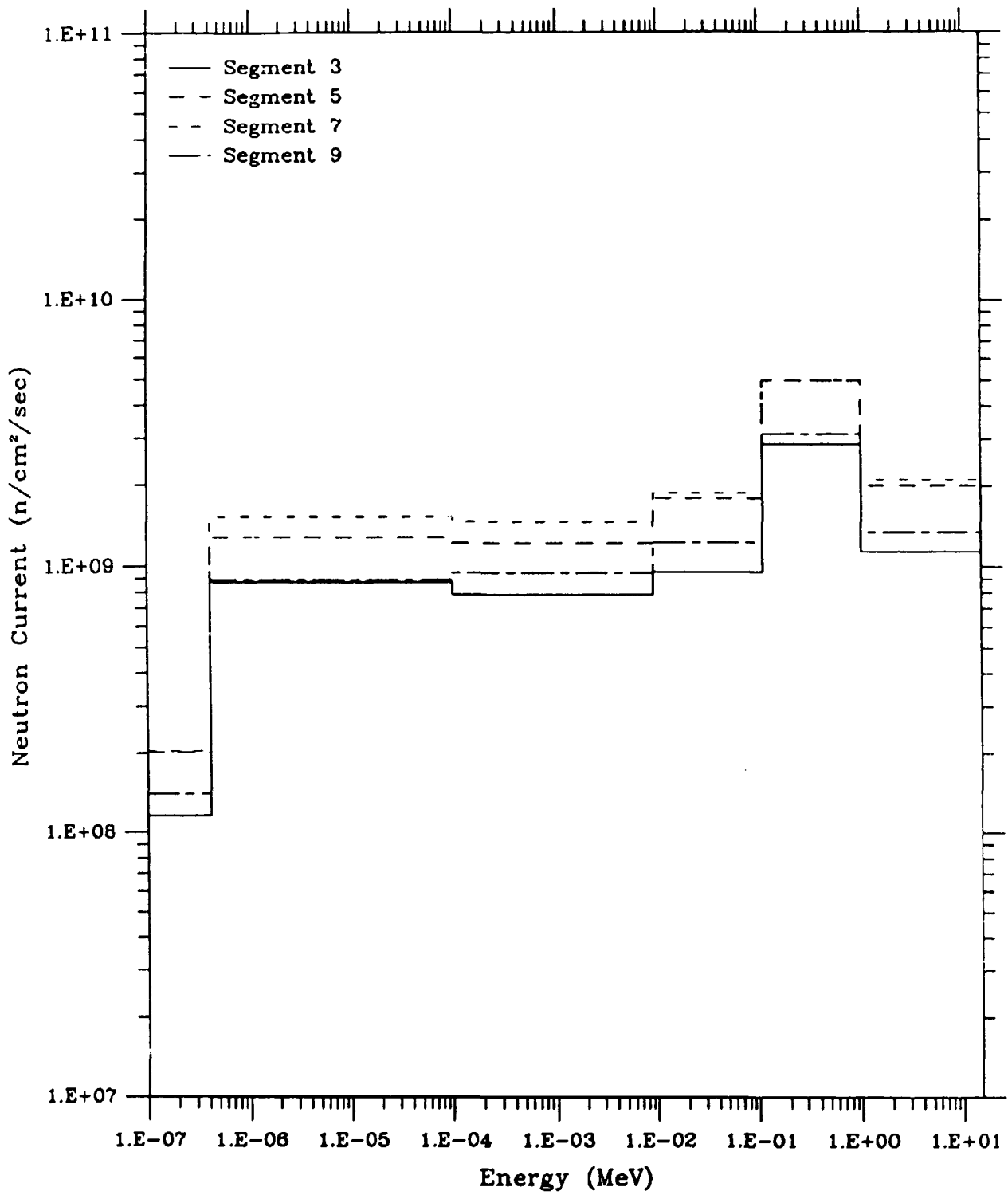
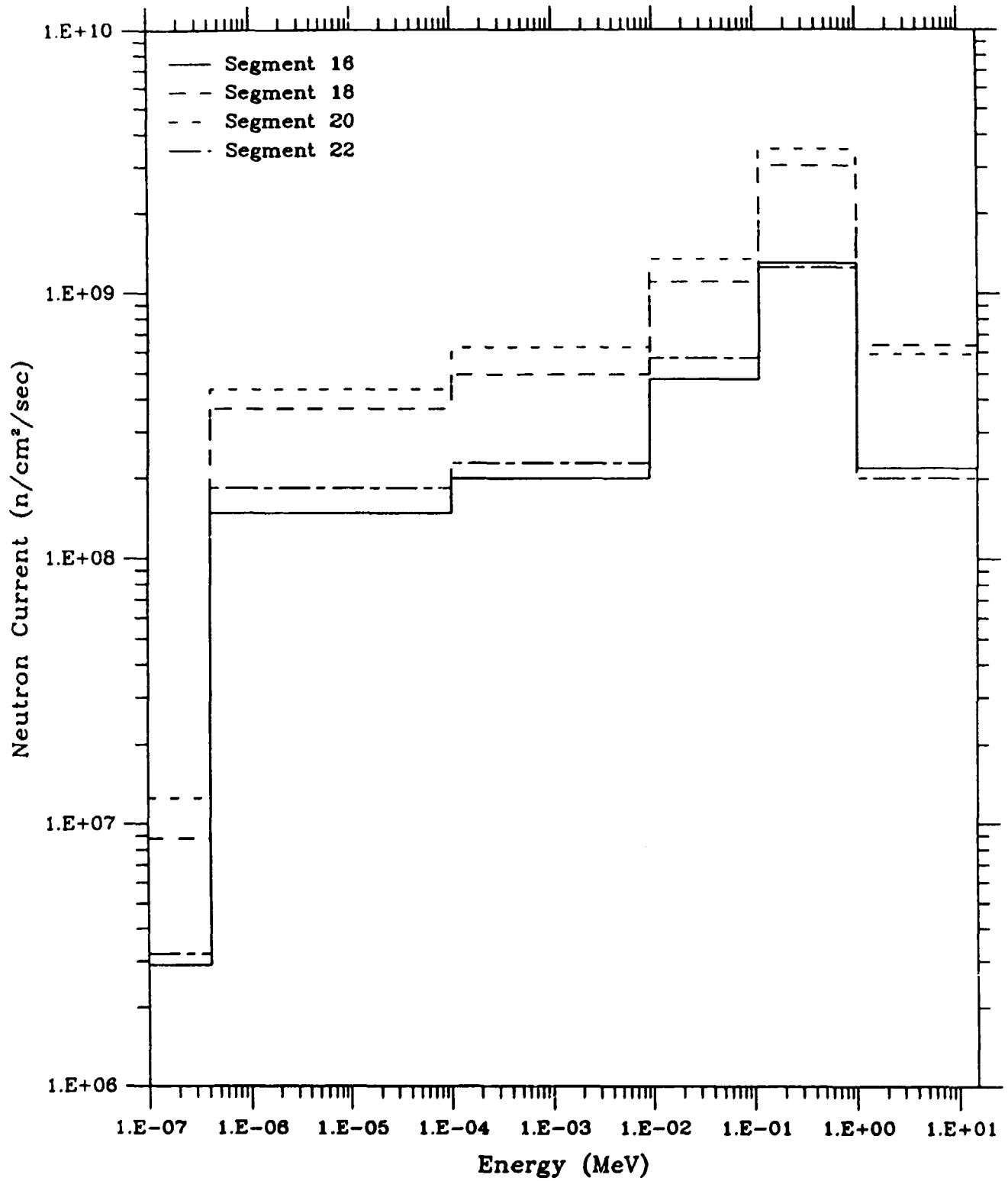**Figure 21:** Outboard Wedge Midsection Neutron Current

56
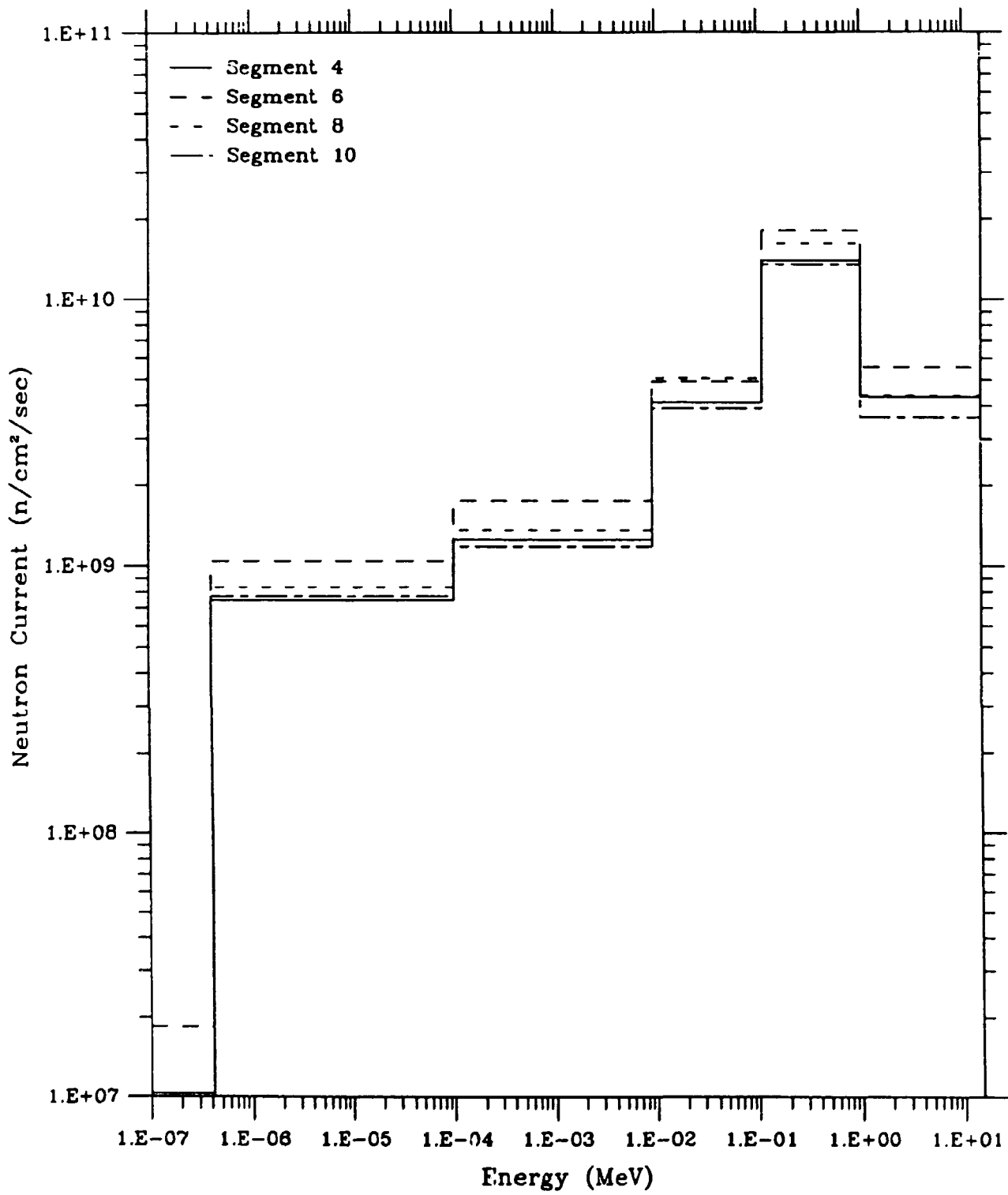
Figure 22: Outboard Parallel Midsection Neutron Current

57
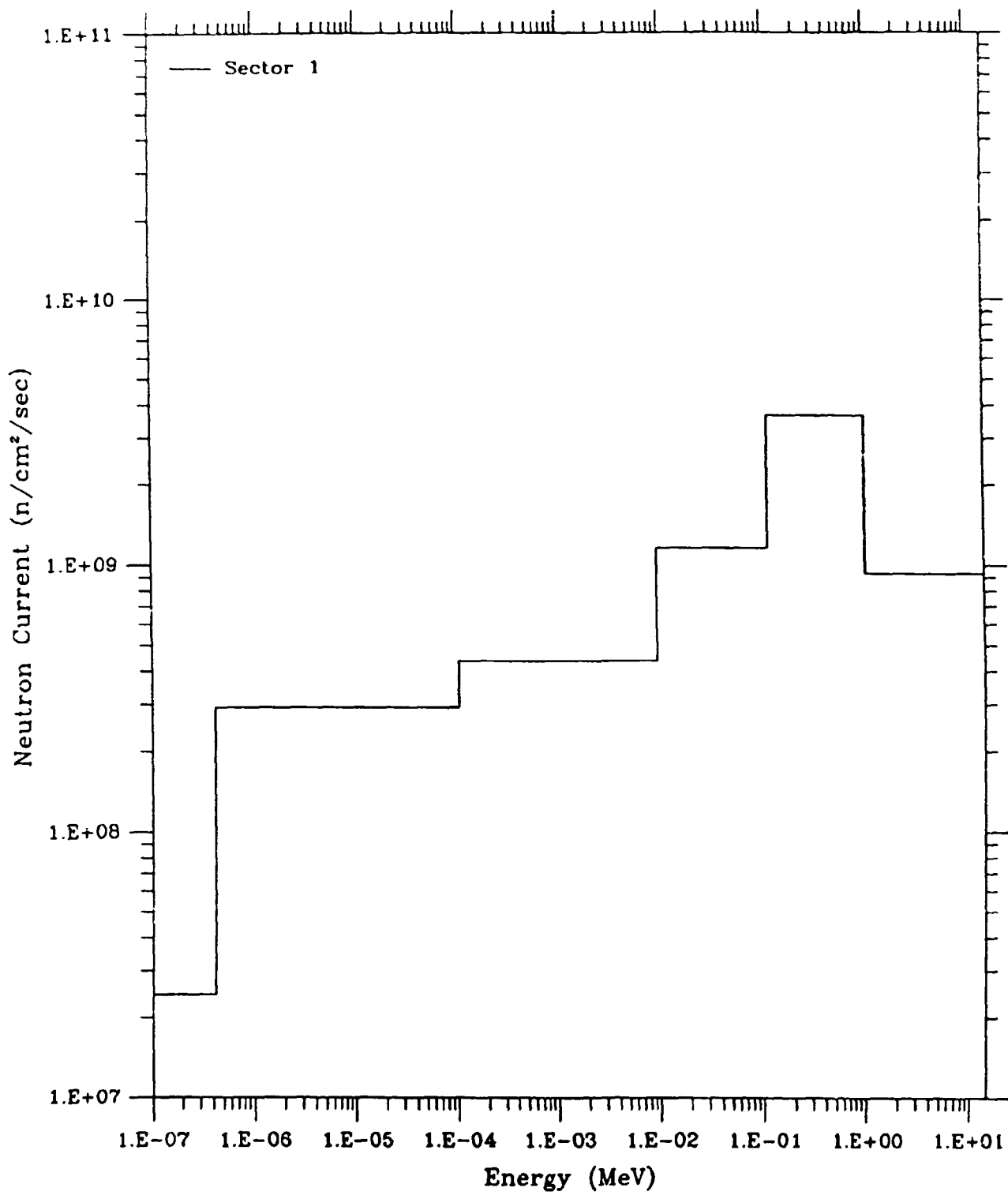
Figure 23: Outboard Top Neutron Current

58
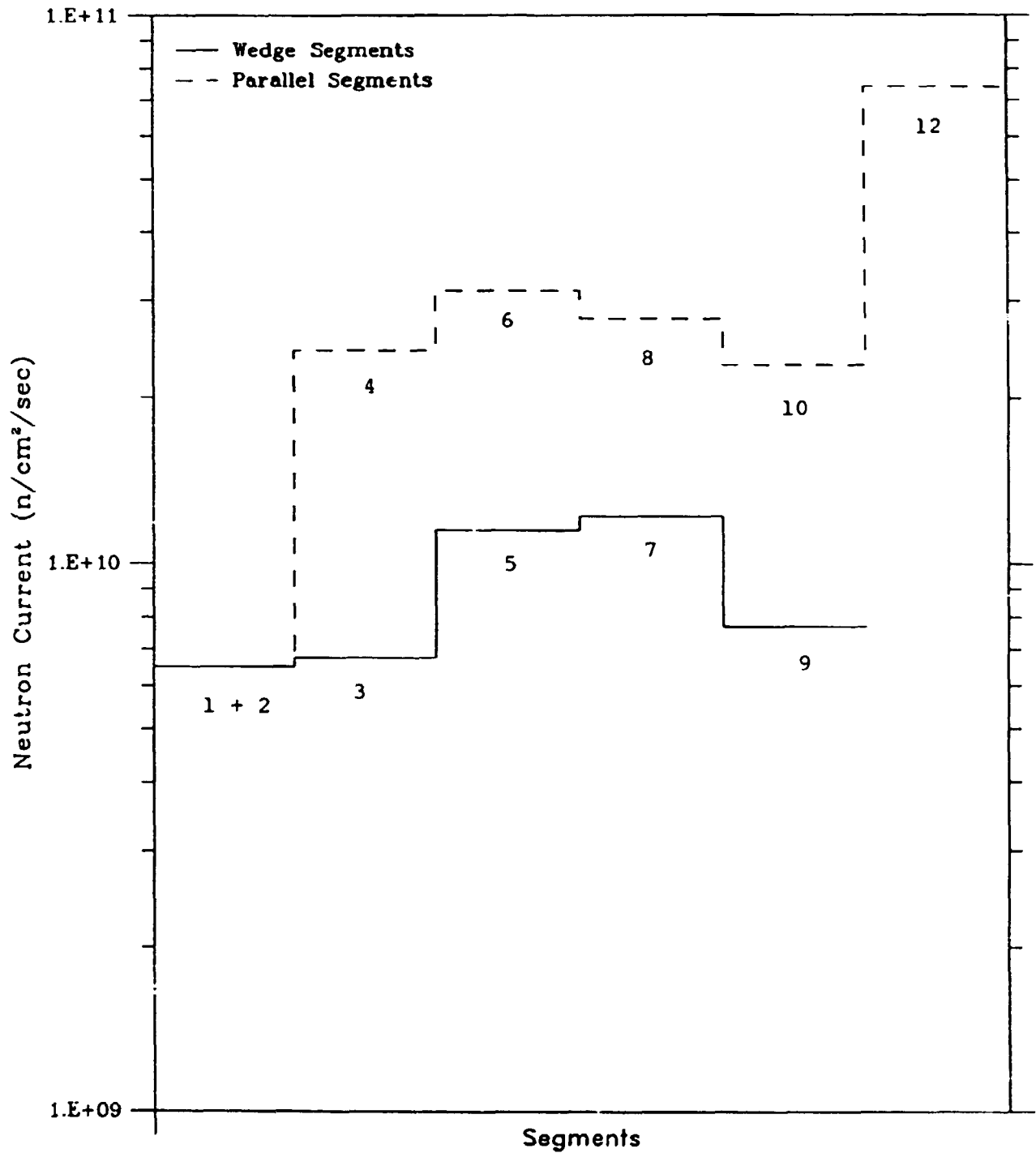
Figure 24: Outboard Total Neutron Current

59
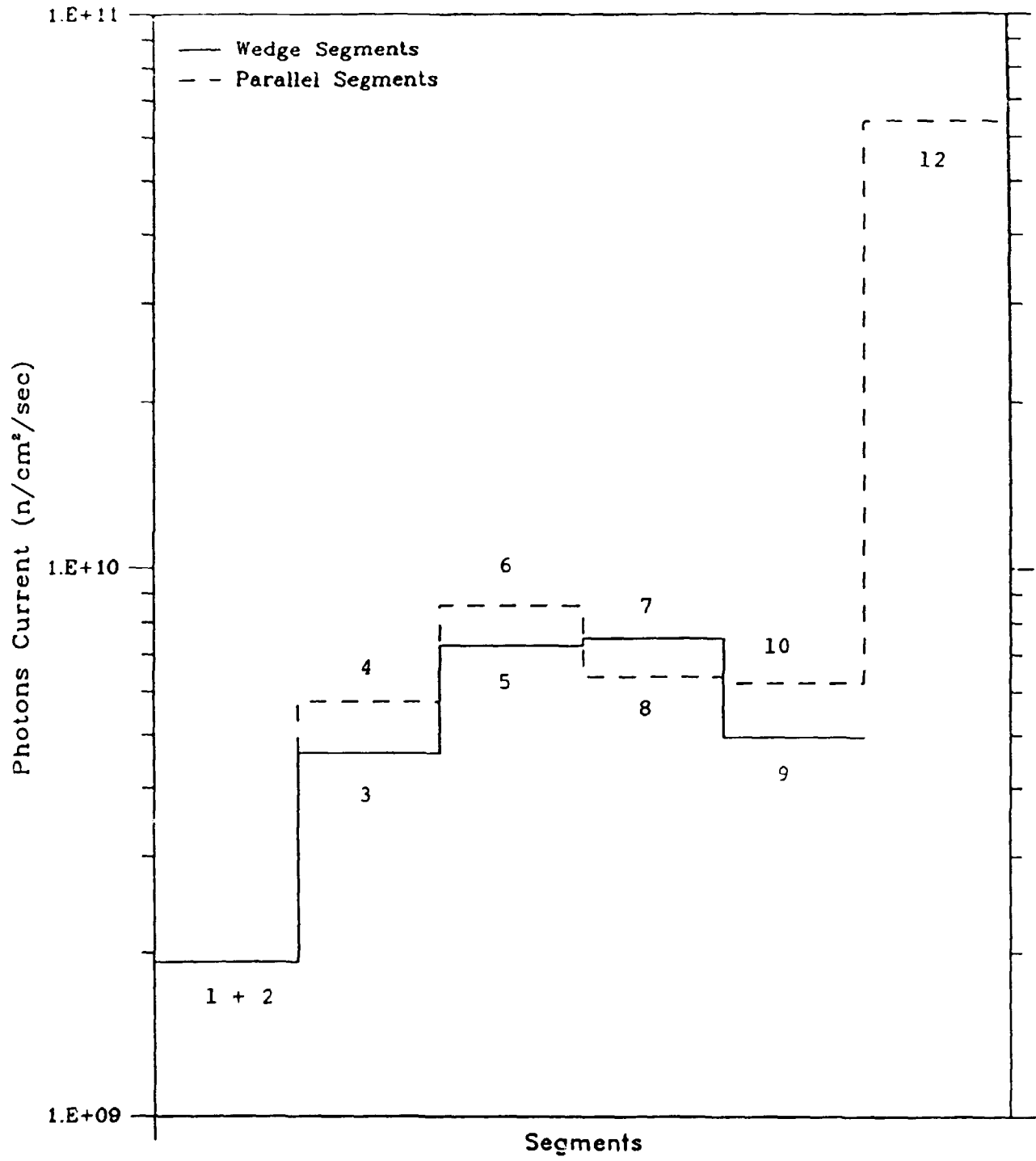
Figure 25: Outboard Total Photon Current

60

Segment 13
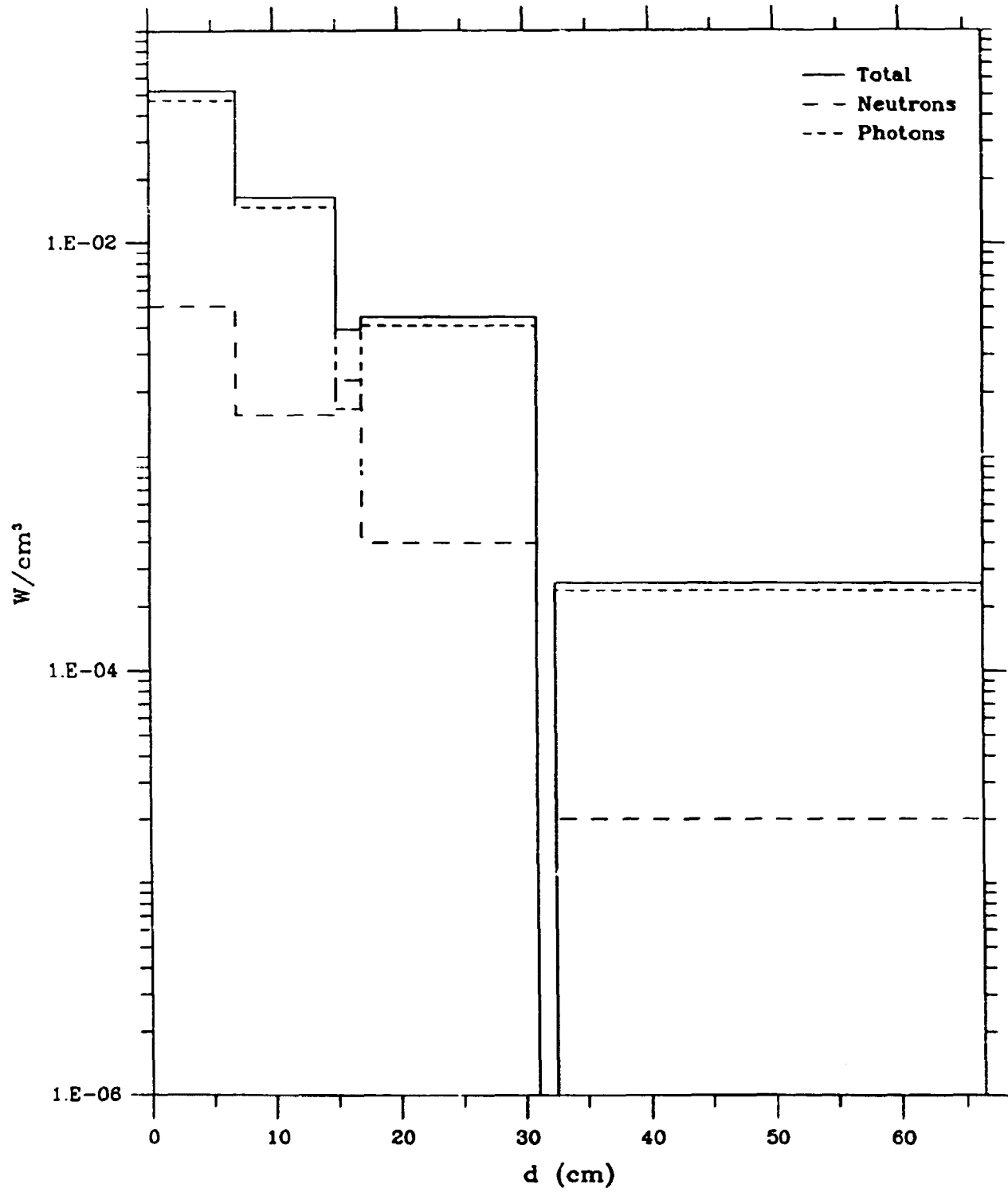
Figure 26: Inboard Power Release

61
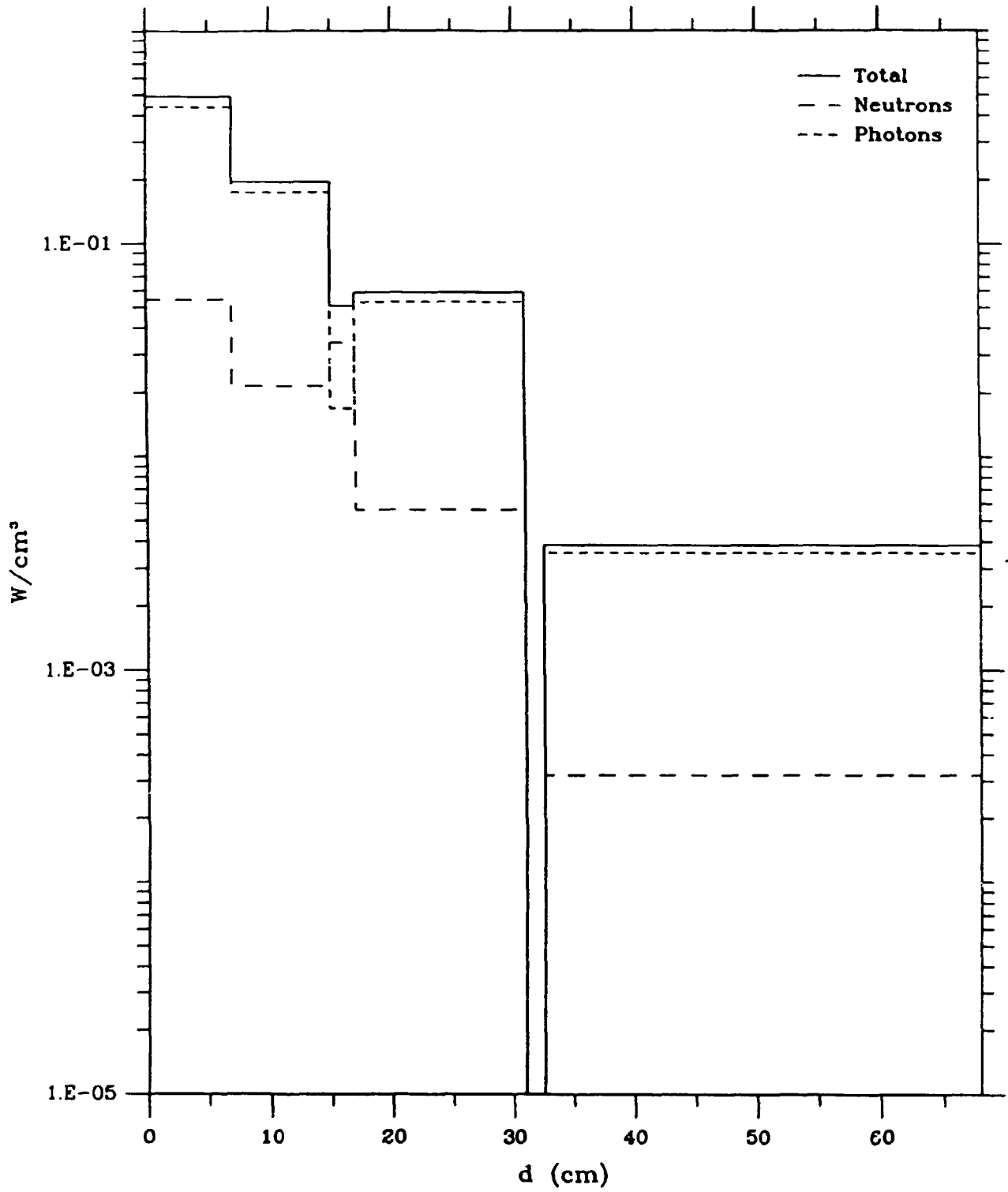
Segment 15

Figure 27: Inboard Power Release

62
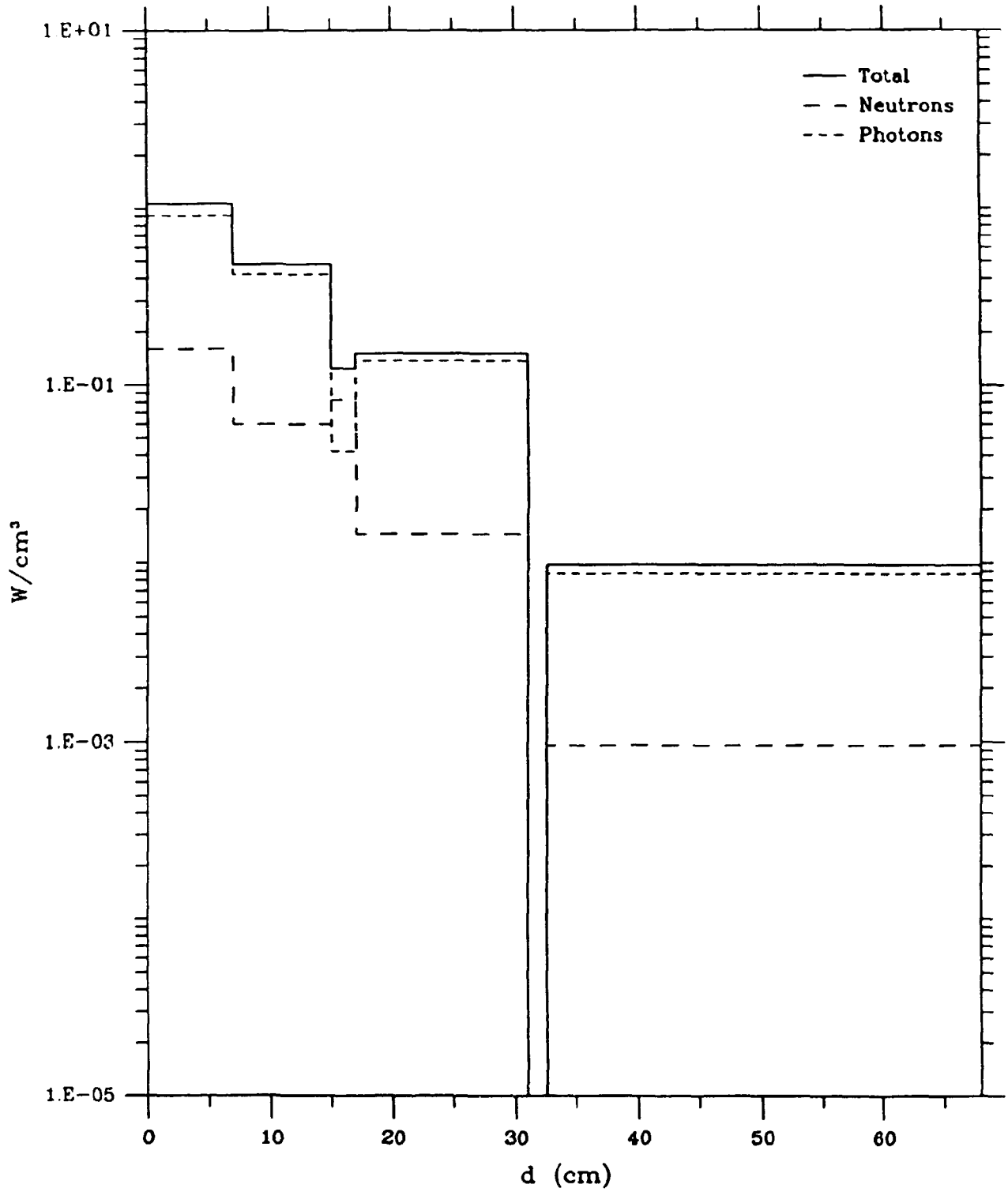
Segment 17

Figure 28: Inboard Power Release

Segment 19
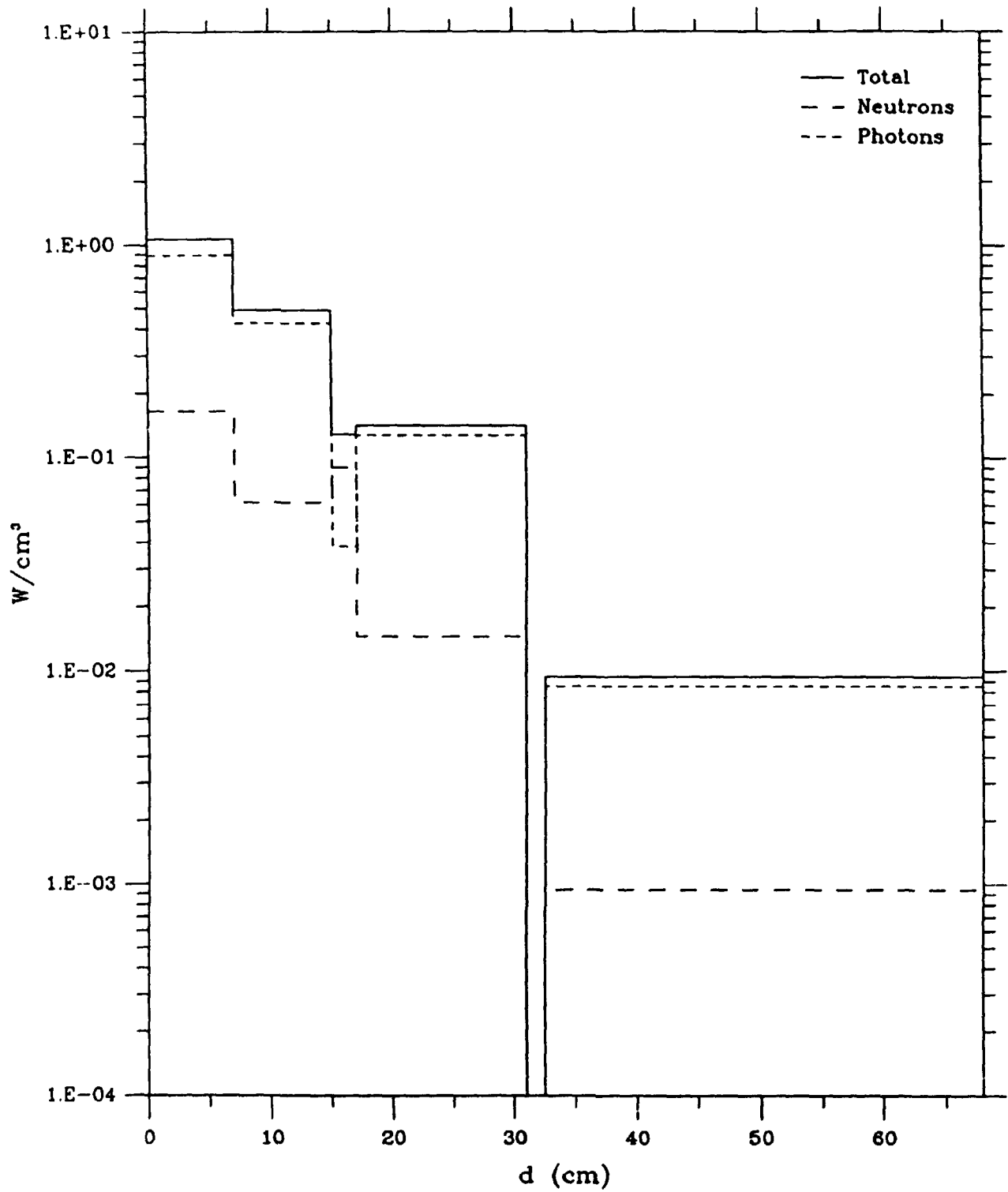
Figure 29: Inboard Power Release

64
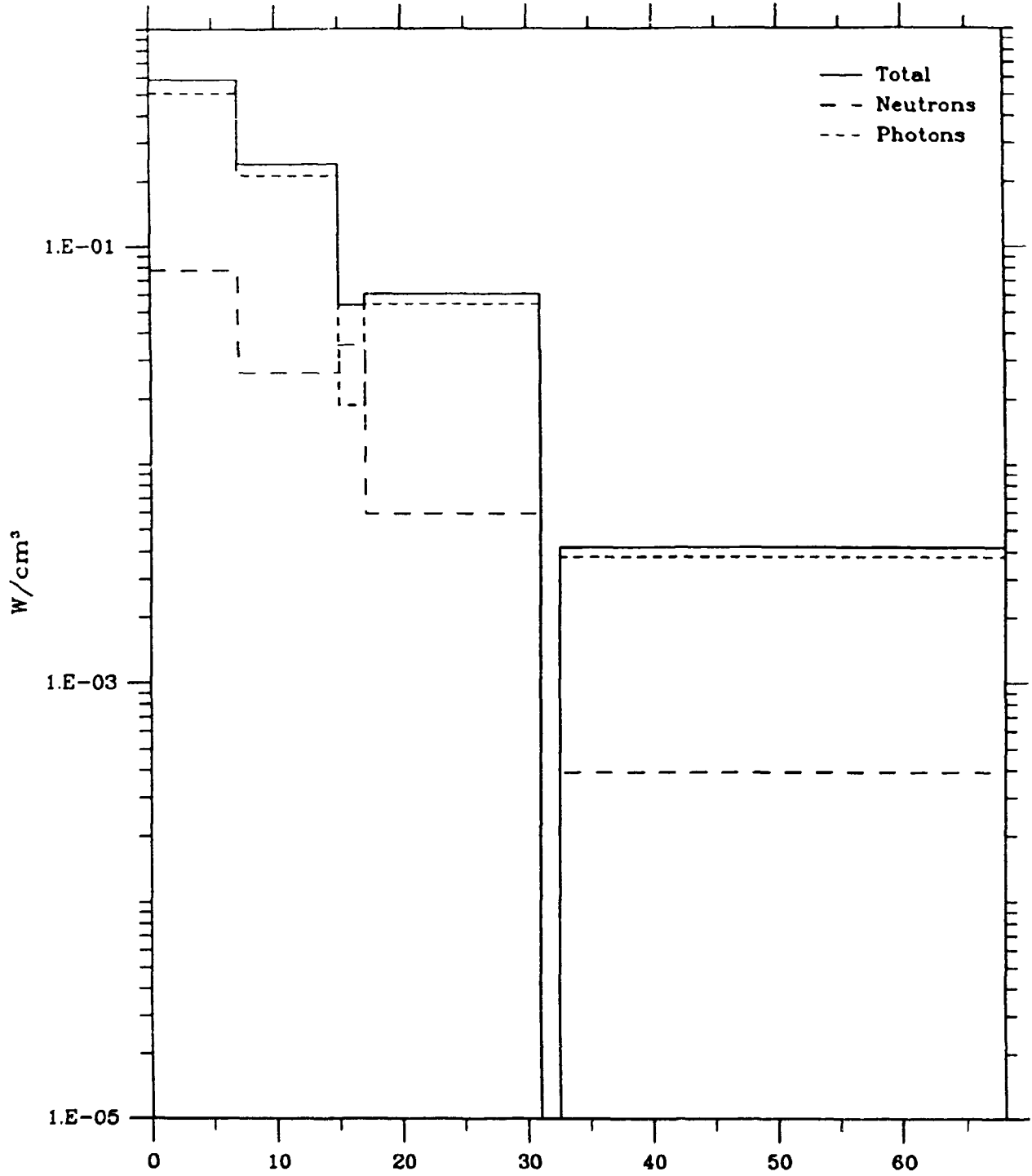
Figure 30: Inboard Power Release

Segment 23
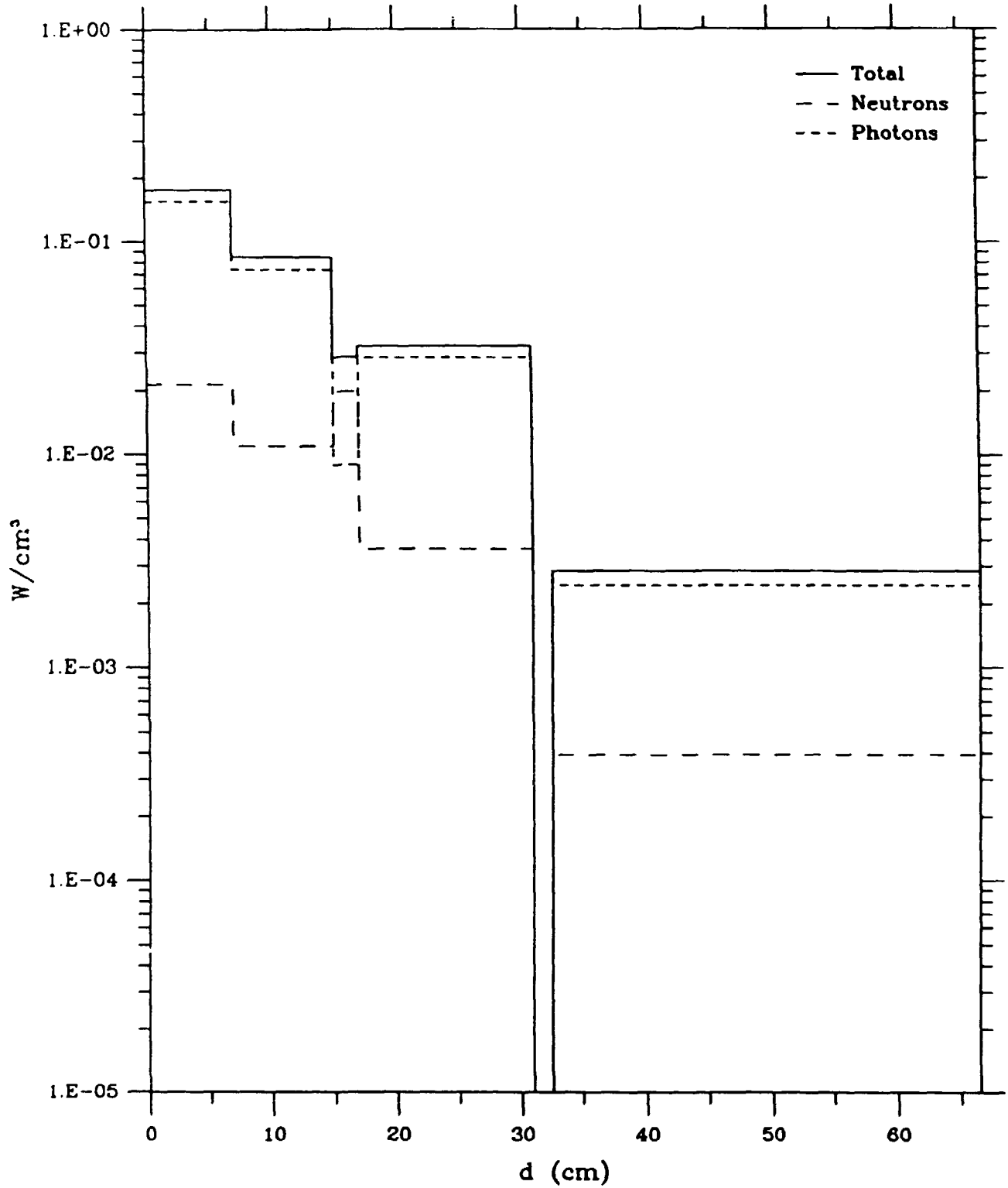
Figure 31: Inboard Power Release

Segment 14
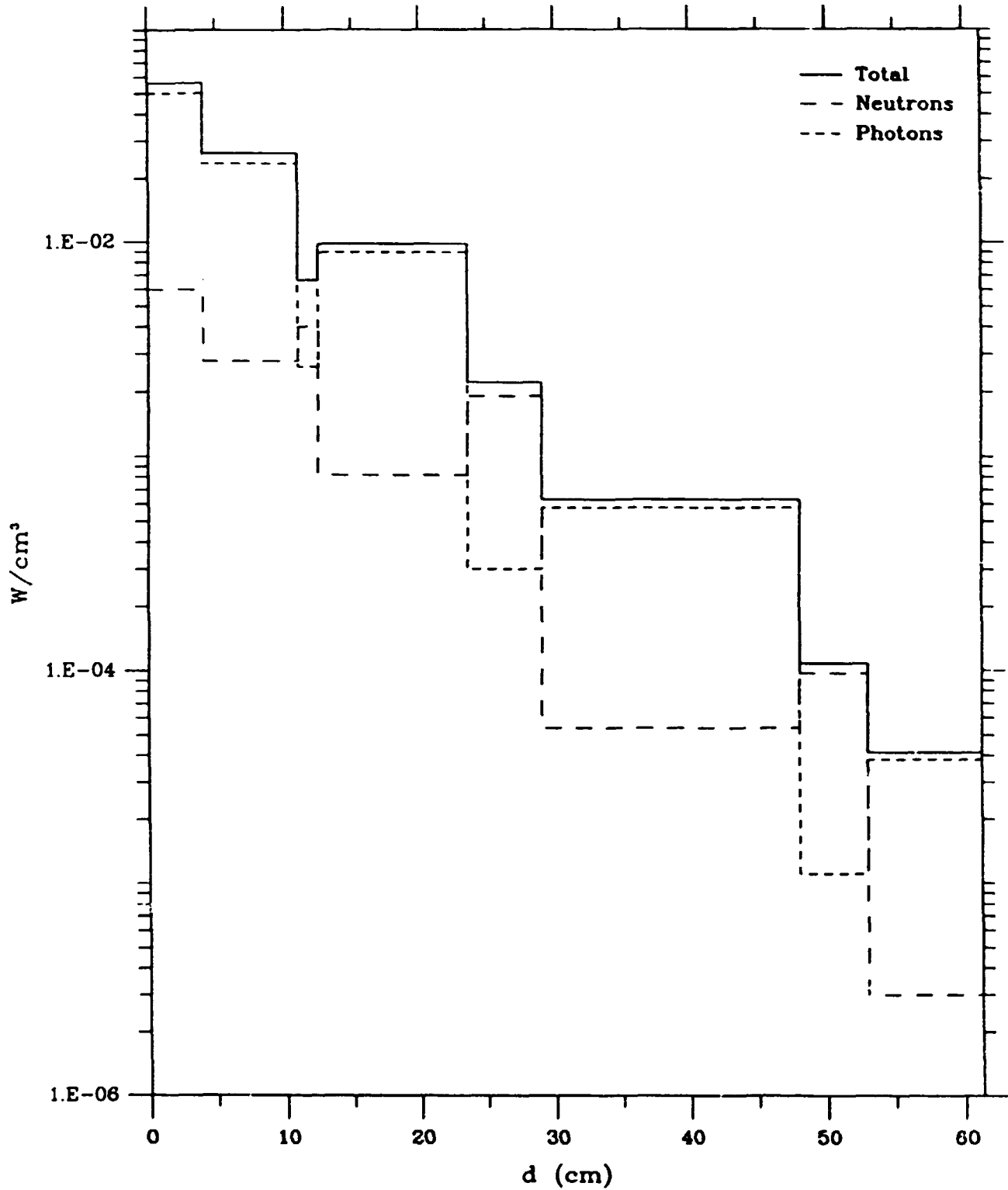
Figure 32: Inboard Power Release
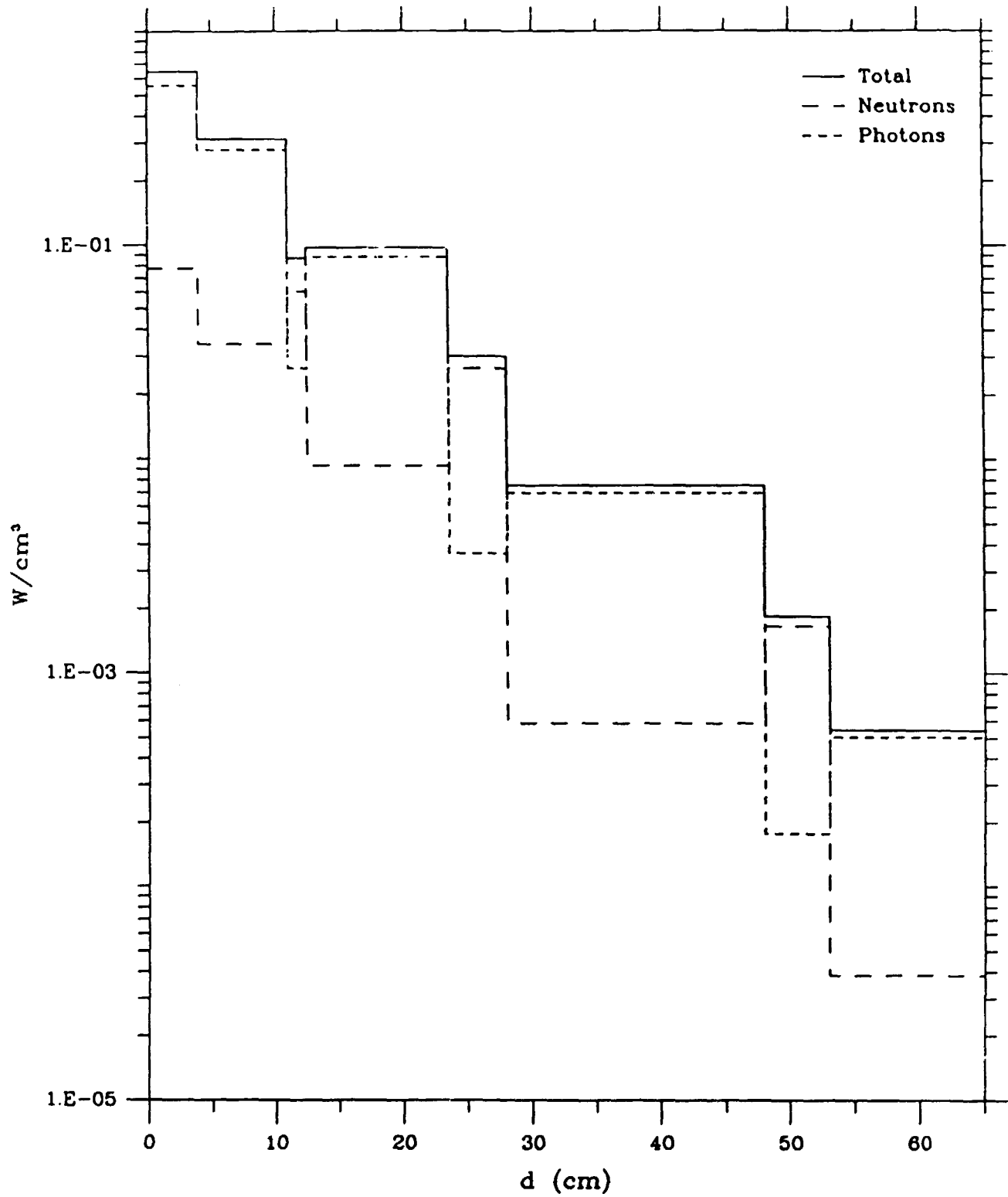
Figure 33: Inboard Power Release

Segment 18
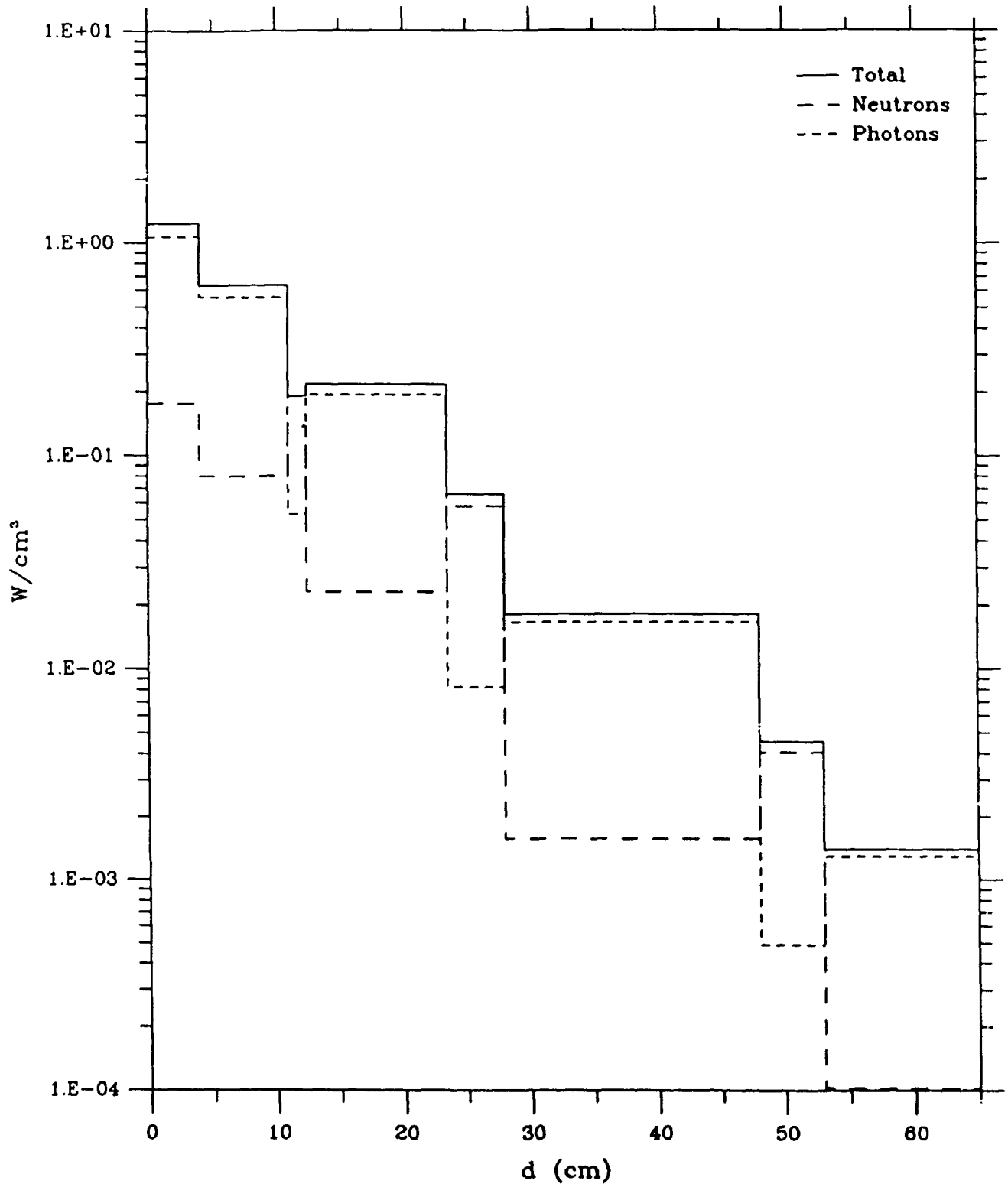
Figure 34: Inboard Power Release

69
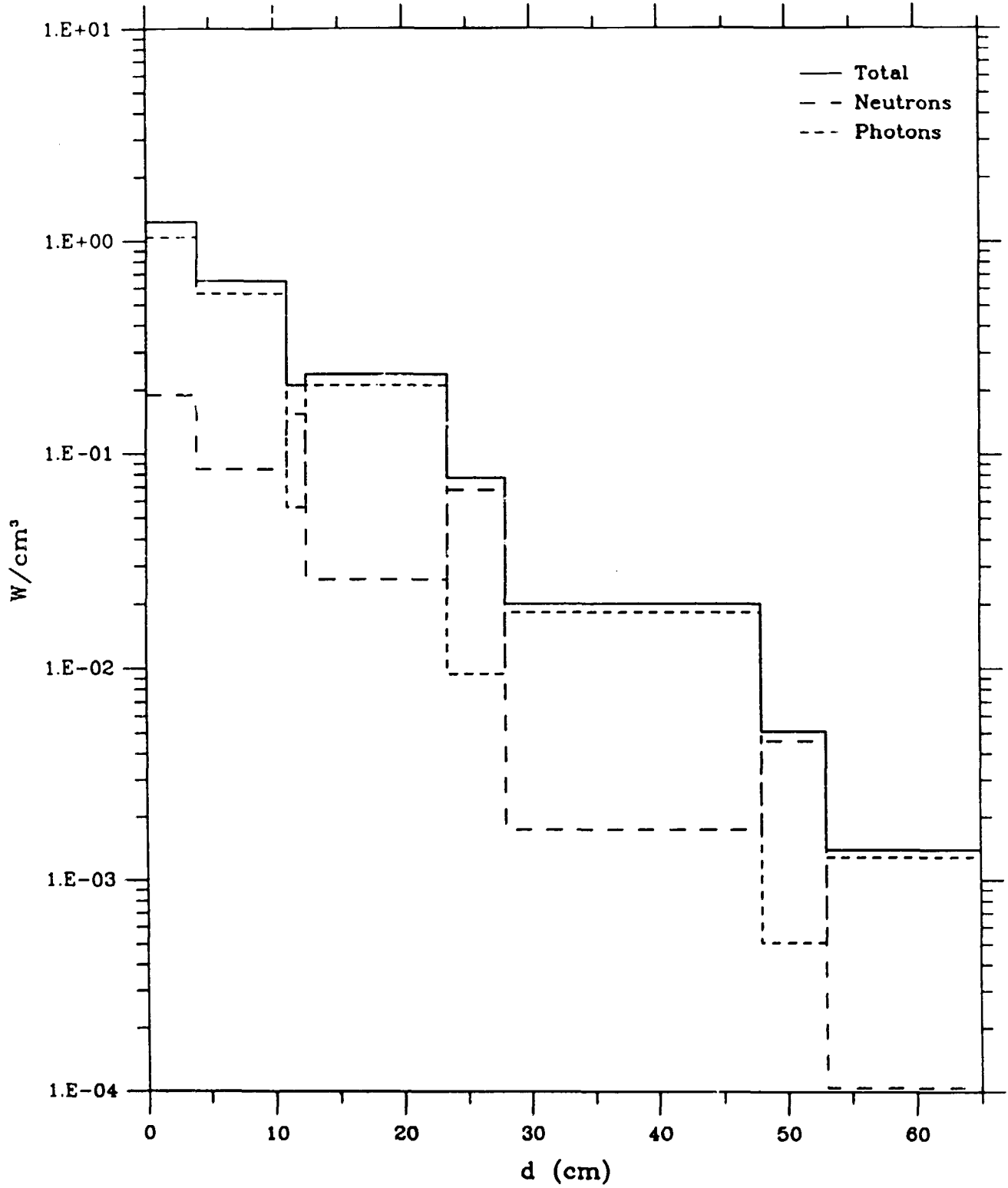
Segment 20

Figure 35: Inboard Power Release

Segment 22
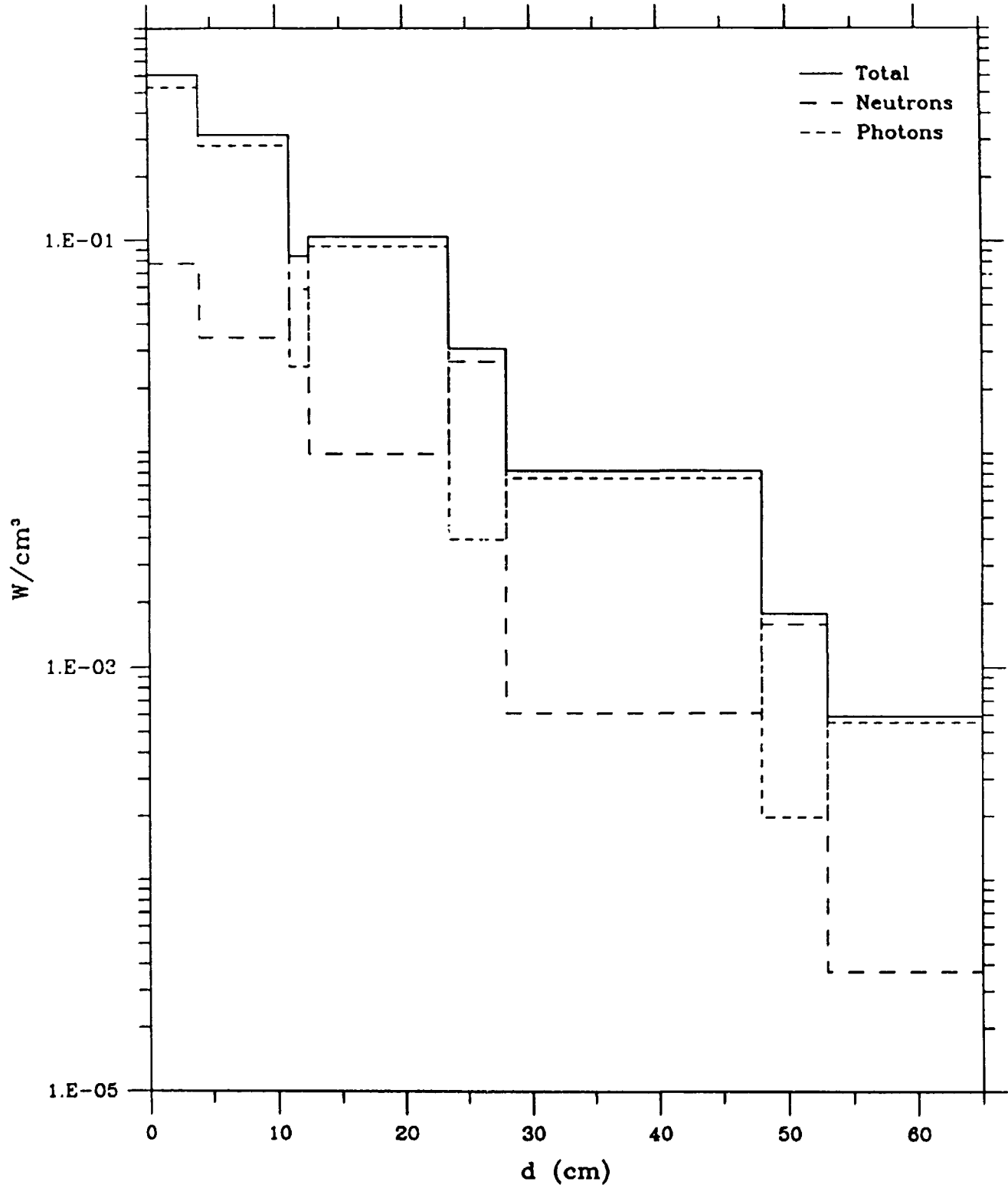
Figure 36: Inboard Power Release

71

Figure 37: Inboard Power Release
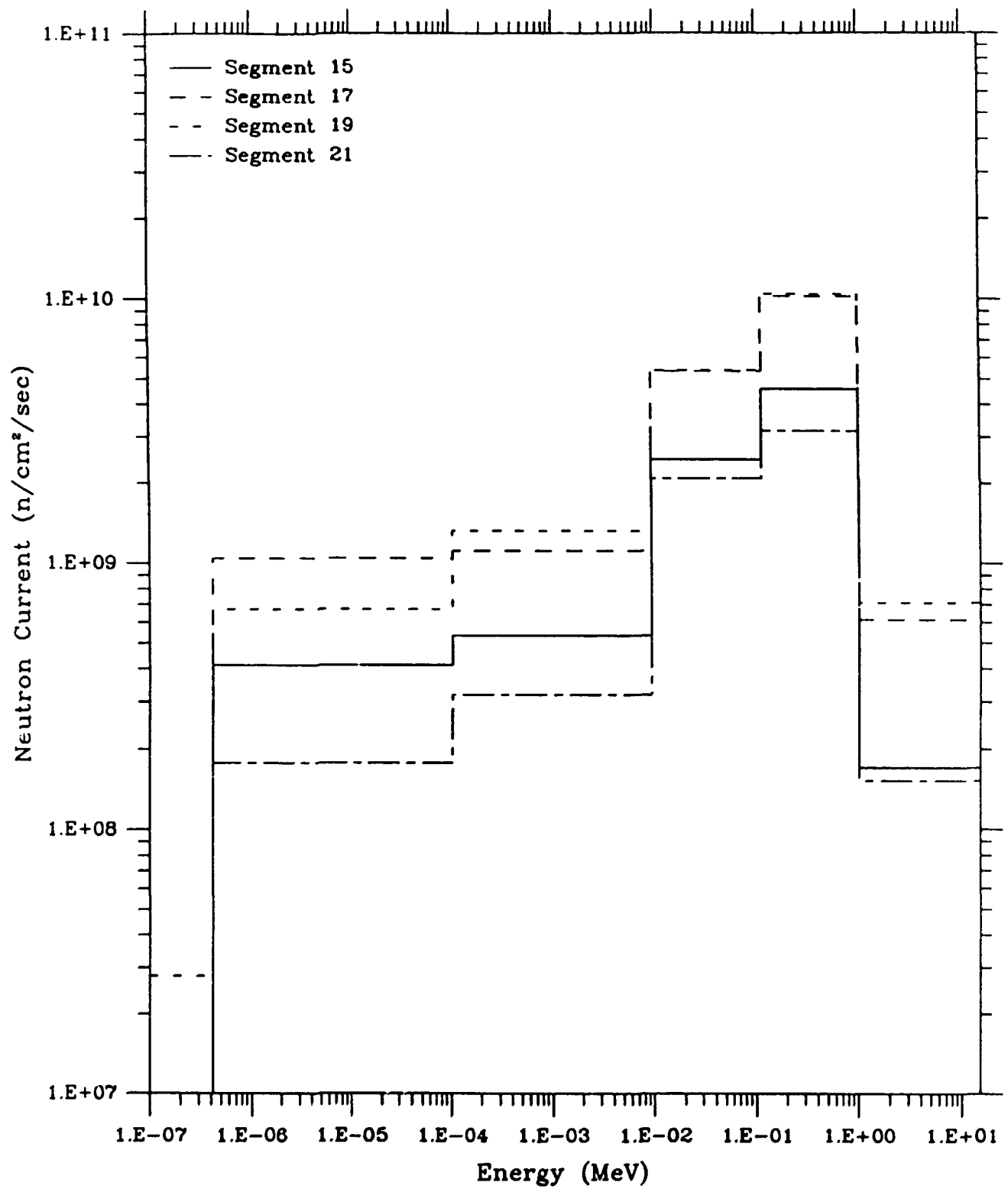
Figure 38: Inboard Wedge Midsection Neutron Current

73

Figure 39: Inboard Parallel Midsection Neutron Current

74
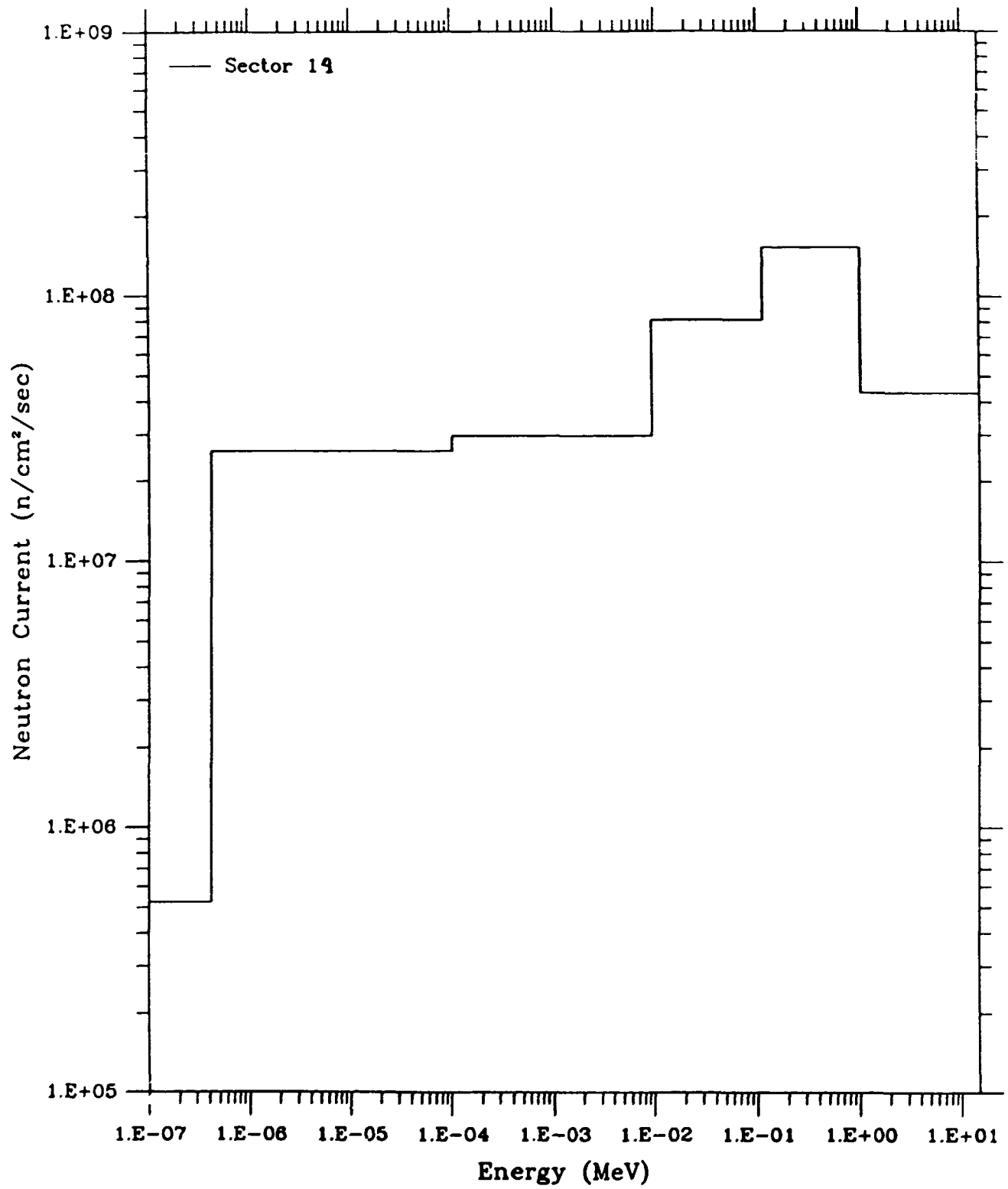
Figure 40: Inboard Top Neutron Current

75
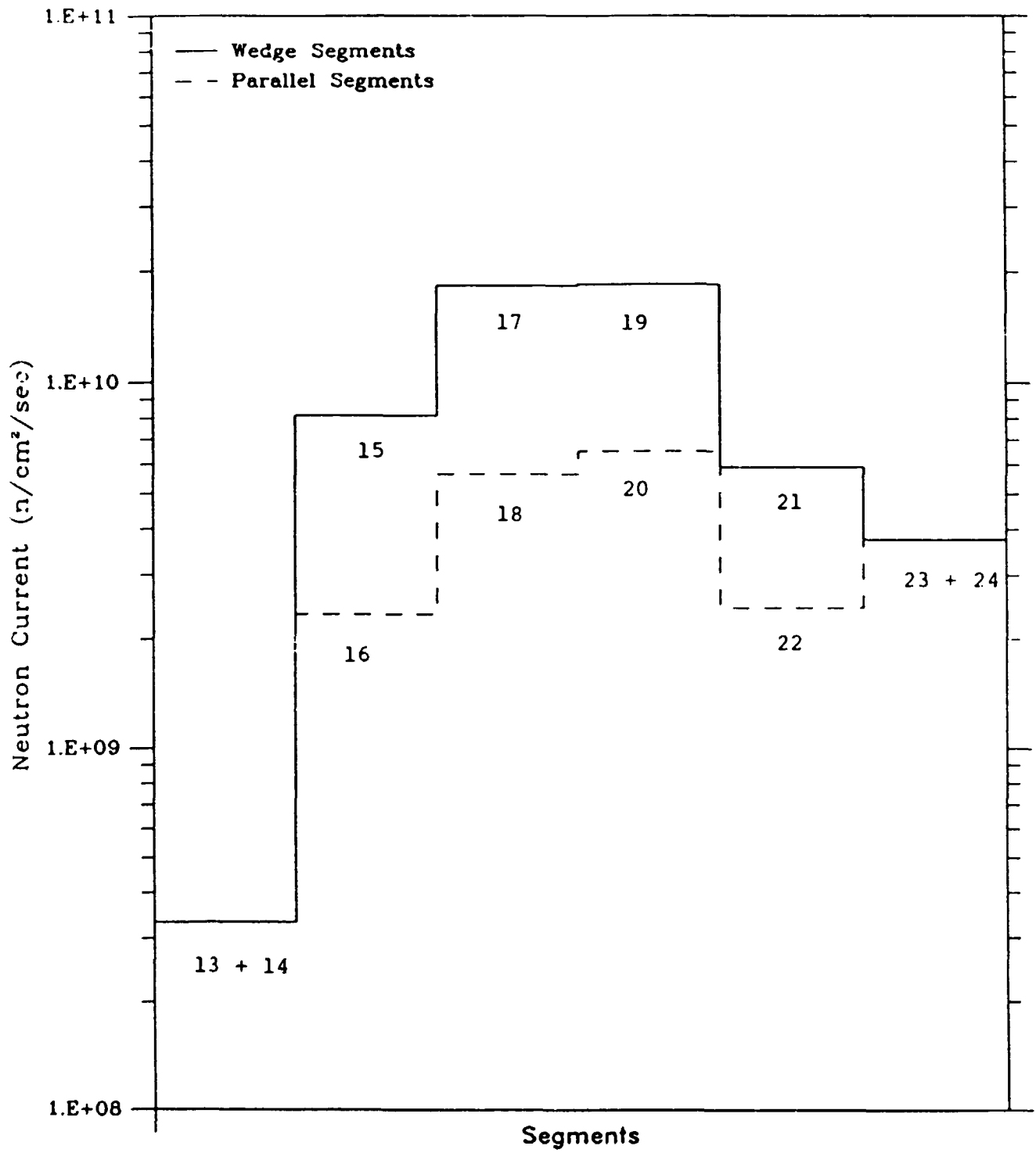
Figure 41: Inboard Total Neutron Current
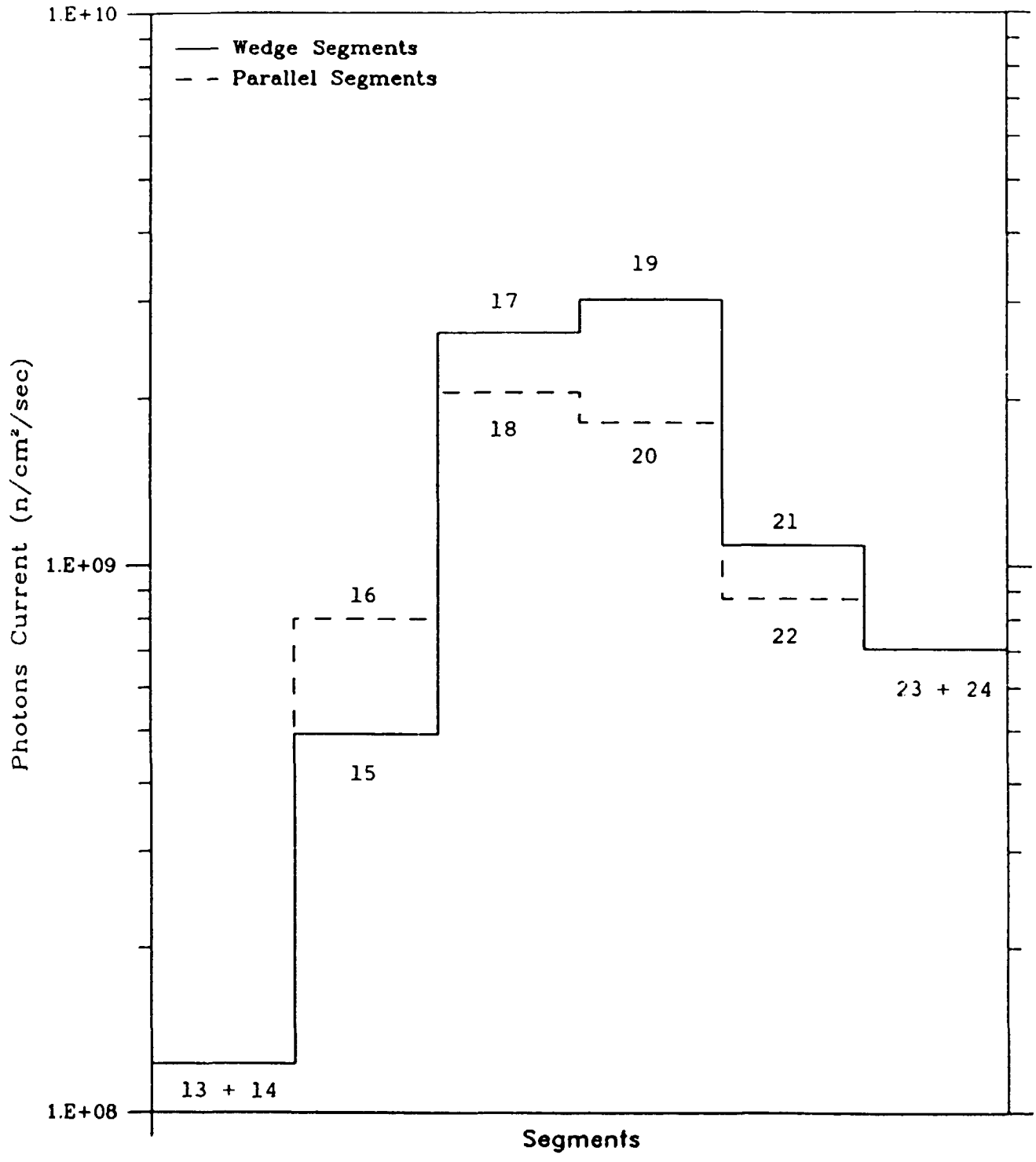
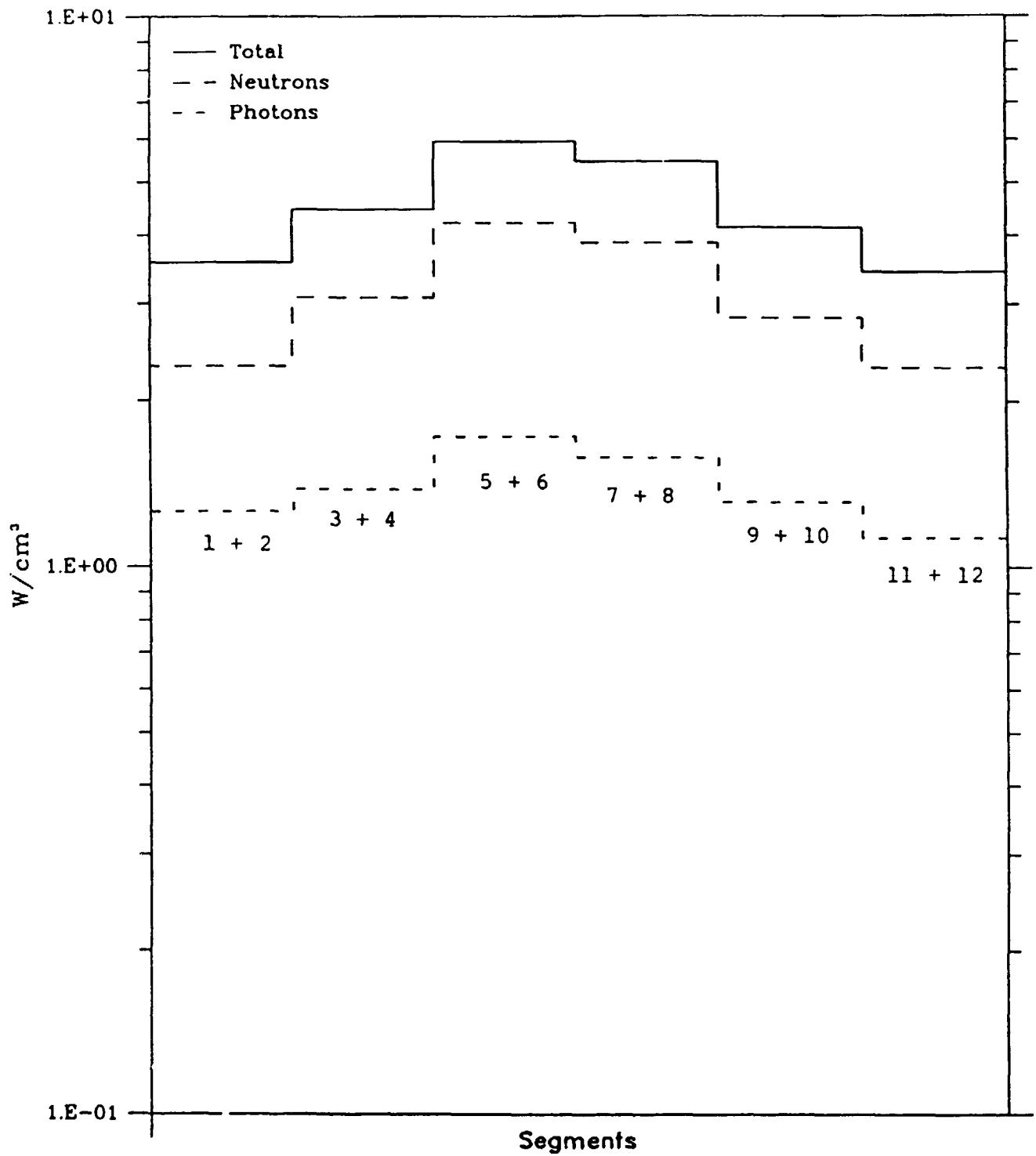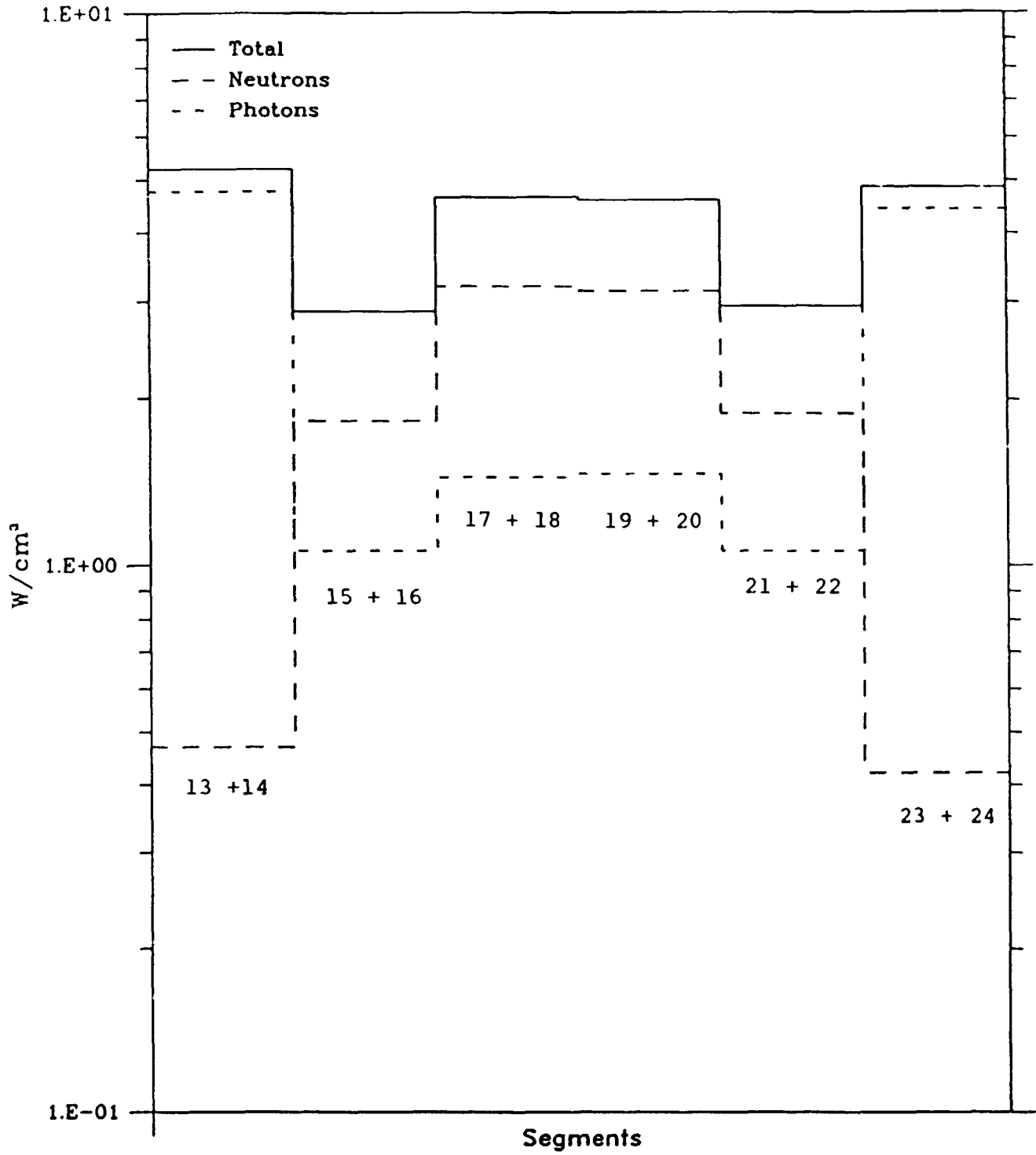**Figure 42**: Inboard Total Photon Current

77

Figure 43: Outboard Blanket Power Release

78

Figure 44: Inboard Blanket Power Release

79